NUMERICAL ANALYSIS FOR THE OPTIMAL DESIGNS FOR THERMAL ENERGY STORAGE SYSTEMS USING PHASE CHANGE MATERIAL (PCM)

FANG YUHANG

M.Phil

The Hong Kong Polytechnic University

2018

The Hong Kong Polytechnic University

Department of Building Services Engineering

Numerical Analysis for the Optimal designs for Thermal Energy Storage Systems Using Phase Change Material (PCM)

Fang Yuhang

A thesis submitted in partial fulfillment of the requirements for the

Degree of Master of Philosophy

March, 2018

CERTIFICATE OF ORIGINALITY

I hereby declare that this thesis is my own work and that, to the best of my knowledge and belief, it reproduces no material previously published or written, nor material that has been accepted for the award of any other degree or diploma, except where due acknowledgement has been made in the text.

_____(Signed)

Fang Yuhang (Name of student)

Abstract

Abstract of thesis entitled: Numerical Analysis for the Optimal Designs for Thermal Energy Storage Systems Using Phase Change Material (PCM)

Using the latent heat of phase change materials (PCM) in latent heat thermal energy storage (LHTES) systems can effectively increase the thermal energy storage capacity while avoiding occupying large volume when using sensible heat of water in stratified water storage (SWS). However, the storage effectiveness of an LHTES can be hindered by low thermal conductivities of PCMs. Previous studies have shown that the insertion of expanded graphite into PCMs could improve their effective thermal conductivity by 50 times (Haillot et al. 2008). Built from the highly developed heat transfer enhancement technique, the work reported in this Thesis systematically analyzed the effect of heat transfer enhancement in PCM and other parameters on the optimal design for the basic unit of a tube-in-tank LHTES system. Firstly, an index of effective energy storage ratio, E_{st}, was proposed to characterize the effective energy storage capacity of an LHTES system with reference to an ideal SWS system at the same volume. Secondly, using a CFD software, the effect of various parameters on E_{st} of an LHTES system was tested. Thirdly, an analytical technique of *required heat transfer length* was developed from the effectiveness-NTU theory and used to predict the optimal designs for an LHTES system under various conditions. Finally, the effect of charging conditions on the subsequent discharging performance was tested in the optimal designs. The results of the current study demonstrated that the improvement in effective thermal conductivity of a PCM would remarkably enhance the effective energy storage of an LHTES system if other parameters, such as compactness factor for PCM,

mass flow rate, tube length of a heat transfer fluid (HTF) and charging conditions, were well designed. Moreover, by enhancing heat transfer in both PCM and HTF, an LHTES could obtain both a high E_{st} and a high COP at little cost of tube materials.

Publications arising from the thesis

Journal publications

- **Y. Fang,** J. Niu, S. Deng, Numerical analysis for maximizing effective energy storage capacity of thermal energy storage systems by enhancing heat transfer in PCM, Energy Build. 160 (2018) 10–18.

-

Manuscripts

- **Y. Fang,** J. Niu, S. Deng, An analytical technique based on required heat transfer length to optimize the effective energy storage capacity of thermal energy storage systems using PCM

- **Y. Fang,** J. Niu, S. Deng, Numerical analysis for the effect of charging conditions on the subsequent discharging process in a tube-in-tank LHTES system.

Conference publications

- **Y. Fang**, J. Niu, Approaching stratified heat discharging rate using tube-in-a-tank design with PCM filled inside, *5th International Symposium on Heat Transfer and Energy Conservation*, Guangzhou, China, 2016,

- **Y. Fang**, J. Niu, S. Deng, Optimizing LHS system using PCM in a tube-in-tank design for emergency cooling, *9th International Conference on Applied Energy*, Cardiff, the U.K, 2017, Energy Procedia. 142 (2017) 3381–3387.

Acknowledgements

This work was supported by the Research Grant Council, Hong Kong, China, under the project No. RGC GRF 152129/14 and carried out at the Hong Kong Polytechnic University

Firstly, I would express my sincere gratitude to my previous chief supervisor, Prof. Niu Jianlei, and my present chief supervisor, Prof. Deng Shiming. Prof. Niu guided me with his judicious intuition on research and helped me focus on the crucial part of the problems. His profound knowledge and patient guidance are the great supports to me. Specially, I would thank Prof. Deng for his supervision after Prof. Niu moved to the University of Sydney. His rigorous attitude to research and his warm concern for students have great impact on me. Also, I would like to acknowledge my co-supervisor, Prof. Asif S Usmani for his kind help in my study. I am very fortunate to be their students, and I wish I could be a professor like them to really care about students and guide students to do the cutting-edge research.

Also, I would like to thank Prof. Adrian Bejan of Duke University for his insightful comments in research, which incented me to deepen my work, and for his generous sharing about his life experience, which encouraged me to persevere in my research.

Many thanks to my former and present colleagues at BSE including Dr. Huang Yu, Dr. Wu Yan, Dr. Liu Jianlin, Dr. Thomas C. W. Tung, Dr. Zhang Xiyao, Taiyang, Caixia, Jianong, Yongxin, Dr. Yan Huaxia, Dr. Xia Yudong, Dr. Du Jing, Guanyu, Wanyi, Long, Shikuan, May and Kendy. I would also like to thank my teammates in Boyan Volleyball Team and PolyU Choir. I really appreciate their companionship, encouragement and assistance during this memorable and wonderful time.

Last but not the least, my great thanks to my parents, my boyfriend, Di, and my roommates, Yaxing and Yuanxi, for their love, understanding, and support throughout my studies.

Table of contents

List of figures

List of tables

Nomenclature

A	heat transfer area, m^2
b	liquid fraction
c_p	specific heat capacity, kJ/(kg·K)
D	tube diameter, m
d	gap width, m
E_{st}	effective energy storage ratio
$E_{st,\infty}$	theoretical energy storage ratio
g	gravity acceleration, m/s^2
H, $H^{'}$, $\Delta \boldsymbol{H}$	enthalpy, J/kg
k	thermal conductivity, W/(m·K)
L	latent heat, J/kg
l	tube length, m
l_p	required heat transfer length, m
l_w	ideal required heat transfer length, m
$\dot{m}$	mass flow rate, kg/s
Nu	Nusselt Number
Pr	Prandtl Number

$\dot{q}$	heat flux, W
Q_{eff}	effective energy storage capacity, J
r	radius, coordinate in the radial direction, m
R	thermal resistance, K/W
Ra	Rayleigh Number
Re	Reynold Number
T	temperature, K
ΔT	operating temperature difference, K
u	local velocity, m/s
V	tank volume, m^3
$\mathbf{v}$	velocity vector
$\dot{W}$	pump power, W

Subscripts

cw	cold wall
cyl	cylinder
d	gap width
eff	effective
hw	hot wall

i	inner tube
in	inlet
m	mass-weighted average
o	outer tube
out	outlet
p	PCM
s	surface
w	water
x	position along tube

Greek letters

α	thermal diffusivity, m^2/s
β	expansion coefficient, K^{-1}
δ	thickness of melted PCM layer, m
φ	capacity effectiveness
η	heat transfer (HT) effectiveness
λ	compactness factor (*CF*)
μ	dynamic viscosity, kg·m/s

ν	kinetic viscosity, m^2/s
ϑ	material factor
ρ	density, kg/m^3
τ	time, s
ω	power factor

Abbreviations

CF	compactness factor
COP	coefficient of performance
EG	expanded graphite
GNP	graphene nanoplatelet
HT	heat transfer
HTF	heat transfer fluid
LHS	latent heat storage
LHTES	latent heat thermal energy storage
NTU	number of heat transfer unit
PCM	phase change material
SWS	stratified water storage
TES	thermal energy storage

Chapter 1 Introduction

1.1 Background

Maintaining a suitable thermal environment for human, goods or instruments requires heating or cooling at the expense of consuming energy. On the other hand, the Sun releases heat at the daytime, while sky and ground could cool the air at the night-time. If the available heat and cold could be stored and then released when needed, a large amount of energy can be saved. For this reason, thermal energy storage (TES) systems were developed. Using TES systems, thermal energy could be added to a storage medium, and removed from that medium for use at a latter time. TES enables the typical, temporal disparity between the supply and the demand, and have many applications in cooling. Firstly, the use of TES could balance the cooling load between peak hours and off-peak hours, allowing smaller dimension of technical equipment by reducing peak cooling load (Kalnas & Jelle 2015). Secondly, charging TES during off-peak hours, usually night-time, also enables water chillers to operate at a higher COP due to a higher evaporating temperature and consume electricity at a lower price due to the energy policy in some regions (Yau & Rismanchi 2012). Thirdly, TES could be charged at one place and then moved to another place to provide cooling for mobile vehicles or distributed systems (Liu et al. 2012).

TES can be classified according to how thermal energy is stored in a storage medium, i.e., by sensible heat, latent heat, or chemical reaction heat. Stratified water storage (SWS) system is a typical sensible heat storage system, which charges the sensible heat at a designed temperature while no additional heat transfer is required during a discharging process. The storage capacity of SWS depends on the amount and specific heat of storage medium for water (4.18 kJ/kg K), and the range of working temperature. Using phase change materials (PCM) in latent heat thermal

energy storage (LHTES) systems could take advantage of the large latent heat of PCM during liquid-solid phase change without large temperature variation and enlarge the storage capacity of LHTES, as compared to using SWS. However, an additional heat transfer process between PCM and heat transfer fluid (HTF) is required to discharge the thermal energy in LHTES. This results in the temperature difference between the storage medium and discharging fluid. Compared to the heat convection in charging fluid side, the heat conduction in PCM side has smaller heat transfer coefficient and higher thermal resistance (Tay et al. 2012b). This is because PCM seldom has fluidity, so the low thermal conductivity of the PCMs hinders the heat transfer between a charging fluid and PCMs.

Enhancing heat transfer in PCMs has been, therefore, the focus of many previous studies (Khan et al. 2016). According to the experimental results by Liu et al. (2005), the use of annular fins was able to improve the effective thermal conductivity of PCM by three times. Haillot et al. (2008) reported an increase in the effective thermal conductivity from 0.2–1 W/(m·K) to 5–50 W/(m·K) by compositing compressed expanded natural graphite in a pure PCM.

Although the heat transfer enhancement technique has been largely improved, the development of optimization method is somewhat delayed, which limits the benefit of PCM in LHTES. Numerical method has been widely used to test the impact of relevant design/ operating parameters on LHTES performances (Tay et al. 2012b), however, only a few researchers paid attention to the effectiveness of thermal energy storage. Tay et al. (2012a) and Belusko et al. (2012) applied the effectiveness-NTU method to a tube-in-tank LHTES system, and proposed to use the average HT effectiveness over the entire phase change process as a system performance indicator. Zhao and Tan (2015) described that their proposed shell-and-tube LHTES system had an average HT effectiveness of over 0.5. Amin et al. (Amin et al. 2012) also multiplied the energy storage

effectiveness with the total storage capacity of LHTES and then compared the result with the total storage capacity of SWS in the index of comparative energy storage ratio. Note that all the indices were developed on the basis of average HT effectiveness. However, when the average HT effectiveness met the cooling demand, a portion of discharged thermal energy was actually ineffective for the cooling demand. Since the purpose of LHTES is to provide more effective thermal energy than SWS, we could keep a portion of stored energy undischarged if the effective storage capacity of an LHTES system is already higher than that of an SWS system. The purpose of the optimization is to maximize the effective storage capacity of an LHTES system in comparison with that of an SWS system.

1.2 Statement of the problems

The use of PCM is to further improve the thermal energy storage capacity on the basis of sensible heat thermal energy storage, such as stratified water storage (SWS). When charging an SWS system with an HTF at 285K, energy at 285 K could be discharged from the system in a discharging process; However, for an LHTES system using PCM, the HTF temperature would increase from 285K to the inlet temperature, due to the additional heat transfer process between PCM and HTF. Apparently, when the outlet temperature of HTF is near the inlet temperature, the discharged thermal energy is ineffective; and when the variation of outlet temperature is very large, it would influence the cooling performance only if the LHTES is assisted by a water chiller in operation. Therefore, the total thermal energy storage capacity of LHTES systems might be larger than that of SWS systems, however, the effective thermal energy storage capacity of an LHTES system might not. The existing indices used to characterize an LHTES system lack the concern about its effective storage capacity and the comparison between LHTES and SWS. Thus, the existing optimization guidelines according to the existing characteristic indices are somewhat ineffective.

On the other hand, the low thermal conductivity of PCM has long been regarded as the short-slab for the use of PCM in TES. A lot of work has been done in this area, and the effective thermal conductivity of PCM could be easily improved by 50 times in literature (Haillot et al. 2008). Researchers have reported the improvement in discharging rate in systems using PCM with high effective thermal conductivity. However, the analyses are always specific and vary case by case. The effect of effective thermal conductivity of PCM on the effective thermal energy storage capacity is also neglected.

There are two important questions to be answered: 1) how does the heat transfer enhancement in PCM affect the effective thermal storage capacity of an LHTES system? 2) what is the highest effective storage capacity could an LHTES system obtain?

1.3 Objectives and significance

In this work, we aim to illustrate whether the use of PCM in an LHTES system could provide a higher effective energy storage capacity than that of a sensible thermal energy storage system, and how to obtain a higher effective storage capacity by existing techniques. For this aim, the discharging and charging process of the basic unit in a tube-in-tank LHTES system would be simulated in FLUENT 13.0. An extensive analysis would be organized for the following objectives.

- Define an appropriate index to characterize the effective energy storage capacity of an LHTES system with reference to an ideal SWS system having the same volume;
- Test the effects of relevant design/ operating parameters, especially the heat transfer enhancement in PCM and convection enhancement in HTF, on LHTES performance, and examine if an optimal design exists;

- Develop an analytical technique to predict the LHTES performance without numerical calculation and find the optimal design for any HTF and any PCM;
- Test the effect of charging conditions on the performance of optimal designs in subsequent discharging process

By addressing the above objectives, the Thesis would provide both qualitative and quantitative implications on the optimal design for a tube-in-tank LHTES system.

1.4 Outline of the thesis

This thesis is composed of seven chapters, which include an introduction of the research, a literature review of related studies, the methodology employed in the research, three chapters that discuss the main contents, and a conclusion.

Chapter 1 introduces the background, statement of the problems, objectives and significance of the research.

Chapter 2 presents a literature review on the achievements in developing optimal designs for LHTES systems from the aspects of PCM material, heat transfer enhancement technique, numerical method, and system characteristic analysis method.

Chapter 3 details the methodology of the current research, which includes the physical configuration, the numerical method, the proposed indices, and the analytical technique of *required heat transfer length*.

Chapter 4 firstly describes the discharging process in a tube-in-tank LHTES system and secondly characterizes the system performances by the index of effective energy storage ratio, E_{st}. A series of parameters, including the effective thermal conductivity of PCM, the inlet velocity, the

inner tube diameter, the tube length and the compactness factor for PCM would be tested to see their effects on the effective energy storage ratio, E_{st}. The effective heat transfer length would be observed to well understand the variation of E_{st} over the parameters. The definition of an optimal design for any PCM and any HTF would be finally proposed.

Chapter 5 demonstrates how to use the analytical technique of *required heat transfer length* to predict the optimal designs for LHTES. The analytical technique would be firstly validated by numerical results, and secondly used to make predications under various conditions. The effect of the above parameters on E_{st} and COP of the optimal design would be tested and guidelines on the optimization of LHTES system would be finally provided.

Chapter 6 illustrates the effect of charging conditions on the subsequent discharging performance in an optimal design for LHTES. Since not all the thermal energy in PCM could be discharged from the system at the end of a discharging process, the charging process would be initiated in the system with the existence of an initial dead zone. The effect of inlet direction, inlet temperature and inlet velocity in a charging process on the subsequent discharging process would be analysed from the perspective of both storage capacity and power consumption.

Chapter 7 concludes the Thesis and provides suggestions on the future work of optimal designs for tube-in-tank LHTES systems.

Chapter 2 Literature review

2.1 Properties of phase change material

Early in 1983, Abhat (1983) made a classification of storage medium in TES systems, as shown in Figure 2-1. Among the PCMs, organic PCMs, such as paraffins and fatty acids, are non-corrosive, non-toxic, and have almost no supercooling. Inorganic PCMs, such as water, metal, or molten salt, are non-flammable and low-cost, with high latent heat. Ideally, PCMs should have high latent heat, high thermal conductivity and suitable phase change temperature. However, the reality is not that ideal. The PCM with a high latent heat usually has a low thermal conductivity. As shown in Table 2-1, the available PCMs have different values of latent heat, and the thermal conductivities of PCMs are usually in the range of 0.15-2W/(m·K), which are at the magnitude of thermal insulating materials. The selection of PCM for an LHTES system should firstly consider the desirable phase change temperature, secondly make trade-off between a higher latent heat and a higher thermal conductivity, and finally take the chemical properties, physical properties and kinetic properties into consideration.

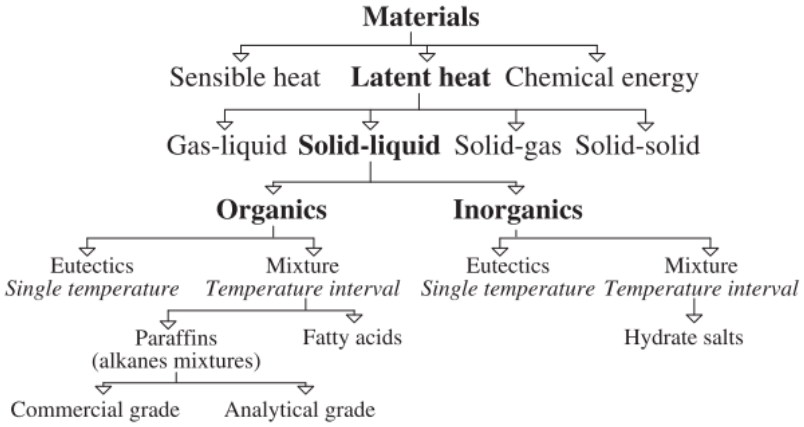

Figure 2-1 Classification of storage medium for TES uses (Abhat 1983)

Ice is frequently used as PCM in LHTES for its high value of latent heat. The low melting temperature of ice ensures a large temperature difference between return water of a cooling system and the ice melting front (Cabeza et al. 2011), thus compensating for the low thermal conductivity of ice. However, for a charging process, using ice as the PCM reduces the working temperature of water chillers by 8–10 K, resulting in a 30–40% loss in energy efficiency (Zhai et al. 2013). For a discharging process, LHTES using ice operates mostly with water chillers due to a decreased heat transfer rate caused by low thermal conductivity of ice (Liu & Wang 2002). These systems are not energy efficient from the aspects of both charging and discharging when the power consumption of water chillers is taken into consideration.

As seen, the melting temperature of PCM is a crucial parameter for LHTES performance. For conventional air-conditioning systems, the temperature of the chilled water is usually at about 280K (7℃), and that for high temperature cooling would be at around 285 K (12℃). Table 2-1 and Table 2-2 list some suitable PCMs that have melting temperatures in the range of 278 K ~ 288K (5~15℃).

Table 2-1 Thermal properties of eutectics slat and salt hydrates (Li et al. 2012)

PCM component/PCM type	Phase change temperature (°C)	Fusion heat (kJ kg^{-1})	Thermal conductivity (W m^{-1} K^{-1})	Density (kg m^{-3})	Specific heat capacity (kJ kg^{-1} K^{-1})	Company
Na_2SO_4, H_2O, NaCl, NH_4Cl	7.5	121	0.55 (liquid), 0.70 (solid)	1490	–	Calor group
$Na_2SO_4 \cdot 10H_2O$, NaCl, NH_4Cl, $Na_2B_4O_7 \cdot 10H_2O$, NH_4Br	9.5–10 (melting point) 8.0 (freezing point)	179, 122 (after 100 recycles)	0.75 (liquid), 0.93 (solid)	1470	–	Kyushu electric power, Mitsubishi
Type 41	5.0–5.5	123.3	–	–	–	Transphase
Type 47	8–9	95.4	–	–	–	Transphase
S7	7	150	0.40	1700	1.85	PCM products
S8	8	150	0.44	1475	1.90	PCM products
S10	10	155	0.43	1470	1.90	PCM products

Table 2-2 Thermal properties of paraffin waxes and fatty acids (Li et al. 2012)

	PCM	Melting temperature (°C)	Fusion heat (kJ kg^{-1})	Density (kg m^{-3})	Thermal conductivity (W m^{-1} K^{-1})	Specific heat (kJ kg^{-1} K^{-1})
Single paraffin wax	$C_{14}H_{30}$ (n-Tetradecane)	6	230	760 (liquid, 20 °C)	0.21 (solid)	–
	$C_{15}H_{32}$ (n-Pentadecane)	10	212	770 (liquid, 20 °C)	–	–
	$C_{16}H_{34}$ (n-Hexadecane)	18	210, 238	760 (liquid, 20 °C)	0.21 (solid)	–
	$C_{17}H_{36}$ (n-Heptadecane)	19	240	776 (liquid, 20 °C)	–	–
Paraffin wax mixture[a]	50:50 Tetradecane: Hexadecane (vol.%)	Sensor: 4–6 DSC: 4.9	154.839	–	–	–
	Rubitherm RT5	Sensor: 4–6 DSC: 5.2	158.332	–	–	–
Fatty acid[b] with pentadecane or additives	90:10 C-L Acid:P (vol.%)	13.3	142.2	883.2 (liquid) 891.3 (solid)	–	2.42 (liquid) 2.08 (solid)
	70:30 C-L Acid:P (vol.%)	11.3	149.2	858.0 (liquid) 872.7 (solid)	–	2.57 (liquid) 2.27 (solid)
	50:50 C-L Acid:P (vol.%)	10.2	157.8	827.8 (liquid) 850.4 (solid)	–	2.89 (liquid) 2.44 (solid)
	90:10 C-L Acid: Methyl Salicylate (mol. %)	12.5	126.7	1182.0 (liquid) 1272.9 (solid)	–	2.41 (liquid) 1.92 (solid)
	90:10 C-L Acid: Cineole (mol. %)	12.3	111.6	927.0 (liquid) – (solid)	–	2.37 (liquid) 1.71 (solid)
	90:10 C-L Acid: Eugenol (mol. %)	13.9	117.8	1091.0 (liquid) – (solid)	–	2.63 (liquid) 2.01 (solid)

a Carbon distribution of Rubitherm RT5 is 33.4 wt.% C14 (No. of carbon atoms), 47.3 wt.% C15, 16.3 wt.% C16, 2.6 wt.% C17 and 0.4 wt.% C18. Freezing temperature for paraffin wax mixture by test is 7.0 °C.
b C–L Acid is composed with 65 mol % capric acid and 35 mol % lauric acid.

2.2 Heat transfer enhancement in PCM

The heat transfer enhancement in PCM is to reduce the thermal resistance between PCM melting front and the heat transfer fluid. There are three ways to reduce the thermal resistance, modifying configurations of PCM containers; enlarging surface area of heat exchangers and increasing effective thermal conductivities of PCMs (Khan et al. 2016).

PCM containers are usually of rectangular (Lamberg et al. 2004), spherical (Tan 2008), cylindrical (Jones et al. 2006) and shell and tube configurations (Trp 2005). The configuration of a tube-in-tank (shell and tube) was considered as the optimal taking compactness factor (Castell et al. 2011) and thermal resistance (Vyshak & Jilani 2007) into consideration.

Fins are usually used to extend heat transfer surface area of heat exchangers. The thickness (Shatikian et al. 2005), number (Akhilesh et al. 2005), configuration (Mat et al. 2013) and orientation (Francis et al. 2009) of fins were widely studied. To further improve effective thermal conductivities of PCMs, many additives of high thermal conductivities were inserted into PCMs, such as porous matrix (Py et al. 2001) and nanoparticles (Khodadadi & Hosseinizadeh 2007). In addition to the improvement in effective thermal conductivity, inserting porous matrix into PCM could also build a shape-stabilized PCM composite, in which the matrix could hold liquid PCM by large capillary effect and surface tension forces caused by small pores (Zhang & Fang 2006). Tables 2-3 and Table 2-4 list the properties of several common additives used in PCM.

Table 2-3 Thermal conductivities of metal additives (Liu et al. 2016)

Metal additives	Density (kg/m^3)	Specific heat (J/ (kg·K))	Thermal conductivity (W/(m·K))
Au nanoparticle (Jana et al. 2007)	19,300	–	318
Cu nanoparticle (Jana et al. 2007)	8960	–	400
Nickel particle (Oya et al. 2013a)	8910	440	90.3
Copper foam (Xiao et al. 2014)	8930	–	398
Nickel foam (Xiao et al. 2014)	8900	–	91.4

Table 2-4 Thermal conductivities of carbon additives (Liu et al. 2016)

Carbon additives	Density (kg/m^3)	Specific heat (J/ (kg·K))	Thermal conductivity (W/(m·K))
Graphite matrix (Mills et al. 2006)	–	–	10–70
Spherical graphite (Oya et al. 2013b)	2270	710	80
Carbon fiber (Nomura et al. 2015)	2220	690	900
Expanded graphite (Ling et al. 2015)	–	–	129
Graphene nanoplatelets (Mehrali et al. 2013)	2200	–	Parallel to surface: 3000 Perpendicular to surface: 6
Graphene (Park & Kim 2014)	2200	–	3000
Graphite powder (Azeem & Zain-Ul-Abdein 2012)	–	–	130

2.2.1 Fins

Fins have been widely used on PCM side to extend heat transfer surface area between PCM and HTF. Due to the limited numbers of fins, heat transfer is locally enhanced around the fins. Accordingly, the effect of fins on the system performance varies when the configuration of PCM container or thermal conditions change. The following reviews the effect of fins in LHTES systems with the configuration of concentric cylinders, in which HTF locates in the inner tube and PCM in the outer tube.

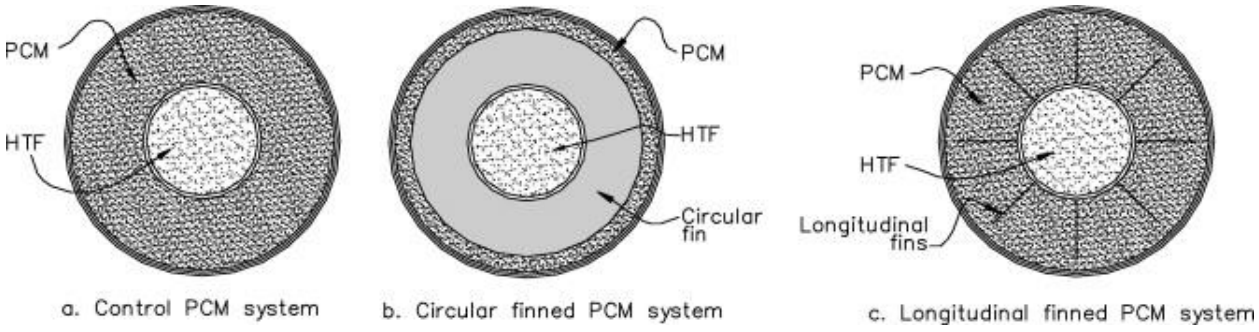

Figure 2-2 Cross-sectional views of the control and finned experimental concentric tube PCM systems used to investigate the improvement in charging of the Erythritol achieved by using fins (Francis et al. 2009)

Agyenim et al. (2009) experimentally compared the effect of circular fins and longitudinal fins in horizontal concentric tubes storage units, where the number of fins and the amount of PCM were controlled. As shown, a longitudinal finned system was recommended, because a circular finned system did not improve the heat transfer from HTF to the PCM. This also indirectly validated the assumption that heat transfer of PCM in axial direction could be ignored, which was used in many numerical models. Tay et al. (2013) numerically compared a pinned tube design (circular fins) and a finned tube design (longitudinal fins) during freezing process which was dominated by heat conduction. It was observed that the finned tube design performed 20-40%

better in terms of average effectiveness and 25% faster in terms of phase change duration. It was also found that the increase in tube volume could reduce phase change duration. However, when the ratio of tube volume to the total volume exceeded 0.03, phase change duration remained unchanged.

Ismail et al. (2001) experimentally and numerically studied the effect of longitudinal-fin parameters on the solidification process of PCM in an LHTES system. The location of solidification interface and the solidification fraction over time, and the total solidification time were used to characterize the system performance. According to their results, the increases in fin number and length could improve the solidification rate, but fin thickness had insignificant effect.

Mat et al. (2013) compared the different designs of internal fins, external fins, and internal-external fins in a triplex-tube LHTES system. As shown in Figure 2-3, HTF flows inside the internal tube and external tube, and PCM locates between the two tubes. The results suggested no significant difference among the three types of fin-arrangement in terms of PCM melting rate. The claimed time for a complete melting in the internal-external fin design was reduced to 43.3% of that in the no fin design.

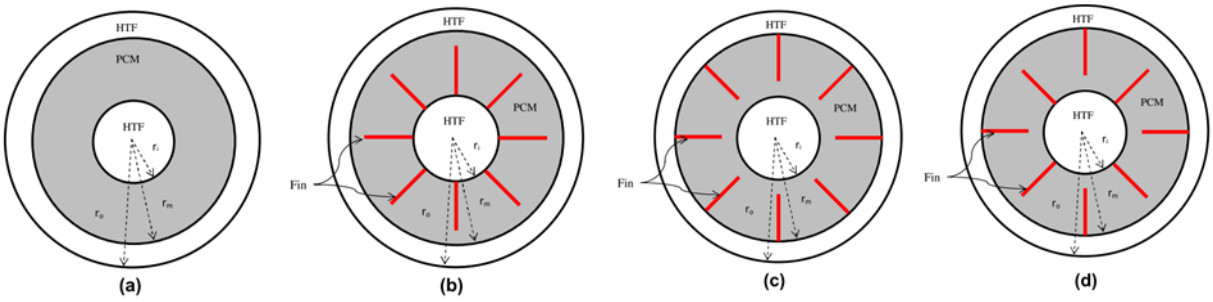

Figure 2-3 The physical configuration of the triplex-tube LHTES designs, (a)the design without fins, (b) the design with internal fins, (c) the design with external fins, (d) the design with internal–external fins (Mat et al. 2013)

For the effect of heat transfer enhancement by longitudinal fins, the results available in open literature are quite diversified. Liu et al. (2005) reported that the use of annular fins was able to improve the effective thermal conductivity of PCM by three times. Rathod and Banerjee (2015) claimed about 43.6% reduction in solidification time by installing three longitudinal fins.

The different dimension of the configurations, different thermal boundary conditions, different designs of the fins might account for the different enhancement in heat transfer. However, if fins could be distributed more widely and uniformly, the heat transfer area could be further increased and make more improvement in the system performance. To do this, additives with high thermal conductivities are inserted into PCMs.

2.2.2 Carbon additives

Carbon-based materials with high thermal conductivities and low densities are one of the most popular additives. As compared with metal, carbon has high chemical stability to avoid reaction with PCMs. Carbon-additives could be made into many morphological structures, such as expanded graphite (EG), carbon fibers or graphene nanoplatelets (GNPs).

Graphite is one typical allotrope of carbon, which has the thermal conductivity of 129 W/(m·K). EG in a worm-like structure can be made by handling expandable graphite particles in vacuum and then in a microwave oven. After this, the composite of EG-PCM can be obtained by absorbing the liquid PCM into the expanded graphite (Lv et al. 2016). The insertion of EG would not change the phase change point, and the latent heat of the composite was equal to the product of the mass fraction and phase change enthalpy of a pure PCM (Xu et al. 2016). Ling et al.(2015) studied the effect of EG mass fraction and composite density on the effective thermal conductivity of PCM/EG composite. During experiments, EG mass fractions of 35 wt% or 25 wt% were inserted

to RT44HC (thermal conductivity of about 0.22 W/(m·K)) to make the composite to have various densities (300 kg/m^3, 500 kg/m^3, 700 kg/m^3 and 900 kg/m^3). On the aspect of EG mass fraction, the thermal conductivity of composites with 35% EG was 30% higher than that with 25% EG. On the aspect of composite density, the effective thermal conductivity of composites with 25 wt% EG could increase from 4.3 W/(m·K) to 10.7 W/(m·K) when the composite density raised from 300 kg/m^3 to 900 kg/m^3. The 150% increase in the effective thermal conductivity was due to the shortening of the heat conduct pathway, as the density was increased.

Carbon fiber, an inorganic fibrous carbon compound, possesses thermal conductivity of 900 W/(m·K) in fiber direction, but about 10 W/(m·K) in circumferential direction. Nomura et al. (2015) compared the melt-dispersion method and the hot-press method to prepare the Erythritol (0.73 W/(m·K)) /carbon fiber composites. As shown in Figure 2-4, the former disperses carbon fiber in liquid PCM, and the latter presses the carbon fiber with solid PCM particles. The results showed that the hot-press method could form percolating filler network more easily and present a higher effective thermal conductivity of the composite with less carbon fiber, compared to the melt-dispersion method. In addition, using the PCM particles with a higher packing ratio in the hot-press method, the composite could achieve a higher effective thermal conductivity. At 20 vol% of carbon fiber, the effective thermal conductivity of the composite prepared by the melt-dispersion method was about 2.5 W/(m·K), and that by the hot-press method using PCM with a packing ratio of 0.58 was about 18 W/(m·K), and that by hot-press method using PCM with a packing ratio of 0.71 was about 27 W/(m·K).

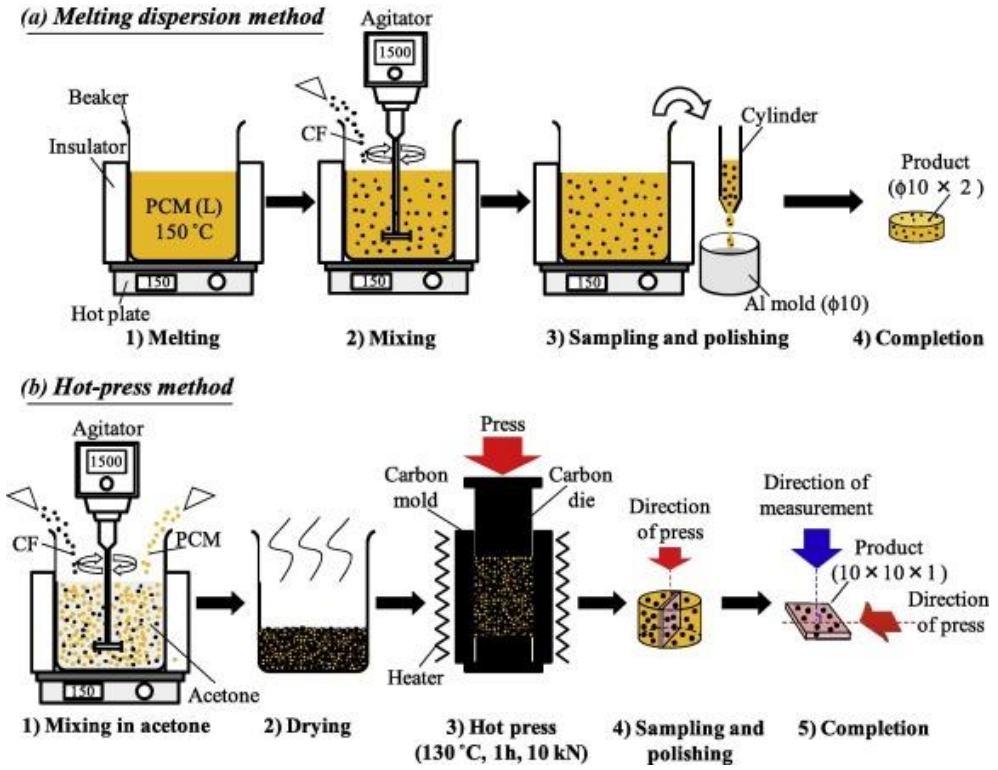

Figure 2-4 Schematic diagram for producing a PCM/ carbon fiber composite by (a) the melting dispersion method and (b) the hot-press method along with the sample preparation for laser flash measurements (Nomura et al. 2015)

Zhang et. al (2017) studied the effect of carbon fiber length on the effective thermal conductivity of the PCM/ carbon fiber composite. The carbon fibers were at the diameter of 9 μm with aspect ratios of 5 (carbon fiber -5) and 25 (carbon fiber -25), respectively. For 10 wt% loading of carbon fiber, the effective thermal conductivity of PCM/ carbon fiber -25 and PCM/ carbon fiber -5 were 3.91 W/(m·K) and 2.46 W/(m·K), which were enhanced by 407.8% and 242.9%, respectively, compared to that of pure erythritol. These can be explained from two aspects, the total thermal resistance and the formation of thermal conductive network. On the one hand, there were more top and bottom interfaces for shorter fibers, carbon fiber -5, resulting in a larger thermal resistance per unit. Furthermore, longer fibers, i.e. carbon fiber -25, were more likely to build the

percolating network throughout the whole PCM. However, larger size fillers are not always good, since they cannot be well dispersed in the PCM due to agglomerating (Fan et al. 2013).

Graphene, another allotrope of carbon, has a single layer two-dimensional structure. Graphene nanoplatelets (GNPs) possess thermal conductivity of 3000 W/(m·K) parallel to surface, and that of 6 W/(m·K) perpendicular to surface. Mehrali et al. (2013) used the impregnation method to prepare palmitic acid/GNPs. According to their results, about 10 wt% of GNPs insertion could improve the effective thermal conductivity of the composite by 10 times. GNPs with larger specific surface areas could absorb more PCM, but a smaller specific surface area of GNPs was more effective on thermal conductivity improvement. Fu et al. (2014) compared the effects of graphene sheet, graphite nanoflake and graphite power on effective thermal conductivity of resin epoxy composites. With only 10.10 wt% of graphene sheets, an effective thermal conductivity of 4.01 W/(m·K) could be obtained, which was 22 times improvement. However, 16.81 wt% of graphite nanoflakes could only improve the thermal conductivity by 2.2 times, and 44.3 wt% of natural graphite powder by 2.4 times.

The heat transfer enhancement of other carbon additives, such as exfoliated graphite sheet, carbon nanotubes, or nano-graphite, could be found in Table 2-5.

Table 2-5 Comparison of thermal conductivities of PCM composites with different carbon material additives (Lin et al. 2018)

PCM	Thermal conductivity of PCM (W/(m·K))	Carbon material additive	Thermal conductivity of additive (W/(m·K))	Fraction of additive	Thermal conductivity of composite PCM (W/(m·K))	Magnification
RT44HC	0.22	Expanded graphite	129	25 wt%	–	20–60 times (depend on its packing density)
Beeswax	0.25	Graphene nanoplatelets	Parallel to surface: 3000 Perpendicular to surface:6	0.3 wt%	2.89	11.56 times
Paraffin	–	Graphene	3000–5000	2.0 wt%	0.46	58.6%
Paraffin	–	Exfoliated graphite sheet	300–400	2.0 wt%	0.41	41.4%
N-eicosane	0.22	Carbon nanotube	2000–6000	1 wt%	0.32	1.45 times
Binary carbonate eutectic salts	–	Graphene	–	1.5 wt%	–	26.11%
Na_2CO_3/MgO	0.881	Multi-wall carbon nanotubes	–	0.5 wt%	1.489 (120 °C)	1.69 times
Paraffin	0.1264	Nano-graphite	–	10 wt%	0.9362	7.41 times
OP10E/water emulsions	0.306	Graphite nanoparticles	–	4 wt%	0.648	2.12 times

2.2.3 Metal-based materials

Metal is another material with its thermal conductivity of two magnitudes higher than that of PCMs. The composite of PCM and metal foam was prepared as shown in Figure 2-5. Xiao et al. (2014) impregnated cooper foam and nickel foam of various porosities and pore sizes with pure paraffin with vacuum assistance. Paraffin/copper foam composites fabricated by the foam porosities of 96.95%, 92.31%, 88.89% and pore size of 25 PPI could achieve effective thermal conductivities of 5.04 W/(m·K), 11.33 W/(m·K) and 16.01 W/(m·K), which were about thirteen, thirty-one, and forty-four times larger than that of pure paraffin, respectively; Paraffin/nickel foam composites fabricated by the foam porosities of 97.45%, 94.24%, 90.61% and pore size of 25 PPI were 1.24 W/(m·K), 1.70 W/(m·K), 2.33 W/(m·K), which were about three, four, five times larger than that of pure paraffin, respectively. Although copper foam is more effective than nickel foam to improve the thermal conductivity of the composite due to its higher thermal conductivity (copper foam: 398 W/(m·K); nickel foam: 91.4 W/(m·K)), copper is easier to be corroded than nickel. Moreover, the increase in porosity both for copper foam and nickel foam decreases the effective thermal conductivities of the composites, and the decrease in pore size at the same porosity has insignificant influence on the effective thermal conductivities of the composites.

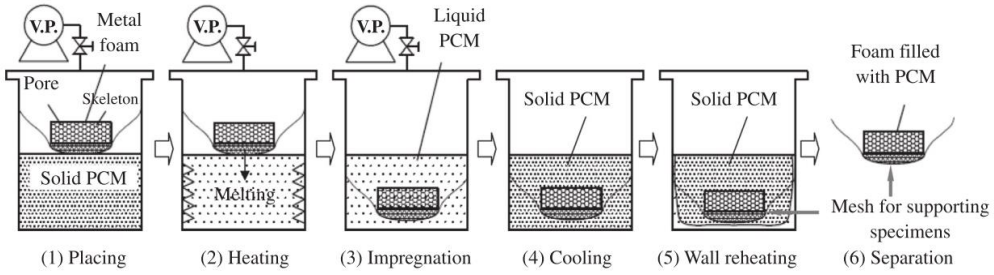

Figure 2-5 Procedure of impregnation treatment for preparing composite PCMs (Xiao et al. 2013)

Metal particles are nanostructured metal materials. Ghossein et al. (2017) used three solidification routes, namely ice-water bath, room temperature and oven solidification, to prepare eicosane/silver nanoparticle composites at different loadings of silver nanoparticles. The loading of silver nanoparticles determined the effective thermal conductivity of the composite. When the loading was larger than 2 wt%, the effective thermal conductivities of the composites would firstly decrease and then increase until the loading of silver nanoparticles was increased to 10 wt% achieving the highest value. Among the three routes, ice-water bath approach showed the lowest improvement on effective thermal conductivity, and the oven solidification approach. With 10 wt% loading of silver particles, the composites obtained by the three solidification approaches could achieve effective thermal conductivities of 0.8319 W/(m·K), 0.8534 W/(m·K) and 0.8754 W/(m·K), respectively, but the thermal conductivity of eicosane is about 0.45 W/(m·K).

Metals are easily oxidized. Although the thermal conductivity of metal oxide is lower than that of metal, it is still much higher than that of most PCMs. Sahan et al.(2015) dispersed Fe_3O_4 nanoparticles into paraffin to form the paraffin-nanomagnetite composites. Loading 10 wt% and 20 wt% of Fe_3O_4 nanoparticles could improve the thermal conductivity by 48% and 60%, respectively. Babapoor and Karimi (2015) compared the use of nanoparticles, namely SiO_2, Al_2O_3, Fe_2O_3,and ZnO in paraffin-nanoparticle composites. It was shown that Al_2O_3 nanoparticles achieved the highest effective thermal conductivity and the highest latent heat of the composite at the same nanoparticle loading. With 8 wt% Al_2O_3 nanoparticles in paraffin, the effective thermal conductivity of the composite was about 1 W/(m·K).

Table 2-6 Comparison of thermal conductivities of PCM composites with different metal material additives (Lin et al. 2018)

PCM	Thermal conductivity of PCM (W/(m·K))	Metal material additive	Thermal conductivity of additive (W/(m·K))	Fraction of additive	Thermal conductivity of composite PCM (W/(m·K))	Magnification
Paraffin	0.305	Nickel foam (porosities > 95%)	91.4	–	1.2	3.93 times
Paraffin	0.305	Copper foam (porosities > 95%)	398.0	–	4.9	16.06 times
Paraffin	0.354	Nickel foam (porosities: 90.61%)	91.4	–	2.33	6.58 times
Paraffin	0.354	Copper foam (porosities: 88.89%)	398.0	–	16.01	45.23 times
Icosane wax	0.20	Copper foam	–	7 vol%	3.78	18.9 times
Paraffin	0.21/0.29 (liquid/solid)	Aluminum foam	218	–	46.04/46.12 (liquid/solid)	218 times
Sodium acetate trihydrate	0.777 (30 ℃℃)	Copper nanoparticles	–	0.5 wt%	0.936	1.20 times
Paraffin	0.25	Fe_3O_4	9.7	20 wt%	0.40	1.6 times
Paraffin	0.418	Al_2O_3	41.1	4 wt%	0.919	2.199 times
Paraffin	0.418	Fe_2O_3	6.4	8 wt%	1.020	2.44 times
Polyethylene glycol	0.06	Silver nanowire	429	19.3 wt%	0.68	11.3 times

2.3 Using numerical method to simulate an LHTES system

Solving the phase change process in PCM is the main difficulty in the simulation of LHTES systems. The phase change problem is a difficult moving boundary problem (Stefan Problem) in physics. Very few analytical solutions are available in closed form (Dutil et al. 2011). Accordingly, numerical calculation is essential to analyzing a phase change problem. This section classifies and compares the applications of fixed grid method and deforming grid method.

2.3.1 Stefan problem

To utilize latent heat of PCM, the heat transfer process of thermal energy storage is based on the melting and solidification phenomena. During melting, the liquid-solid interface would be moving and the domain of each phase would also be time-dependent. This phase change problem is known as one of the moving boundary problems in scientific literature, Stefan problem, which considers only conduction in one-dimensional heat transfer. The following equations would generally describe the phenomenon.

The melting domain can be divided into three regions, namely a liquid phase, a solid phase and a melting front. Accordingly, there are two heat transfer equations to describe the heat transfer in both phases separately, and one energy conservation equation to describe the heat balance in the solid-liquid moving interface where the heat is absorbed or released at the phase change temperature during melting and solidification.

Heat transfer in liquid phase:

$$\rho_l c_{p,l} \frac{\partial T_l}{\partial \tau} = \nabla \cdot (k_l \nabla T_l) \tag{2-1}$$

Heat transfer in solid phase:

$$\rho_s c_{p,s} \frac{\partial T_s}{\partial \tau} = \nabla \cdot (k_s \nabla T_s) \tag{2-2}$$

The heat balance or the Stefan condition imposed at the solid-liquid interface can be expressed by:

$$k_s \nabla T_s \cdot \mathbf{n} - k_l \nabla T_l \cdot \mathbf{n} = \rho L \mathbf{v} \cdot \mathbf{n} \tag{2-3}$$

where **n** is the unit normal to the phase interface, **v** the velocity vector of the interface and *L* the latent heat per unit mass. The equations describe the heat transfer between the solid (*s*) and liquid (*l*) regions, involving the corresponding thermal properties, and the density may be constant or different between the regions.

In Stefan condition, the heat absorbed/released at the melting/solidification front, is conducted through the phases themselves. Thus, the displacement rate of moving interface is controlled by the fusion heat transferred at the boundary.

$$\lambda \rho \left(\frac{ds(\tau)}{\tau} \right) = k_s \left(\frac{\delta T_s}{\delta \tau} \right) - k_l \left(\frac{\delta T_l}{\delta \tau} \right) \tag{2-4}$$

The major challenge for phase change problems is to correctly describe the location of the solid–liquid interface and to capture the abrupt change of the associated thermophysical properties (Wang et al. 2010). Moreover, multidimensional configurations of a container, and natural convection in the liquid phase also complicates the problem, which could be only numerically solved.

The numerical methods for phase change problems can be divided into three types: fixed grid, deforming grid and the hybrid. In the deforming grid method (the front tracking scheme), the coordinate system is transformed to track the phase change interface according to the Stefan

condition, leading to high computational costs. On the contrary, the fixed grid method containing fixed grids and auxiliary function (i.e., enthalpy-based function or heat-capacity-based function) is needed to describe the phase change interface. Lastly, the hybrid method is a combination of the fixed grid and deforming grid methods.

2.3.2 Fixed grid method

In the fixed grid method, the region where phase change occurs is defined as a mushy zone, in which the PCM is in a condition between liquid and solid. In the mushy zone, the phase change of PCM is described in the form of enthalpy or heat capacity to avoid numerical instability. However, enthalpy or heat capacity would still have an evident increase within the mushy zone. Consequently, the thickness of the mushy zone as well as the grid discretization in the mushy zone are critical to the numerical correctness.

The fixed grid method in the formation of enthalpy includes enthalpy and temperature in the energy equation (Zalba et al. 2003). For conduction-dominated heat transfer, the energy equation could be rewritten as follows:

$$\rho \frac{\partial h}{\partial \tau} = \nabla \cdot (k \nabla T) \tag{2-5}$$

The solution to this equation obviously requires description of enthalpy-temperature function, and also the relationship between thermal conductivity and temperature if necessary. Here is an example of the enthalpy-temperature function:

$$h = \begin{cases} c_{ps} T & @\ T < T_m \\ c_{pl} T + (c_{ps} - c_{pl}) T_m + L & @\ T \geq T_m \end{cases} \tag{2-6}$$

For a pure substance, its solidification process takes place at a single temperature. However, for PCM mixtures in commercial applications, the solidification takes place over a range of temperature, and a two-phase zone would appear between its solid and liquid zones. Therefore, the enthalpy method is preferred for estimating the transition of phase change.

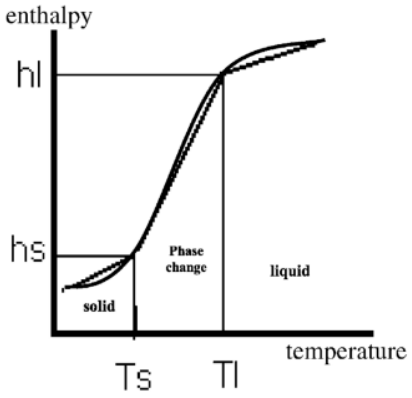

Figure 2-6 The variation of enthalpy over temperature

If the variation of enthalpy during phase change is represented in the form of heat source, the energy equation could be rewritten as follows (Swaminathan & Voller 1997).

$$\rho C \frac{\partial T}{\partial \tau} = \nabla \cdot (k \nabla T) - \rho L \frac{\partial f_l}{\partial \tau} \tag{2-7}$$

The source term can be approximated using the following auxiliary equation, in which the liquid fraction is linearized and dependent on temperature only.

$$f_l = \begin{cases} 0, & \text{if } T \le T_m - \epsilon \\ \frac{(T - T_s)}{(T_L - T_s)}, & \text{if } T_m - \epsilon < T < T_m + \epsilon \\ 1, & \text{if } T \ge T_m + \epsilon \end{cases} \tag{2-8}$$

For the fixed grid method in the formation of heat capacity (Hashemi & Sliepcevich 1967), the heat capacity varies during phase changing stage, and there is no sharp increase in enthalpy. Thus, there is no variable of enthalpy in the energy equation, as shown in Eq. (2-9).

$$\rho C(T)\frac{\partial T}{\partial \tau} = \nabla \cdot (k \nabla T) \tag{2-9}$$

The fixed grid method in the formation of heat capacity is widely used since temperature is the only prime variable to be solved in discretization. Then the approximation of the heat capacity dominates. Eq. (2-10) gives an example of the function of specific heat over temperature.

$$c_p^{eff}(T) = \begin{cases} c_p & @\ T < T_m - \Delta T \\ \dfrac{L}{2\Delta T} + c_p & @\ T_m - \Delta T < T < T_m + \Delta T \\ c_p & @\ T > T_m + \Delta T \end{cases} \tag{2-10}$$

One derivation of the heat capacity based fixed grid method is the temperature transforming method, which is also called “the improved temperature-based equivalent heat capacity method”. In this method, equation is based on the modification of heat capacity terms. Compared to the heat capacity method, this method includes an additional source term in the form of heat capacity and accordingly overcomes the time and spatial limitations in the heat capacity method(Cao & Faghri 1990).

$$\rho C(T)\frac{\partial T}{\partial \tau} = \nabla \cdot (k \nabla T) - \rho \frac{\partial S}{\partial \tau} \tag{2-11}$$

This source term is represented by the following equation (Faghri 2008)

$$S(T) = \begin{cases} C_s \times \in, & T < T_m - \in \\ \left(\frac{C_s + C_l}{2}\right) \times \in + \frac{L}{2}, & T_m - \in < T < T_m + \in \\ C_l \times \in + L, & T > T_m + \in \end{cases} \tag{2-12}$$

In the heat capacity method, the sum of latent heat and sensible heat is in the form of a modified heat capacity. As shown in Figure 2-7, there is a large peak of the modified heat capacity around the freezing point. Due to the abrupt peak, a large number of iterations should be conducted at each time step. Thus, the calculation is difficult to converge and the latent heat might be underestimated.

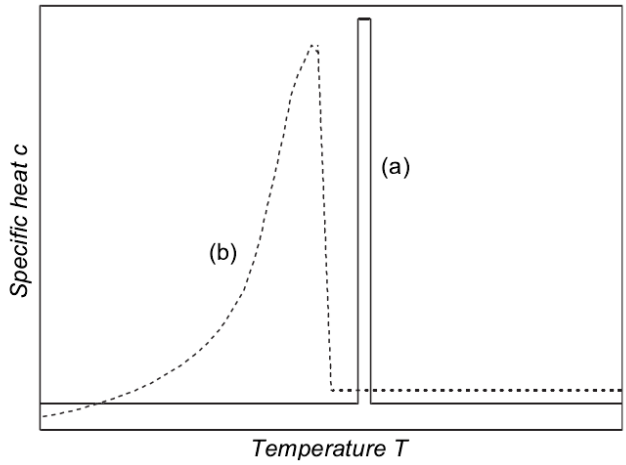

Figure 2-7 Apparent specific heat for (a)a material with sharp phase change, (b) a material with gradual phase change (Pham 2006)

Table 2-7 compares the features of the above fixed grid methods. Among the four methods, the enthalpy method is the most attractive for its high computational efficiency and modeling accuracy (Kalaiselvam & Parameshwaran 2014).

Table 2-7 Feature, advantages and disadvantages of mathematical methods used for phase change problems (Al-Saadi & Zhai 2013)

Mathematical model for latent heat evolution	Main feature	Advantages	Disadvantages	Possible solution schemes	References
Enthalpy method	Enthalpy accounts for sensible and latent heat	• Fast if proper scheme is selected • Deal with sharp as well as gradual phase change	• Difficult to handle supercooling problems • The temperature at a typical grid point may oscillate with time	Iterative scheme with Non-linear solvers (e.g., Newton's methods) Linearized-Enthalpy: Corrective iterative scheme Quasi-Enthalpy: Non-iterative Temperature correction scheme	[24,55] [22,35] [42]
Heat capacity method	Heat capacity accounts for both sensible and latent heat	• Intuitive since dealing with one dependent variable "Temperature" • Easy to program • Suitable for gradual phase change	• Lack of computational efficiency • Small time step and fine grids are required for accuracy • Difficult in handling cases where the phase-change temperature range is small • Difficult to obtain convergence with this technique, and there is always a chance that the latent heat is underestimated • Not applicable for cases where phase change occurs at fixed temperature	Iterative Scheme (e.g., Gauss–Seidel iterative scheme) if a proper heat capacity approximation is selected	[22,27,29,61,63,64]
Temperature transforming method	Heat capacity and source term are used to account for sensible and latent heat	• Deal with sharp and gradual phase change • Handle large time step and course grids	• Not a common method and therefore not tested to evaluate the pros and cons	Iterative Scheme (e.g., Gauss–Seidel iterative scheme) after linearizing the source term	[43–46,80,81]
Heat source method	Latent heat is treated as a source term	• Intuitive due to separating the latent heat from sensible • Deal with sharp and gradual phase change	• Requires under-relaxation and therefore extra efforts is needed to determine the optimum relaxation factor • Lack of computational efficiency • Problems with round off errors if melting occurs over temperature range	Iterative Scheme (e.g., Gauss–Seidel iterative scheme) after linearizing the source term	[23,38,47,49]

2.3.3 Deforming grid method (Front tracking scheme)

In deforming grid method, either the spatial grid or the temporal grid is deformed as the phase change proceeds to capture the location of the phase change interface. One approach is to fix the spatial step, Δx, and float the time step, Δt_n, and the other is to fix the time step, Δt, and allow the spatial step, Δx_n, to float. In both approaches, the phase change interface would pass through one node (x_j, t_n) after one time step. Since this method explicitly tracks the interface, it is also called as front tracking scheme in literature. Other names, such as adaptive grid method, variable grid method, or grid deforming method, address the property of the deforming grid in numerical analysis. When mesh is adaptive, the mesh topology and number of mesh points are fixed in the calculation. The calculation starts with a uniform mesh and then moves the mesh points to meet the requisite of "one grid, one time step" for the moving of phase change front.

Mackenzie and Robertson (2002) used the deforming grid method to solve a one-dimensional phase-change problem. The numerical results were compared with the classical solution of the Stefan test problems. Although the numerical algorithm was relatively simple, it validated the effectiveness of using deforming grid method to solve phase change problems.

Lacroix and Voller (1990) compared the use of the fixed grid method and the deforming grid method in solving phase-change problem in a rectangular cavity. According to their results, the mesh in the fixed grid method must be finer to capture the phase change interface, and an additional coordinate generator was required to generate the moving mesh at each time step in the deforming grid method.

Viswanath and Jaluria (1993) also compared the use of the above two methods. It was found that the deforming grid method would fail to simulate the transition from liquid to solid when there is no macroscopic phase change interface but a mushy zone instead.

On the whole, the fixed grid methods are much easier to set and cost less computational resources, and therefore are more commonly used in the commercial software.

2.4 Characteristics of LHTES systems

2.4.1 Effect of operating conditions

Numerical method has been widely used to assist the optimization of LHTES systems (Tay et al. 2012b). Lacroix (1993) numerically studied the performances of an LHTES system, where the heat transfer inside PCM was enhanced by annular fins. A maximum improvement in heat transfer was observed when the system was operated at a moderate mass flow rate and a low inlet temperature. In addition, it was illustrated that either a larger mass flow rate or a larger temperature difference between the inlet and the melting front could shorten charging time (Xiao & Zhang 2015). Tay et al. (2012c) experimentally verified a decrease in HT effectiveness caused by a larger HTF mass flow rate. According to the numerical results by Trp et al. (2006), operating conditions and geometric parameters of LHTES systems can be selected based on expected heat transfer rates and expected durations within which the thermal energy had to be stored.

2.4.2 Effect of charging flow direction

Many studies analyzed the parameters of HTF during charging processes, including flow direction, flow rate or temperature, although the existence of dead zone has never been taken into consideration. Languri et al. (2013) experimentally compared upward charging and downward discharging in a vertical tube-in-tank system and revealed that upward charging achieved a 70%

reduction in charging time compared to downward charging due to the enhanced natural convection. Gong and Mujumdar (1997) compared the parallel charging, where charging direction was the same as that of the discharging direction, and counter charging, where charging direction was opposite to that of the discharging direction. The comparison between the charging directions are drawn in Figure 2-8. Their results showed that the use of parallel charging increased the heat transfer rate by 5% compared to the use of counter charging as a result of a higher temperature difference when the hot and cold fluids entered from the same end. Moreover, it was verified that either a smaller mass flow rate or a larger temperature difference between the inlet temperature and phase change temperature could shorten the charging time (Xiao & Zhang 2015). However, all the above results were obtained at an initial condition when the PCM was all in solid form before melting or all in liquid form before solidification. There has been a lack of performance comparison when taking initial dead zone into consideration.

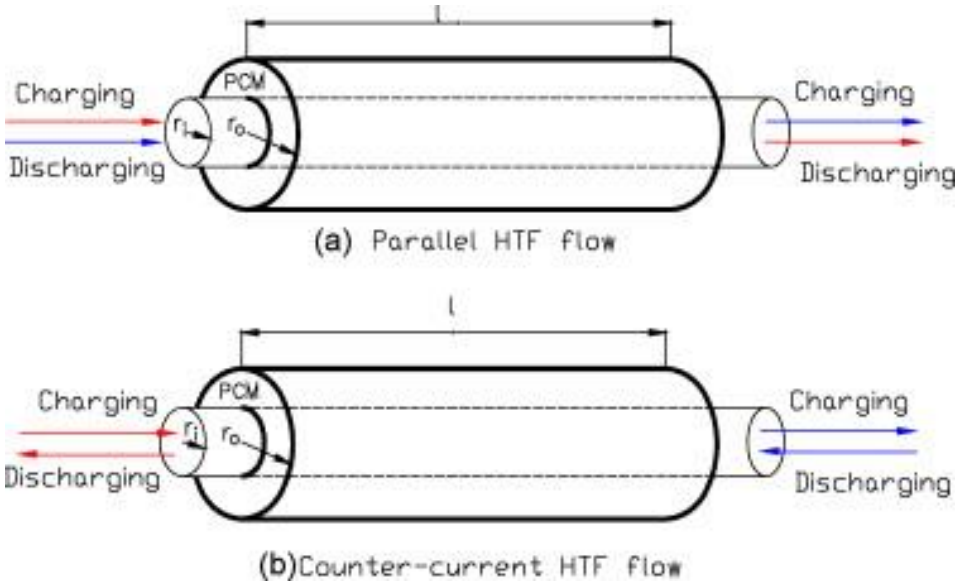

Figure 2-8 The physical model illustrating parallel and counter-current HTF flow in a shell and tube system (Gong & Majumdar 1997)

In literature, the undischarged region was called a dead zone, indicating a particular region inside a PCM tank, where heat diffusion was extremely low, and PCM barely reacts (melts or solidifies) to the heat transfer process during a discharging or charging process in an LHTES system (Belmonte et al. 2016). Lele et al. (2015) numerically analyzed the thermal decomposition kinetics of salt hydrate in a heat storage system, where there were two dead zones in the bottom corner of the reactor tank due to the geometry of two tubes in the tank. López-Navarro et al. (2014) and Gil et al. (2014) respectively noticed a dead zone which occupied over 20% volume in PCM-TES systems for off-peak cooling strategy due to the actual discharging time.

2.4.3 Indices for characterizing LHTES systems

Since the system performance is dynamic, special indices are required to characterize the LTHES systems. Phase change duration (Trp et al. 2006), heat fraction of total energy storage capacity (Sari & Kaygusuz 2001), effective thermal conductivity of PCM (Py et al. 2001) and effective Nusselt number (Li & Wu 2015) were commonly used in experimental studies, and phase change fraction of PCM (Belusko et al. 2012) and the location of phase change interface over time in numerical studies. In addition, the local/ average temperature in PCM (Rahimi et al. 2014), the fluid outlet temperature (Gong & Majumdar 1997), the phase change fraction over certain period of time were also used in some other studies. However, such indices were not effective to assess LHTES systems in different designs. Tay et al. (2012a) and Belusko et al. (2012) applied the effectiveness-NTU method to a tube-in-tank LHTES system, and proposed to use the average HT effectiveness over the entire phase change process as a system performance indicator. Several other performance indices were proposed by Amin et al. (2012) to characterize a slab-type LHTES system, including energy storage effectiveness to quantify the potential exergy loss, and comparative energy storage ratio to quantify the comparative volumetric energy storage capacity.

They consequently analyzed the design parameters that affected these indices of a slab-type LHTES system.

Wang et al. proposed to use the index of energy efficiency ratio (2015) and heat storage rate (2016) to characterize LHTES systems. The former was defined as the amount of thermal energy that can be discharged from the system by unit power consumption, and the power consumption of pump in charging process was also considered in the dimensionless form of energy efficiency ratio. The latter was equal to average heat storage rate during the whole phase change process, and the dimensionless form of heat storage rate was actually the average HT effectiveness in the work by Chen et al. (2014).

2.5 Summary

As presented in this Chapter, numerical method is effective to calculate the performances of tube-in-tank LHTES systems. Although the effect of operating parameters on the system performances has been studied, the characterization of the performance does not illustrate how much stored thermal energy could be utilized and whether the use of PCM in LHTES could provide a higher effective energy storage capacity than the use of water in sensible thermal energy storage systems. Moreover, there lacks quantitative guidelines in optimizing LHTES systems. Accordingly, even though the heat transfer enhancement technique in PCM has been largely developed, its benefit has not been well explored. These issues would be addressed in this Thesis.

Chapter 3 Methodology

This Chapter firstly describes the physical configuration of the basic unit of a tube-in-tank LHTES system. Secondly, a conjugate numerical fluid flow and heat transfer method is validated to solve the physical model. Finally, a series of indices are proposed to characterize the LHTES performance and an analytical technique of *required heat transfer length* is developed to predict effective storage capacity of any design.

3.1 Description of the physical configuration

As shown in Figure 3-1, the basic unit of a tube-in-tank LHTES system is a concentric cylinder, which includes one tube and the surrounding PCM. In operation, HTF flows through the inner tube and PCM melts or solidifies around the inner tube. When the geometric parameters or operating conditions of the system are changed, various designs of tube-in-tank LHTES systems could be obtained. The physical configuration of the default design is a six-meter-long concentric cylinder with an inner tube diameter of 5mm and an outer tube diameter of 10mm.

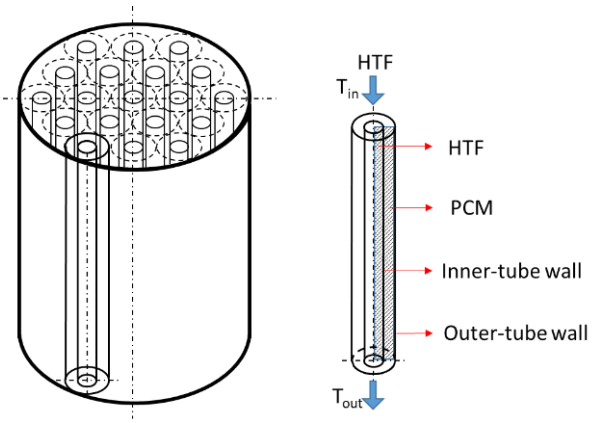

Figure 3-1 Physical configuration of a tube-in-tank LHTES system: a) the complete system; b) one of the concentric cylinders (Trp 2005)

In many cases, natural convection could effectively enhance the heat transfer in PCM (Longeon et al. 2013). Mills (1999) characterized the effect of natural convection on heat transfer using the parameter of effective thermal conductivity, k_{eff}. For a fluid layer locating between parallel plates at different temperatures, the circulation occurred when Ra_d >1000; and when Ra_d <1000, the heat transfer was dominated by pure conduction. For concentric cylinders, the definition of Rayleigh number in Eq. (3-1) was modified as Ra_{cyl} in Eq. (3-2). Eq. (3-2) shows the effect of heat transfer enhancement caused by natural convection on the basis of original thermal conductivity, *k*.

$$Ra_d = \frac{g\beta(T_{hw} - T_{cw})d^3}{\nu\alpha} \tag{3-1}$$

$$\frac{k_{eff}}{k} = 0.386\left(\frac{\Pr}{0.861+\Pr}\right)^{1/4} Ra_{cyl}^{1/4} \quad 10^2 < Ra_{cyl} < 10^7 \tag{3-2}$$

where $Ra_{cyl} = \frac{[\ln(D_0 / D_i)]^4}{d^3(D_i^{-3/5} + D_0^{-3/5})^5} Ra_l$ and $d = （D_0\text{-}D_i）/2$ is the gap width.

However, the effect of natural convection in this study was subtle. During a melting process, the melting front or the heat sink, moved from inner tube to outer tube, while the inner tube or the heat source was static. The location of the melting front was between the inner tube and the outer tube, and the surface temperature of inner tube was below the inlet temperature. The effect of natural convection could be estimated under an extreme condition. Under the extreme condition, the inner tube, where HTF located, served as a hot wall at 290K and the outer tube, where melting front located, a cold wall at 285K. For the default design under the extreme condition, the calculated Rayleigh number, Ra_{cyl}, was at 261, and k_{eff}, could be 2.83 times of *k*. On one hand, this effect could be easily overtaken by inserting metal foam or expanded graphite in the PCM, and

insertion would also hinder the formation of natural convection (Mills et al. 2006). On the other hand, long tubes could be folded or spirally shaped instead of being vertically distributed in the tank, which would further weaken natural convection. To simplify the numerical calculation, natural convection in PCM was neglected, and the focus was on the effect of heat transfer enhancement in PCM. It should, however, be noted that the natural convection may need to be considered at different geometric and thermal boundary conditions.

3.2 Numerical method

A conjugate numerical fluid flow and heat transfer method was used to investigate the discharging process in a concentric cylinder.

The governing equations for the HTF were as follows:

Continuity equation:
$$\nabla \mathbf{v} = 0 \tag{3-3}$$

Momentum equation:
$$\frac{\partial}{\partial \tau}(\rho_w \mathbf{v}) + \nabla \cdot (\rho_w \mathbf{v}\mathbf{v}) = -\nabla p + \nabla \cdot (\mu_w \nabla \mathbf{v}) \tag{3-4}$$

Energy equation:
$$\frac{\partial}{\partial \tau}(T) + \nabla(\mathbf{v}T) = \nabla \cdot (\alpha_w \nabla T) \tag{3-5}$$

For the PCM, neither momentum equation nor continuity equation was solved since natural convection was neglected. In addition, it was reported that the porosity of metal foam could be as high as 96%, and the degree of heat transfer enhancement was determined by the pore size (Xiao et al. 2013). Thus, the effect of metal foam on the enthalpy of PCM composite could be up to 4%, which might be neglected; and the effect on the heat transfer enhancement in PCM could be described in the form of the effective thermal conductivity of PCM composite. By describing the

phase change of PCM in a function of enthalpy, *H*, and liquid fraction, *b*, the energy equation could be obtained and solved.

$$\frac{\partial}{\partial t}(\rho_p H) = \nabla \cdot (k_p \nabla T) \tag{3-6}$$

$$H = H^{'} + \Delta H \text{ , where } \Delta H = bL \tag{3-7}$$

$$b = \begin{cases} 0 & if \quad T \le T_{solidus} \\ \dfrac{T - T_{solidus}}{T_{liquidus} - T_{solidus}} & if \quad T_{solidus} < T < T_{liquidus} \\ 1 & if \quad T_{liquidus} \le T \end{cases} \tag{3-8}$$

Given that the PCM was heated by the HTF in the center of the concentric cylinder, the temperature distribution in the tangential direction was always identical. The above governing equations were simplified from 3D to 2D, and the centerline of the concentric cylinder could be regarded as an axial symmetry.

Boundary conditions were as follows:

1) The HTF was in laminar flow region and had a parabolic velocity inlet at a uniform temperature and a pressure outlet;

2) The no-slip boundary condition was applied to the inner tube, and the thermal resistance of the inner tube neglected;

3) The outer tube was thermally insulated.

2D axisymmetric models were built in ANSYS FLUENT 13.0. The Solidification and Melting module, based on the fixed grid method, was selected to solve the phase change in PCM, and the Laminar module to solve the fluid flow in the HTF. The SIMPLE algorithm was used for

pressure-velocity coupling and the standard pressure staggering option for pressure correction. A second order upwind scheme was adopted to discretize convective terms, and a double precision to reduce trade-off errors.

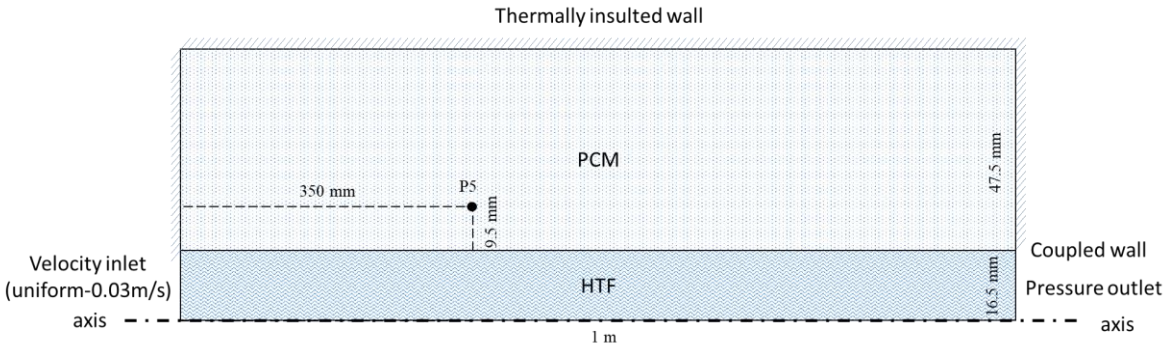

(a)

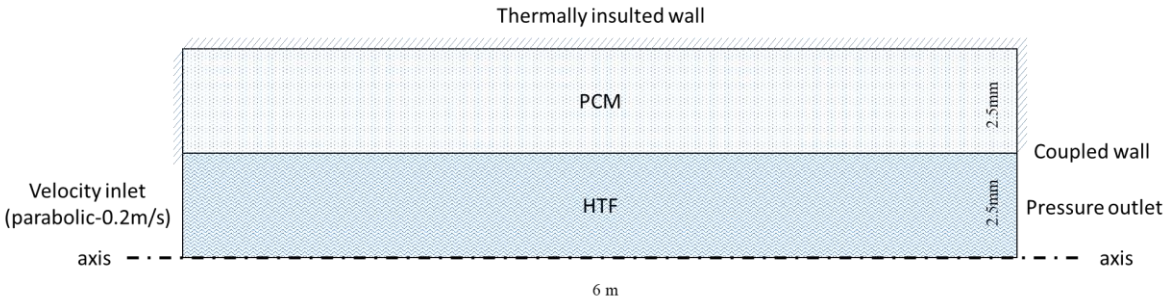

(b)

Figure 3-2 Diagrams of 2D numerical models in FLUENT. a) the model for Trp's experiment; b) the model for default design in this study

3.2.1 Validation of numerical method

A numerical model based on the Trp's (2006) experimental work was built to validate the conjugate numerical fluid flow and heat transfer method in the current study. Figure 3-2(a) shows the numerical model according to Trp's work. The initial temperatures of the PCM and the HTF were 293K, and the HTF inlet velocity was at 0.03m/s at the temperature of 323K. The melting temperature of selected PCM was at 300.7K. Other detailed properties of the PCM and the HTF could be found in Trp's full paper.

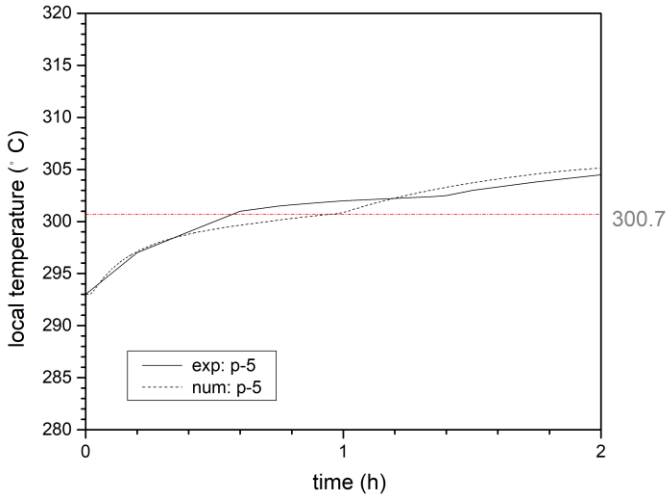

Figure 3-3 The comparison between the numerical results (dotted curve) and the experimental results (Trp et al. 2006) (solid curve) of the temperature at a monitored point of P5 illustrated in Figure 3-2(a)

Lorente et. al. (2014) theoretically and numerically studied the transition from the melting dominated by heat conduction to that by natural convection. The critical time can be estimated by $(Lv/\alpha g\beta\Delta T)^{1/2}$. In Trp's study, the melting would begin to be dominated by natural convection before one hour. Therefore, the local temperature at Point 5, locating 9.5mm from the inner tube, was monitored in the first two hours' melting. Three sets of mesh, 320×50, 640×100, and 1280×200, were compared under the time step of 0.01s, 0.1s and 1s to ensure the mesh's independence. The mesh containing 64,000 grids (640×100) with a time step of 0.1s was finally selected, since finer mesh and smaller time step only made a subtle improvement in the accuracy. As shown in Figure 3-3, the experimental result and numerical result overlapped in the first half of hour, but they were slightly different there afterwards. This was because the actual PCM used in the experiment melted over a range of temperature, but the PCM in the numerical model melt at a single point, 300.7K. Therefore, there were two turning points in the experiment but one in numerical calculation. Overall, the conjugate fluid flow and heat transfer method was validated to reasonably calculate a heat-conduction dominated melting process.

3.2.2 Parametric studies

In this study, the numerical model for the default design is shown in Figure 3-2(b). As shown in Table 3-1, water was used as the HTF, and one type of tetradecane and hexadecane binary mixtures as PCM (Bo et al. 1999). The HTF inlet was at 0.2m/s and 290K, and the initial temperatures of both the PCM and the HTF were equal to the PCM melting point at 285K.

To test the effect of heat transfer enhancement in PCM and the effect of compactness factor (*CF*) for PCM, parametric studies were conducted for a number of other designs than the default

design. Four sets of effective thermal conductivities of PCM, k_{eff}, at 0.14 W/(m·K), 1.4 W/(m·K), 7 W/(m·K) and 14 W/(m·K), respectively, were selected. By default, the thermal conductivity of the selected PCM was 0.14 W/(m·K), but a higher k_{eff} can be achieved by filling metal foam or graphite matrix into the PCM (Mills et al. 2006). Ten sets of outer tube diameter, at 6mm, 8mm, 10mm, 12mm, 14mm, 16mm, 18mm, 20mm, 24mm and 30mm, respectively, were selected. The default diameter of inner tube was 5mm, and the default diameter of outer tube 10mm.

Other parametric studies were set as follows. To test the effect of tube length, four sets of tube length at 6m, 12m, 24m and 48m, respectively were selected. The default tube length was 6m. To test the effect of inlet velocity, three sets of inlet velocity at 0.05m/s, 0.1m/s and 0.2m/s, respectively were selected. By default, the inlet velocity was at 0.2m/s. To test the effect of inner tube diameter, three sets of inner tube diameter at 5mm, 10mm and 20mm, respectively were selected. By default, the inlet velocity was at 5mm.

Table 3-1 Parameters of the materials used in this study

Material	*Density*	*Thermal conductivity*	*Specific heat capacity*	*Dynamic viscosity*	*Latent heat*	*Melting point*
	kg/m^3	*W/(m·K)*	*J/(kg·K)*	*kg·m/s*	*J/kg*	*K*
PCM (Bo et al. 1999)	*770*	*0.14*	*2200*	*0.008*	*182,700*	*285-285.001*
water	*998.2*	*0.6*	*4180*	*0.001003*	-	-

During mesh independence check, the domain was discretized into 5 grid/mm, 10 grids/mm, or 20 grids/mm radially and 1 grid/cm, 2 grids/cm, or 4 grids/cm axially, and the time step was set at 0.01s, 0.1s, or 1s. After the comparison, the meshing of 10 grids/mm radially and 1grid/cm axially with a time step of 0.1s was selected in the designs for both accuracy and efficiency. For example, the mesh of the default design contained 30,000 grids (50×600). The transient calculation met the convergence criterion of 1E-06 in continuity, momentum and energy equations, while the distributions of pressure and velocity in the HTF were verified by the analytical results of laminar flow.

3.3 Characteristic indices for LHTES systems

The HTF temperature is the mass-weighted average temperature of HTF over a truncation surface:

$$T_m = \frac{\int_0^{D_i/2} T_r \cdot u(r) \cdot \rho_w \cdot 2 \cdot \pi \cdot r \cdot dr}{\dot{m}} \tag{3-9}$$

The HT effectiveness as defined by Amin et al. (Belusko et al. 2012) is used:

$$\eta = \left(T_{in} - T_{out}\right) \Big/ \left(T_{in} - T_p\right) \tag{3-10}$$

where T_{in} refers to inlet temperature, T_{out} outlet temperature, T_p PCM melting point.

3.3.1 Definition of effective energy storage ratio and capacity effectiveness

For an LHTES system, its theoretical energy storage capacity, Q_∞ , i.e., the total amount of thermal energy that can be discharged from the system, can be defined as,

$$Q_\infty = \lambda \cdot V \cdot \rho_p \cdot (c_{p,p} \Delta T + L) + (1\text{-}\lambda) \cdot V \cdot \rho_w \cdot c_{p,w} \Delta T \tag{3-11}$$

where λ is the compactness factor (*CF*) for PCM, λ=1-D_i^2/D_o^2 , and ΔT the temperature difference between charging inlet, T_{charge}, and discharging inlet, T_{in}, $\Delta T = T_{in} - T_{charge}$. In reality, the charging temperature, T_{charge}, is lower than the PCM melting point, T_p, and the solidification of PCM usually completes before PCM is fully cooled down to T_{charge}. In this study, both LHTES and SWS are assumed to be at the temperature of T_p before discharging, which may lead to an underestimated energy storage capacity of both systems.

The effective energy storage capacity, Q_{eff}, is defined as the actual amount of discharged thermal energy at the time of τ_{eff} , when the HTF outlet temperature approximately exceeds a specified value, for instance, 286K in this study.

$$Q_{eff} = \int_0^{\tau_{eff}} \dot{m} \cdot c_{p,w} \cdot (T_{in} - T_{out}) \cdot d\tau \tag{3-12}$$

It should be emphasized that the specified value of 286K is an important parameter affecting the effective energy storage capacity of a design. The outlet temperature of 286K, or HT effectiveness of 80%, is used as a constraint in this study.

For an ideal SWS system of the volume, *V*, its effective energy storage capacity, Q_{SWS}, will be

$$Q_{SWS} = \rho_w c_{p,w} V \Delta T \tag{3-13}$$

For comparing the effective energy storage capacity of an LHTES system with that of an ideal SWS system, two energy storage ratios, an effective energy storage ratio, E_{st}, and a theoretical energy storage ratio, $E_{st,\infty}$, are defined as follows:

$$E_{st} = Q_{eff} / Q_{SWS} \tag{3-14}$$

$$E_{st,\infty}=\lambda\cdot\frac{\rho_p}{\rho_w}\cdot\frac{c_{p,p}\Delta T+L}{c_{p,w}\Delta T}+(1-\lambda) \tag{3-15}$$

The capacity effectiveness, φ, is defined as:

$$\varphi=E_{st}/E_{st,\infty} \tag{3-16}$$

The performance of an LHTES system can be assessed using the effective energy storage ratio, E_{st}. A system resulting in an E_{st} lower than 1 is basically a failure, which however did happen in practice.

3.3.2 Definitions of COP, material factor, and power factor

Under the constraint of HT effectiveness, LHTES systems are assessed by the index of discharging COP, material factor, ϑ, and power factor, ω.

The discharging COP, assessing the system performance from the perspective of energy efficiency, can be obtained without the numerical calculation results. Given COP decreases over a discharging process, the local COP at the outlet temperature of 286K, is regarded as the discharging COP in Eq. (3-17).

$$COP=\frac{\dot{q}_{\tau_{eff}}}{\dot{W}} \tag{3-17}$$

where $q_{\tau_{eff}}=\dot{m}c_{p,w}(T_{in}-T_{out})$, $\dot{W}=\dot{m}/\rho\cdot\Delta p$ and Δp can be calculated using Eq. (3-18).

$$\Delta p=f\frac{l}{D_i}\frac{\rho_w u_{\mathrm{m}}^2}{2} \tag{3-18}$$

and $$f=\begin{cases}64/\mathrm{Re} & 0<\mathrm{Re}<3000\\ (0.790\ln\mathrm{Re}-1.64)^{-2} & 3000\le\mathrm{Re}\le5\times10^6\end{cases}$$

Material factor, ϑ, is the ratio of the total heat transfer area at inner tube to that of the default design (inner tube diameter of 5mm), where *N* denotes the number of basic units operating in parallel to achieve the discharging rate for the default design.

$$\vartheta = \frac{N \cdot D_{i,design}}{D_{i,default}} \tag{3-19}$$

The power factor, ω, is defined as the ratio of power consumption in charging process to that in discharging process. This value characterizes the effect of charging process on the discharging process from the perspective of power consumption.

$$\omega = \frac{W_{charging}}{W_{discharging}} \tag{3-20}$$

3.4 Analytical technique of required heat transfer length

According to NTU theory, thermal resistance and heat transfer area together determine the heat transfer performance. For LHTES systems, as PCM melts, the thickness of the liquid PCM layer increases. As a result, the thermal resistance increases and effective heat transfer area decreases over melting. With such characteristics, LHTES is a typical dynamic thermal system, where outlet temperature increases from the initial temperature to the inlet temperature over melting. In this study, we characterize the system at an outlet temperature of 286K, and we aim at optimizing LHTES to obtain better performance at a specific NTU, or HT effectiveness.

To obtain a specific NTU, a larger thermal resistance requires a larger heat transfer area, and a larger heat transfer area corresponds to a smaller volume of melted PCM. The heat transfer area is a good indicator for both thermal resistance and the PCM liquid fraction. For a particular tube,

the heat transfer length represents the heat transfer area. An analytical technique of *required heat transfer length* is generated from the above idea and used to predict E_{st} of a design. Generally, a system with a shorter *required heat transfer length* can obtain a higher capacity effectiveness and a higher E_{st}.

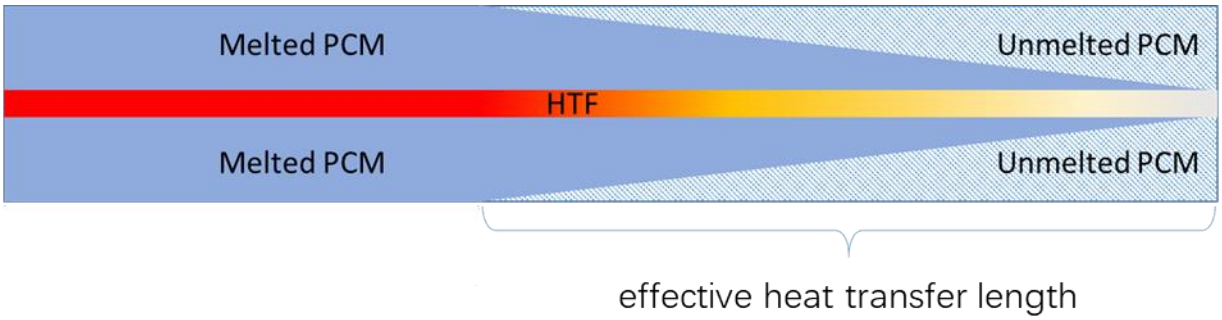

Figure 3-4 The location of effective heat transfer length in the basic unit of a tube-in-tank LHTES system

3.4.1 Function of required heat transfer length

Based on effectiveness-NTU theory, an analytical technique of *required heat transfer length* is proposed to predict the system performance. Several assumptions are made as follows:

1) Assuming melting front as moving boundary at a constant temperature, T_p

2) Assuming an averaged thickness of melted PCM along tube, δ

3) Assuming one-dimensional heat transfer in HTF along the flow direction

The basic heat transfer equations are given in Eqs. (3-21) ~ (3-23)

$$\dot{q} = \dot{m} c_{p,w} dT_m \tag{3-21}$$

$$\dot{q} = h(\mathrm{T}_m - T_s)dA_s \tag{3-22}$$

$$\dot{q} = k_p \frac{T_s - T_p}{\ln[(D_i + 2\delta)/D_i]} \cdot \frac{dA_s}{D_i/2} \tag{3-23}$$

By integrating the three equations, the function of NTU can be obtained as Eq. (3-24)

$$1 - \eta_{eff} = \frac{T_{out} - T_p}{T_{in} - T_p} = \exp(-NTU_{eff}) \tag{3-24}$$

An analogy between a normal LHTES design and a design neglecting thermal resistance in PCM is made. When thermal resistance in PCM is neglected, the surface temperature of inner tube is equal to the PCM melting temperature, T_p, indicating the operating condition of constant wall temperature. When the two designs are to achieve identical HT effectiveness, η_{eff} , the Eq. (3-25) can be obtained.

$$NTU_{eff} = \frac{A_{s,p}}{\dot{m}c_{p,w}(R_w + R_p)} = \frac{A_{s,w}}{\dot{m}c_{p,w}R_w} \tag{3-25}$$

By eliminating repeating terms, the equations can be further simplified to Eq. (3-26).

$$\frac{l_p}{R_w + R_p} = \frac{l_w}{R_w} \tag{3-26}$$

Finally, the functions of *required heat transfer length*, l_p, and *ideal required heat transfer length*, l_w, are derived in Eqs. (3-27) ~ (3-29).

$$l_p = l_w \cdot (1 + \frac{R_p}{R_w}) \tag{3-27}$$

$$\frac{R_p}{R_w} \sim \frac{k_w Nu}{k_p} \tag{3-28}$$

$$l_w = \ln(\frac{1}{1-\eta}) \cdot \frac{c_{p,w}\nu}{4k_w} \cdot D_i \cdot \frac{\mathrm{Re}}{Nu} \tag{3-29}$$

where the thermal resistance in HTF, R_w, is determined by $1/h$, and the thermal resistance in PCM, R_p, is determined by $\ln(1+2\delta/D_i)/k_p \cdot D_i/2$. It is assumed that the tube flow is fully developed both hydrodynamically and thermally from inlet ot outlet. Thus, the Nusselt Number of 3.66 is used to solve HTF in laminar region, which is also the representative Nu value for tube flow with constant wall temperature. And Nusselt for tube flow with Re over 3000 can be calculated by Eq. (3-30). The averaged thickness of the melted PCM layer, δ, will be discussed later.

$$Nu = \frac{(f/8)(\mathrm{Re}-1000)\,\mathrm{Pr}}{1+12.7(f/8)^{0.5}(\mathrm{Pr}^{2/3}-1)} \quad \begin{pmatrix} 0.5 \le \mathrm{Pr} \le 2000 \\ 3\times10^3 < \mathrm{Re} < 5\times10^6 \end{pmatrix} \tag{3-30}$$

As shown in Eq. (3-27), when the thermal resistance ratio between PCM and HTF approaches zero, l_p approaches l_w. Thus, l_p is called as *required heat transfer length*, and l_w the *ideal required heat transfer length*.

3.4.2 Prediction of PCM liquid fraction

According to the definition, l_p describes the heat transfer condition at time of τ_{eff}, and the melted PCM is the resultant of heat transfer over time duration of $0 \sim \tau_{eff}$. It would be desirable if the volume of melted PCM could be estimated by the corresponding value of l_p at HT

effectiveness of η_{eff} . However, the heat flux at inner tube wall is determined by the thickness of PCM melted layer, and the thickness of PCM melted layer again depends on the heat flux at inner tube. To decouple the above relationship, several assumptions are made as follows:

1) An averaged thickness of melted PCM, δ , along the effective heat transfer tube is used to calculate the wall heat flux, $\dot{q}_x$. Accordingly, the heat flux varies with the HTF temperature along effective heat transfer tube.
2) The melted PCM in the effective heat transfer tube is melted by the wall heat flux, $\dot{q}_x$, over time duration of τ_{eff} . Note that the wall heat flux is always in the exponential form as described in Eq. (3-31), thus the assumption is reasonable.

The wall heat flux of inner tube at the position x, ($0 < x < l_p$) can be described in Eq. (3-31).

$$\begin{aligned} \dot{q}_x &= h \cdot (T_m - T_s) \cdot \pi \cdot D_i \cdot dx \\ &= h \cdot \exp(-\frac{NTU}{l_p} x) \cdot (T_{in} - T_s) \cdot \pi \cdot D_i \cdot dx \\ &= h \cdot (1-\eta)^{\frac{x}{l_p}} \cdot (T_{in} - T_s) \cdot \pi \cdot D_i \cdot dx \end{aligned} \tag{3-31}$$

where $T_{in} - T_s = \frac{1}{1 + R_p / R_w} \cdot (T_{in} - T_p)$.

Since the PCM in spent tube is all melted and only the melting front near the inlet of l_p has reached the outer tube wall in the effective heat transfer tube, the heat flux at the inlet of l_p can be presented as:

$$\dot{q}_{x=0} \cdot \tau_{eff} = L \cdot \rho_p \cdot \frac{\pi}{4} \cdot (D_o^2 - D_i^2) \cdot dx \tag{3-32}$$

Accordingly, the liquid fraction of PCM in the effective heat transfer tube can be derived in Eq. (3-33).

$$\varphi_{l_p} = \frac{\int_{x=0}^{x=l_p} \dot{q} \cdot \tau_{eff}}{L \cdot \rho_p \cdot \frac{\pi}{4} \cdot (D_o^2 - D_i^2) \cdot l_p} = \frac{\eta_{eff}}{\ln(\frac{1}{1-\eta_{eff}})} \tag{3-33}$$

For a specific value of η_{eff} =80%, the liquid faction of PCM in l_p is equal to 0.497.

3.4.3 Assumption of averaged thickness of PCM

In the last section, the liquid fraction of PCM in effective heat transfer tube is obtained, the averaged thickness of melted PCM layer in Eq. (3-35) can be calculated from Eq. (3-34).

$$\varphi_{l_p} \cdot \frac{\pi}{4} \cdot (D_o^2 - D_i^2) = \frac{\pi}{4} \cdot \left[(D_i + 2\delta)^2 - D_i^2 \right] \tag{3-34}$$

$$\frac{\delta}{(D_o - D_i)/2} = \frac{\sqrt{\varphi_{l_p} \cdot \lambda + (1-\lambda)} - \sqrt{1-\lambda}}{1 - \sqrt{1-\lambda}} \tag{3-35}$$

For a specific compactness factor (*CF*) for PCM, λ=75%, the averaged thickness of melted PCM layer in effective heat transfer tube is 0.58 of the thickness of total PCM layer between inner tube and outer tube.

3.4.4 Prediction of E_{st}

On the basis of the above results, the liquid fraction of PCM in the whole tube, *l*, can be calculated using Eq. (3-36)

$$\varphi_p = \varphi_{l_p} \cdot \frac{l_p}{l} + 1 \cdot \frac{l - l_p}{l} \tag{3-36}$$

If all the thermal energy in the inner-tube HTF and that in the melted PCM could be discharged, the effective energy storage ratio can be predicted using Eq. (3-37).

$$E_{st} = \varphi_p \cdot \frac{\rho_p}{\rho_w} \cdot \frac{c_{p,p}\Delta T + L}{c_{p,w}\Delta T} + (1 - \lambda) \tag{3-37}$$

3.5 Summary

This Chapter systematically presented the methodology developed in the Thesis. A conjugate numerical fluid flow and heat transfer method was firstly validated to solve the physical model of the basic unit of a tube-in-tank LHTES system. Secondly, the index of effective energy storage ratio, E_{st}, was proposed to characterize the effective energy storage capacity of an LHTES system with reference to an equivalent SWS system. Some other indices were also proposed to characterize the system performances from the perspective of power consumption or material cost. Finally, an analytical technique of *required heat transfer length* was developed from the effectiveness-NTU theory to predict E_{st}. In the following chapters, the above will be used to explore the optimal design for the basic unit of a tube-in-tank LHTES system.

Chapter 4 Parametric studies on discharging performance

4.1 Introduction

This Chapter aims at describing the discharging characteristics of tube-in-tank LHTES systems. To this end, the validated numerical method in Chapter 3 will be used to simulate the designs of tube-in-tank LHTES systems in discharging process. By characterizing the designs by the index of effective energy storage ratio, E_{st}, the effect of parameters on the discharging performance will be analyzed. It is aimed to demonstrate whether E_{st} can be raised by enhancing heat transfer in PCM or HTF, and whether there exists an optimum *CF* to obtain the maximum E_{st} for any PCM and any HTF in a finite-length tube. The effective heat transfer length at the outlet temperature of 286K will be used to interpret E_{st} of any design. The analysis will provide qualitative implications on the optimal designs for tube-in-tank LHTES systems.

4.2 The discharging process of an LHTES system

In the discharging process of an LHTES system, PCM is melted and HTF is cooled. As PCM melts, the thermal resistance between HTF and PCM melting front increases. As a result, the outlet temperature of HTF increases as thermal energy is discharged from the system. Figure 4-1 presents the distribution of temperature in the HTF and liquid fraction in the PCM at specific time points in a discharging process. At 30s, only a small portion of PCM is melted and the outlet temperature is below 286K; at 1569s, most of PCM is melted and the outlet temperature is 289K. As defined in Chapter 3, E_{st} indicates the amount of discharged storage capacity of an LHTES system in comparison with that of an SWS system. It is shown in Figure 4-2 (b) that E_{st} is a function of outlet temperature (HT effectiveness). At an HT effectiveness of 0.8 (outlet 286K), E_{st} is 0.51, indicating

a discharged storage capacity lower than that of an ideal SWS; At an HT effectiveness of 0.2 (outlet 289K), E_{st} is 5.42, indicating a much higher discharged storage capacity than that of an ideal SWS. To avoid large temperature variation in outlet temperature of an LHTES system, the designs with various parameters would be assessed by E_{st} at HT effectiveness of 0.8 (outlet 286K) in the Thesis. In operation, the discharging process should stop when outlet temperature exceeds 286K.

However, at an HT effectiveness of 0.8 (outlet 286K), E_{st} is low and only a small portion of PCM is melted. To improve the E_{st}, it is of great significance of understanding the melting process in PCM.

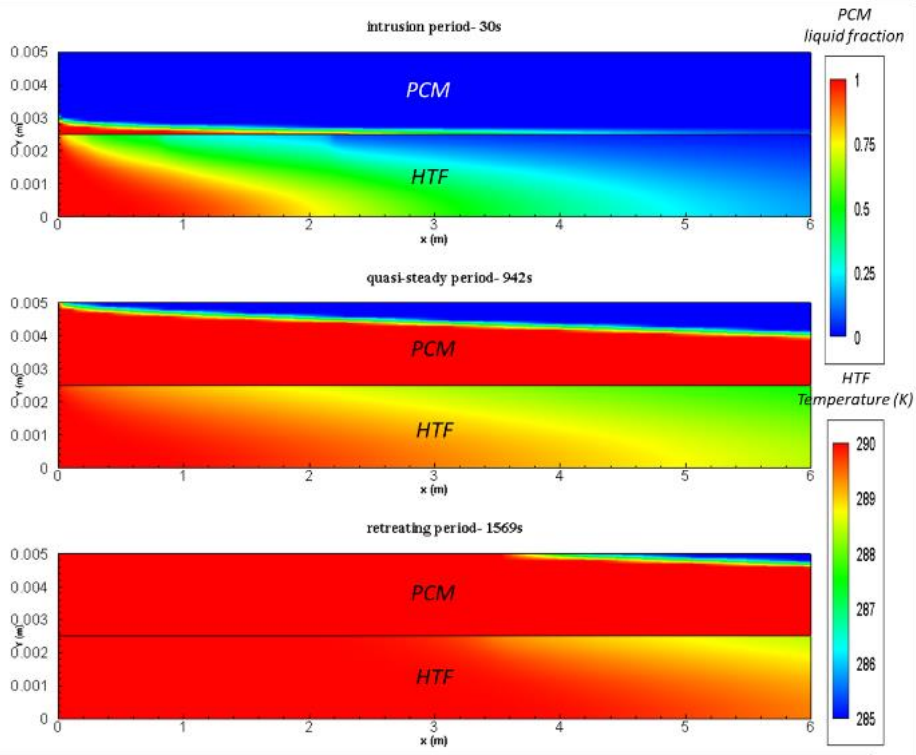

Figure 4-1 Distributions of temperature in the HTF and liquid fraction in the PCM in the axial plane of the default design at specific time points during a discharging process

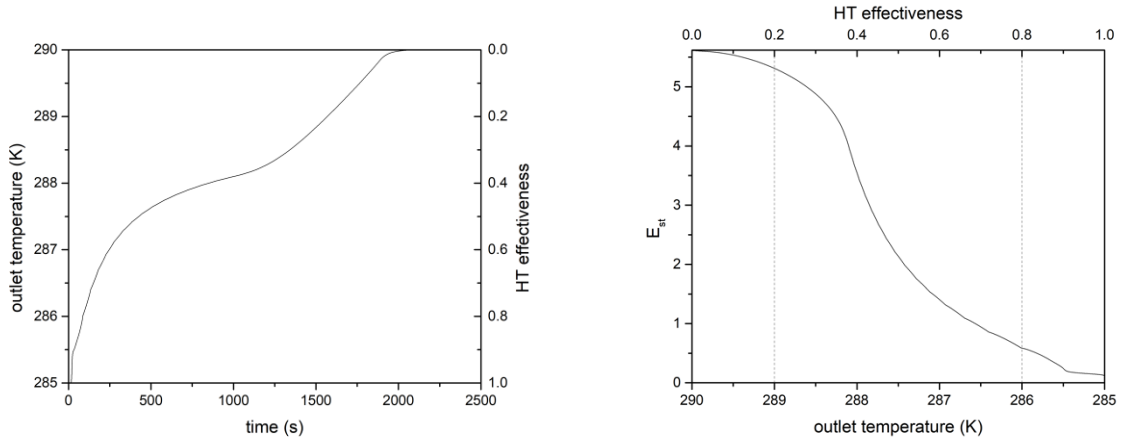

(a) (b)

Figure 4-2 The system performance of the default design: a) the variation of outlet temperature over time; b) the variation of relationship between the effective energy storage ratio, E_{st}, and outlet temperature

As shown in Figure 4-1, the melted PCM is always in a truncated-coned region bundled with an inclined melting front, since there is always a larger temperature difference between the HTF and the melting front in the tube near inlet. The melting front moves both radially and axially over a discharging process. According to the location of melting front, a discharging process can be divided into three periods:

a) Intrusion period ($0 \sim l/u_m$): the melting fronts locates at the inner tube, and the warm HTF ($T_{in}=290\ K$) gradually replaces the stored water ($285\ K$) in the inner tube;

b) quasi-steady period: the melting front moves radially and finally reaches the outer tube;

c) Retreating period: the melting front moves axially to the end.

By the time of 1569s, all the PCM in the first-three-meter-long tube has melted, and the HTF is not cooled when passing through this section. In fact, where there is a melting front, there is an effective heat transfer tube to cool HTF; and if PCM is fully melted, the tube would lose its effectiveness in heat transfer. In retreating period, the length of effective heat transfer tube decreases as melting front moves axially. When the length of effective heat transfer tube is longer than the *required heat transfer length* to achieve outlet temperature of 286K, the melting continues; on the contrary, it stops. On the whole, E_{st} is calculated according to the melted PCM at the outlet temperature of 286K, and the portion of unmelted PCM is described by the *required heat transfer length*. Accordingly, the interpretation of *required heat transfer length* might provide implications on improving E_{st}.

In the following sections, the effect of parameters on E_{st} and *required heat transfer length* would be analyzed. By varying the parameters of a design, E_{st} could be improved.

4.3 Parameter of heat transfer enhancement in PCM

The effect of enhancing heat transfer in PCM was studied in designs with PCM at different effective thermal conductivities. As shown in Figure 4-3(a), with PCM at a higher effective thermal conductivity, k_{eff}, the outlet temperature is lower and the total discharging time shorter. Consequently, E_{st} is largely improved. In Figure 4-3(b), when k_{eff} is improved by 10 times, 50 times and 100 times, E_{st} increases from 0.59 to 3.43, 3.83 and 3.88, respectively. Without heat transfer enhancement, E_{st} of an LHTES system is lower than that of an ideal SWS system; With 50 times heat transfer enhancement (k_{eff} = 7 W/(m·K)), E_{st} of an LHTES system can be increased to more than 3 times of that of an ideal SWS system. Thus, enhancing heat transfer in PCM can effectively improve E_{st}.

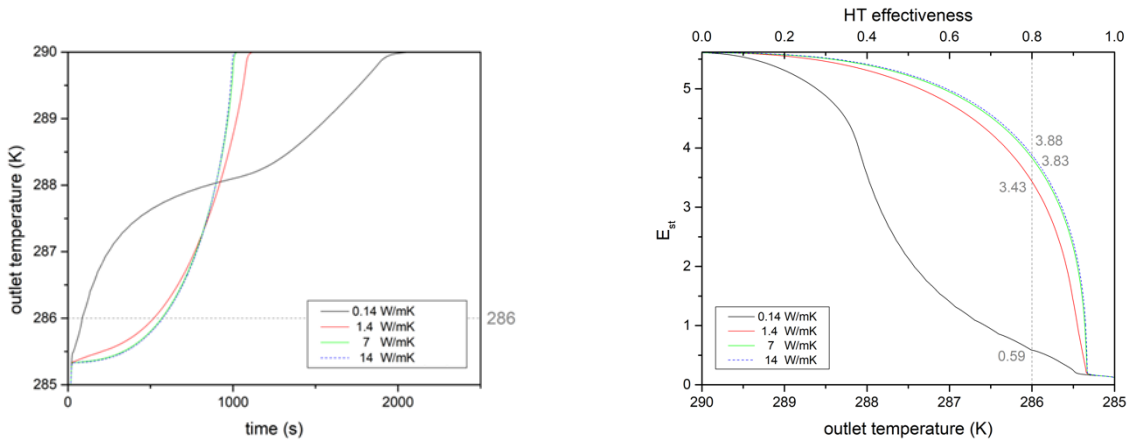

(a) (b)

Figure 4-3 The comparison of designs at different k_{eff}: a) the variation of outlet temperature over time, and b) the relationship between the effective energy storage ratio, E_{st}, and the outlet temperature

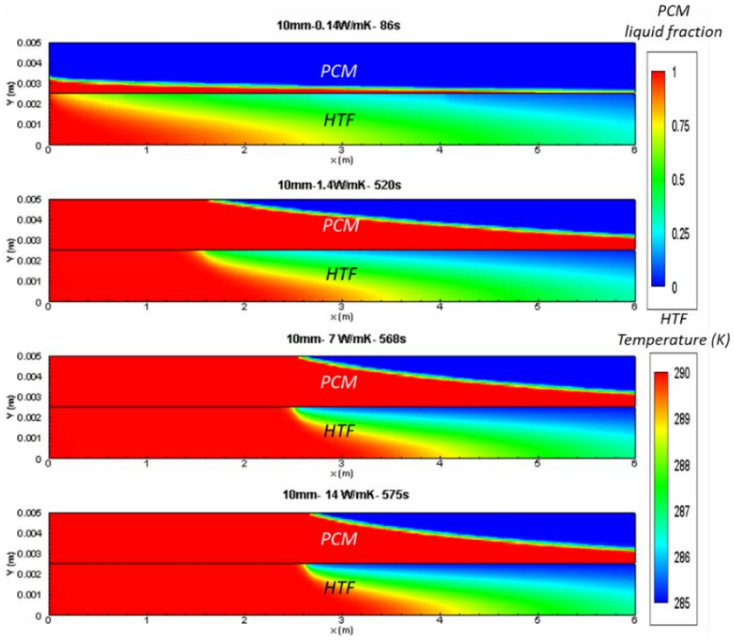

Figure 4-4 Distributions of temperature in the HTF and liquid fraction in the PCM at the instant when outlet temperature is about to exceed 286K after discharging, at four different k_{eff} (The texts above contours describe the value of outer tube diameter, k_{eff} and the local time)

However, when heat transfer enhancement is over a threshold, E_{st} cannot be further improved. This phenomenon could be understood from the heat transfer analysis of a tube-in-tank LHTES system. When effective thermal conductivity of PCM is improved, the thermal resistance in PCM is decreased. According to effectiveness-NTU theory, the decrease in thermal resistance could decrease the *required heat transfer length* in a heat exchanger. However, as indicated in Eq. (3-27), when the thermal resistance in PCM is negligible to that in HTF, a further heat transfer enhancement in PCM would have little effect on the total thermal resistance and the *required heat transfer length*. The *required heat transfer length* is the effective heat transfer length at outlet temperature of 286K in Figure 4-4, and the effective heat transfer length in a tube-in-tank LHTES system indicates the location of melting front and the unmelted PCM. Therefore, it is reasonable that E_{st} cannot be further improved if k_{eff} is over 7 W/(m·K).

4.4 Parameter of inlet velocity

As above, a design with a shorter *required heat transfer length* could obtain a higher E_{st}. According to Eq. (3-27) ~ (3-29), the *required heat transfer length* decreases with Re. Accordingly, when the inner tube diameter is fixed, the decrease in inlet velocity might improve E_{st} of a design. The inlet velocity of HTF was set as 0.2m/s, 0.1m/s and 0.05m/s in respective designs. As shown in Figure 4-5(b), decreasing the inlet velocity from 0.2 m/s to 0.1m/s or 0.2m/s could improve E_{st} from 0.59 to 1.84 or 3.92. Figure 4-6 presents the distribution of temperature in the HTF and liquid fraction in the PCM at the outlet temperature of 286K. With HTF at inlet velocity of 0.2m/s, the *required heat transfer length* for *CF* of 75% is much longer than the LHTES tube, and outlet temperature exceeds 286K before the melting front reaching outer tube. Thus, the effective *CF* for PCM is decreased to enable an effective heat transfer length identical to the tube length. With HTF at inlet velocity of 0.1m/s, although *required heat transfer length* for *CF* of 75% is still longer than

the LHTES tube, a higher effective *CF* is obtained and E_{st} is improved. A further decrease in inlet velocity from 0.1m/s to 0.05m/s finally makes a *required heat transfer length* shorter than the tube length, thus the melting front reaches the outer tube and a higher E_{st} is obtained.

To conclude, for designs with low thermal conductivity of PCM, using HTF at low inlet velocity could improve the effective storage capacity at the expense of lower discharging rate, while discharging energy at high rate would seriously damage the effective storage capacity, resulting in an LHTES system worse than an SWS system.

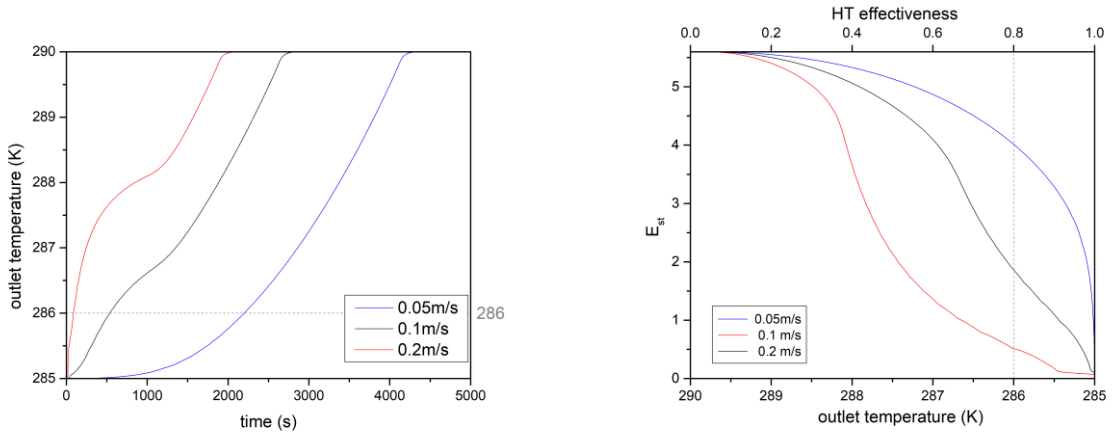

(a) (b)

Figure 4-5 The comparison of designs using different inlet velocities: a) the variation of outlet temperature over time, and b) the relationship between the effective energy storage ratio, E_{st}, and the outlet temperature (k_{eff} = 0.14 W/(m·K))

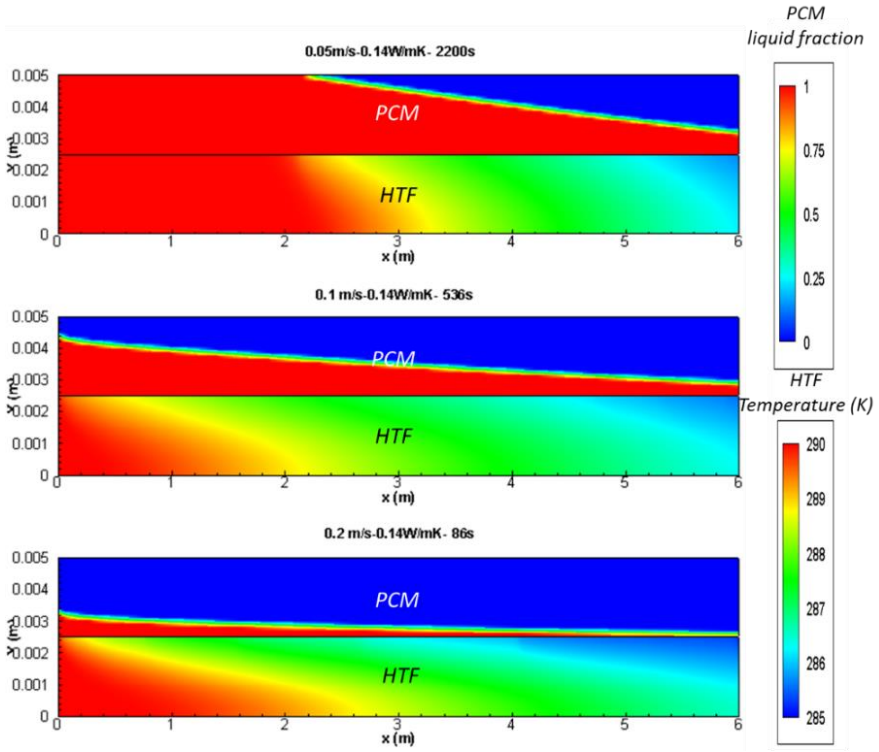

Figure 4-6 Distributions of temperature in the HTF and liquid fraction in the PCM at the instant when outlet temperature is about to exceed 286K after discharging, at three different inlet velocities (k_{eff} = 0.14 W/(m·K)) (The texts above contours describe the value of inlet velocity, k_{eff} and the local time)

4.5 Parameter of inner tube diameter

When inner tube diameter is changed, the value of inlet velocity could obey the rule of constant inlet velocity or constant mass flow rate. To avoid complex effect on *required heat transfer length*, *CF* for PCM is fixed in this comparison. According to Eq. (3-29), when inlet velocity is controlled, *required heat transfer length* increases with the inner tube diameter and Re; and when mass flow rate is controlled, the multiple of inner tube diameter and Re is fixed, thus the *required heat transfer length* is constant. The above prediction is verified in Figure 4-8. And on

the aspect of E_{st}, as shown in Figure 4-7, the increase in inner tube diameter has a negative effect on E_{st} under the condition of constant inlet velocity, while it has no effect on E_{st} when mass flow rate is fixed.

To conclude, it is the value of mass flow rate that determines the *required heat transfer length* and E_{st}. A smaller mass flow rate indicates a higher effective storage capacity and a lower discharging rate. Thus, inner tubes with small diameter and small inlet velocity are prerequisites in industrial application of LHTES, even though the discharging rate might be low.

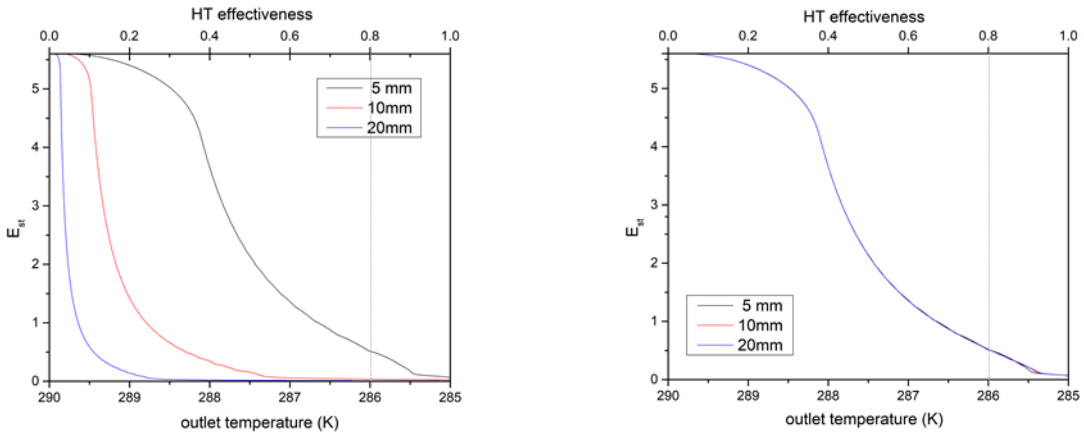

(a) (b)

Figure 4-7 The comparison of the relationships between the effective energy storage ratio, E_{st}, and the outlet temperature, at three different inner tube diameters, a) when inlet velocity is fixed, or b) when mass flow rate is fixed, (k_{eff} = 0.14 W/(m·K))

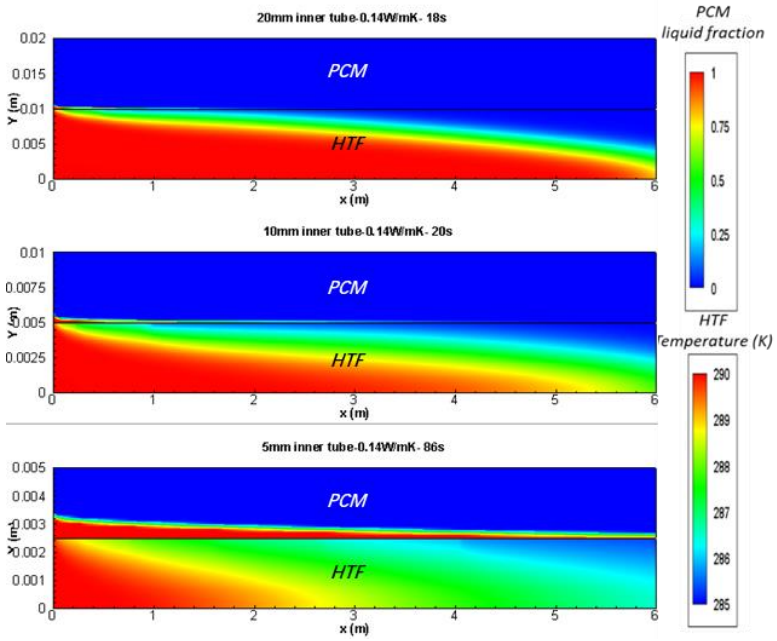

(a)

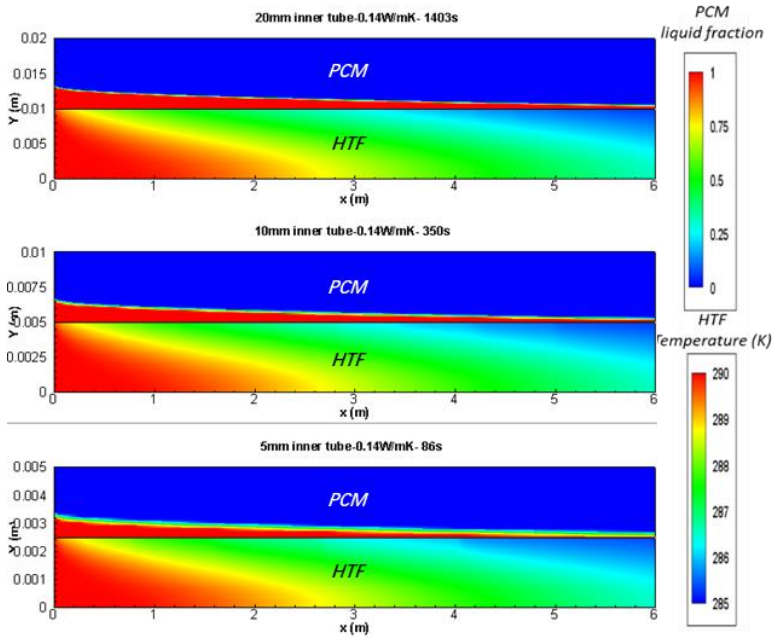

(b)

Figure 4-8 Distributions of temperature in the HTF and liquid fraction in the PCM at the instant when outlet temperature is about to exceed 286K after discharging, at three different inner tube diameters (k_{eff} = 0.14 W/(m·K)) a) when inlet velocity is fixed, or b) when mass flow rate is fixed. (The texts above contours describe the value of inner tube diameter, k_{eff} and the local time)

4.6 Parameter of tube length

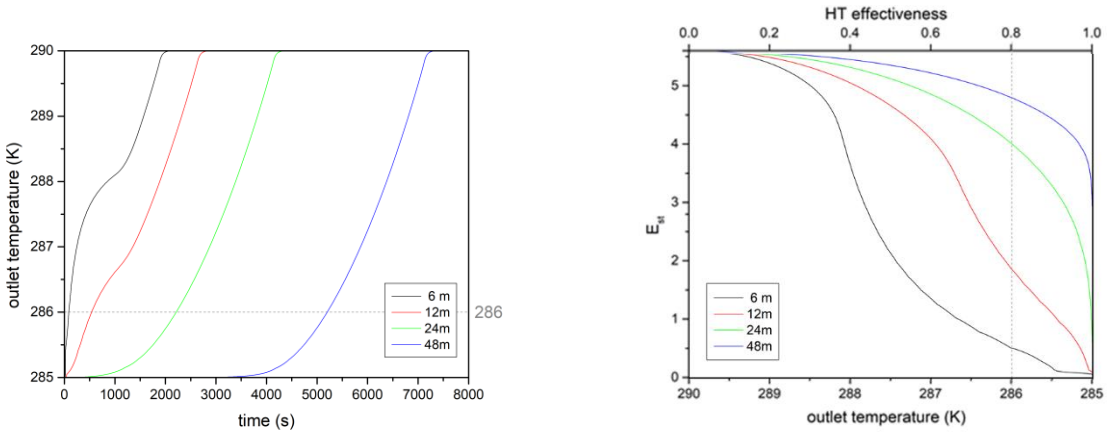

(a) (b)

Figure 4-9 The comparison of designs with different tube lengths: a) the variation of outlet temperature over time, and b) the relationship between the effective energy storage ratio, E_{st}, and the outlet temperature (k_{eff} = 0.14 W/(m·K))

Long tubes are also normally used in industry. According to Eq. (3-27) ~ (3-29), the tube length does not affect the *required heat transfer length*, but does affect the effective *CF* in operation. Designs with different tube lengths, including 6m, 12m, 24m and 48m, were compared. As shown in Figure 4-9(b), E_{st} increases with the increase in tube length. The *required heat transfer length* and the effective *CF* could be obtained from Figure 4-10. It is shown that the *required heat transfer length* for the design with *CF* of 75% is about 15m. Under the condition of short tubes, the effective *CF* increase with the increase in tube length, thus E_{st} is improved; Under the condition of long tubes, the *required heat transfer length* is invariant, and the improvement of E_{st} is due to the decrease in the ratio of the *required heat transfer length* to the total tube length.

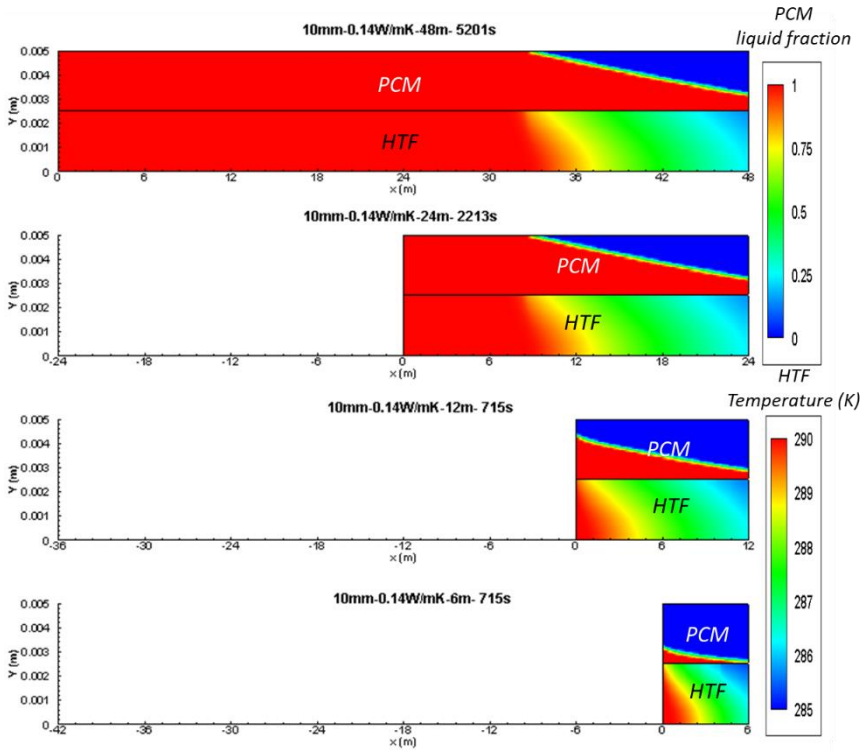

Figure 4-10 Distributions of temperature in the HTF and liquid fraction in the PCM at the instant when outlet temperature is about to exceed 286K after discharging, at four different tube lengths (k_{eff} = 0.14 W/(m·K)). (The texts above contours describe the value of outer tube diameter, k_{eff} and the local time)

The increase in tube length from 6m to 48m could improve E_{st} from 0.59 to 4.81. Ideally, with superconduction in PCM and high convection heat transfer in the tube, the *required heat transfer length* could be extremely short in comparison with tube length and almost all the PCM could be melted at outlet temperature of 286K. Under such a condition, the warm fluid can be immediately cooled down to the PCM temperature, once it flows into the tube, and the PCM will almost melt layer by layer from the beginning to the end of the tube.

4.7 Parameter of compactness factor for PCM

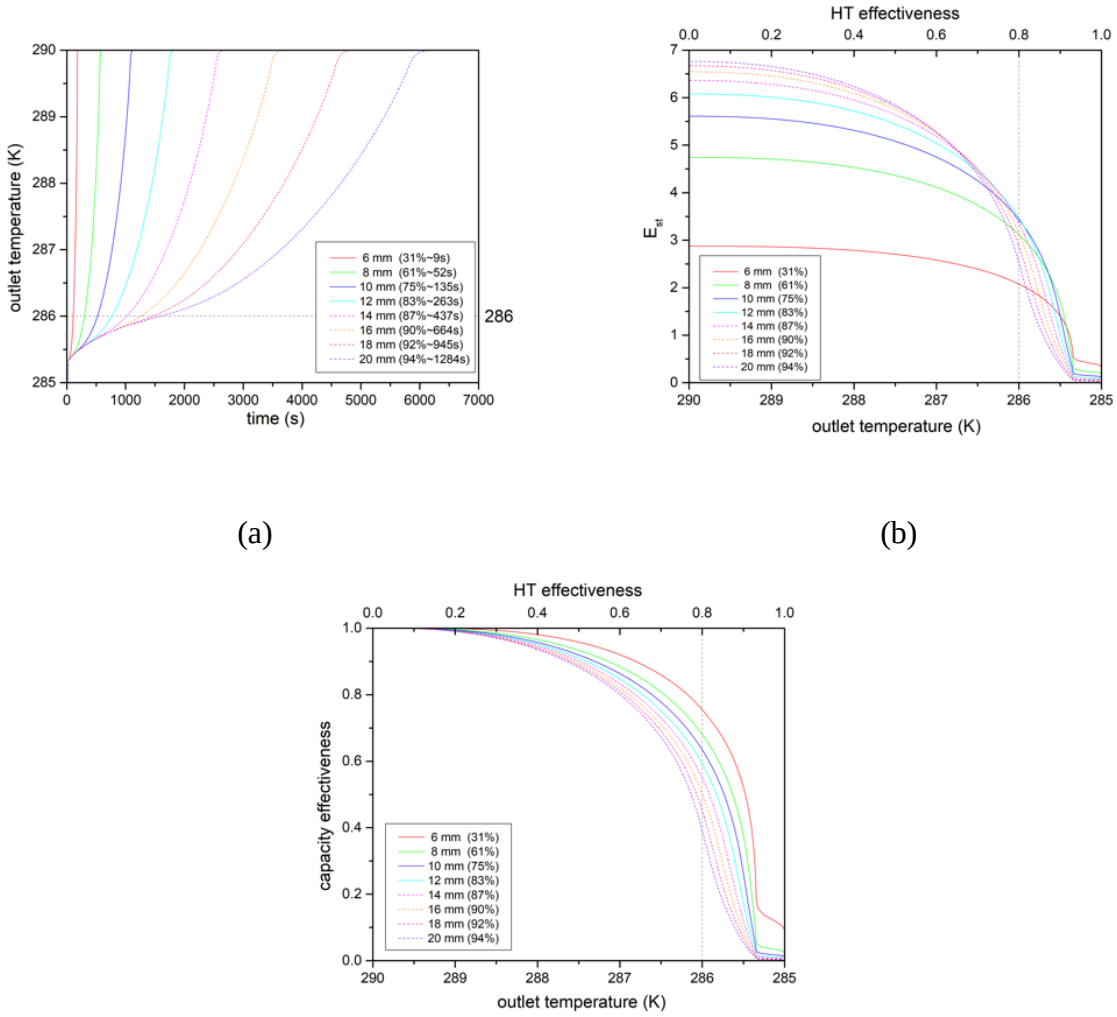

Figure 4-11 The comparison of designs with different compactness factor for PCM: a) the variation of outlet temperature over time, b) the relationship between the effective energy storage ratio, E_{st} and the outlet temperature, and c) the relationship between the capacity effectiveness, and the outlet temperature (k_{eff} = 1.4 W/(m·K)), where the legend describes the outer tube diameter, CF values and the time duration after which the melting front reaches the outer tube.

Designs with different *CF* s for PCM (k_{eff} = 1.4 W/(m·K)) were compared. According to Eq. (3-27), a larger *CF* brings about a larger thermal resistance in PCM, thus the *required heat transfer length* is longer. If the *required heat transfer length* is shorter than the tube length, the increase in *CF* could improve E_{st}; or else, the effective *CF* is invariant and determined by the tube length. Figure 4-11 and Figure 4-12 well verify the above prediction. As *CF* increases, the effective energy storage capacity increases, while the capacity effectiveness decreases. E_{st} is a synthesis of an increased effective energy storage capacity and a decreased capacity effectiveness. Thus, there is a maximum E_{st} corresponding to an optimum *CF* for PCM. At k_{eff} = 1.4 W/(m·K), the design with the 12mm outer tube, corresponding to a *CF* of 83%, is optimal, at which an E_{st} of 3.46 is obtained, indicating that the effective energy storage capacity can reach 3.46 times of that of an ideal SWS system.

To conclude, an optimum *CF* exists, at which a maximum E_{st} can be obtained. The optimization of an LHTES system is to find the optimum *CF* for any HTF and any PCM to achieve a maximum E_{st}.

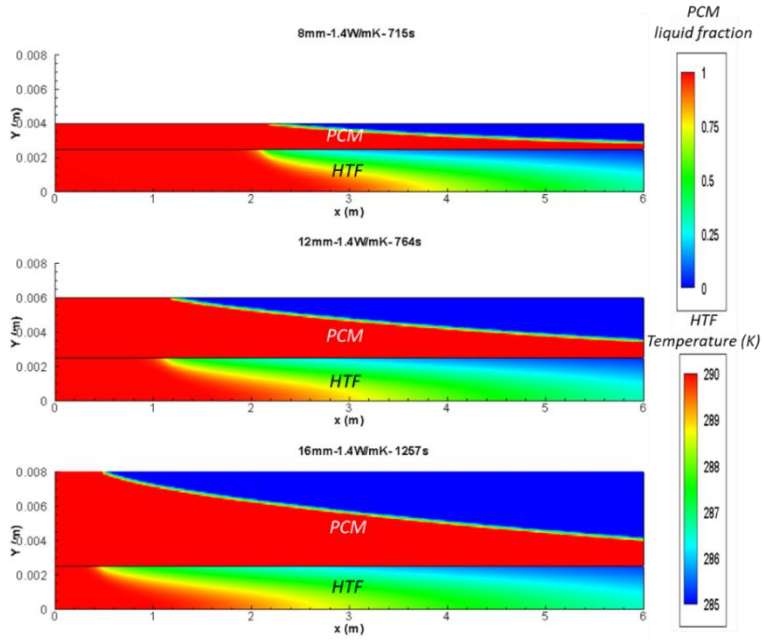

Figure 4-12 Distributions of temperature in the HTF and liquid fraction in the PCM at the instant when outlet temperature is about to exceed 286K after discharging, at three different compactness factors for PCM, (k_{eff} = 1.4 W/(m·K)). (The texts above contours describe the value of outer tube diameter, k_{eff} and the local time)

4.8 Summary

This Chapter characterized the basic unit of a tube-in-tank LHTES system by the index of effective energy storage ratio, E_{st}, and analyzed the effects of parameters on E_{st} and *required heat transfer length*. The results show that the designs with a shorter *required heat transfer length* usually present a higher E_{st}. Several guidelines on the system optimization could be obtained as follows.

-A shorter *required heat transfer length* and a higher E_{st} could be obtained by enhancing heat transfer in PCM or lowering down the mass flow rate of the HTF by decreasing inlet velocity and inner tube diameter.

-Although the tube length has no effect on *required heat transfer length*, a longer tube could improve the effective *CF* or the ratio of tube length to *required heat transfer length*. Thus, E_{st} could be improved by lengthening tube.

-Most importantly, there is an optimal design with an optimum *CF* for PCM to achieve the maximum E_{st}.

To conclude, the optimization of an LHTES system is to find the optimum *CF* for designs with any HTF and any PCM to achieve a maximum E_{st}.

Chapter 5 The optimal designs for LHTES systems

5.1 Introduction

The previous Chapter characterized the basic unit of a tube-in-tank LHTES system by the index of effective energy storage ratio, E_{st}, and analyzed the effects of parameters on E_{st}. It was shown that enhancing heat transfer in PCM, lowering down the mass flow rate of the HTF or lengthening the tube length could improve E_{st} of a design; And there is an optimum *CF* to achieve the maximum E_{st} for a design with any HTF and any PCM. In this Chapter, the analytical technique derived from effectiveness-NTU theory would be firstly validated by the numerical results in Chapter 4, and then used to predict the optimal designs for the basic unit of tube-in-tank LHTES systems. The effects of prementioned parameters on the optimal designs would be tested, and the variation of the optimum *CF* and maximum E_{st} over the tested parameters would be analyzed. It is aimed to demonstrate whether maximum E_{st} could be improved by enhancing heat transfer in HTF and PCM, and whether there is an upper limit for the maximum E_{st}. This analysis would provide quantitative guidelines on the optimal designs for tube-in-tank LHTES system.

5.2 The optimal design for an LHTES system

The optimization of an LHTES system is to find the optimum *CF* for the HTF and the PCM. Figure 5-1 summarizes the variations of E_{st} over *CF* for PCM at three k_{eff} values. At k_{eff} = 0.14 W/(m·K), the optimum *CF* and maximum E_{st} are 31% and 1.57; at k_{eff} = 1.4 W/(m·K), 83% and 3.46; and at k_{eff} = 7 W/(m·K), 96% and 4.40, respectively. With an increase in effective thermal conductivity of PCM, the optimum *CF* increases from 31% to 96%, and the maximum E_{st} increases

from 1.57 to 4.40. At k_{eff} = 7 W/(m·K), the effective energy storage capacity of the LHTES system can reach 4.4 times of that of an ideal SWS system.

Note that the solid curves in Figure 5-1 are drawn according to the predictions by the proposed analytical technique and the scattered points according to the numerical results. As shown, the analytical technique proposed in Chapter 3 could well predict E_{st} of any design and is effective in optimizing tube-in-tank LHTES systems. In the following sections, the effects of various parameters on the optimal design would be analyzed with the assistance of the proposed analytical technique.

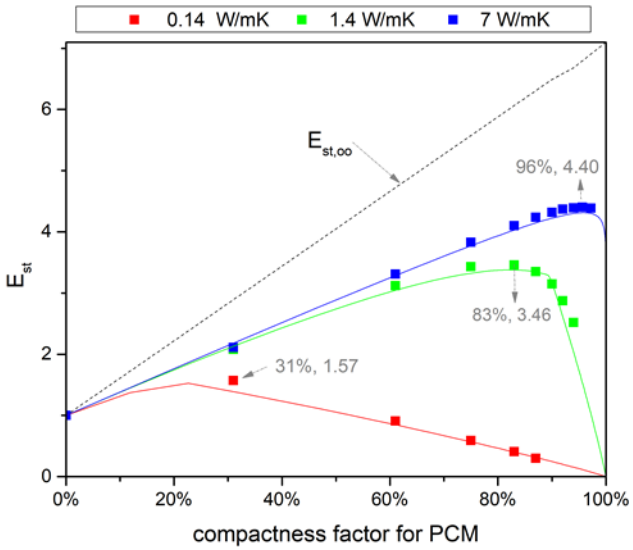

Figure 5-1 The variation of the theoretical and effective energy storage ratios, $E_{st,\infty}$ and E_{st}, over the compactness factor (CF) for PCM at three different effective thermal conductivities, k_{eff}, where solid curves represent analytical predictions and scattered points the numerical results

5.3 Effect of heat transfer enhancement in PCM

As mentioned, an increase in effective thermal conductivity of PCM could improve maximum E_{st} of an optimal design. Figure 5-2 presents the variation of maximum E_{st} over effective thermal conductivity of PCM, k_{eff}, based on analytical predictions. At low k_{eff}, the optimum *CF* for PCM is low, resulting in a low maximum E_{st} of an optimal design, however, with the increase in k_{eff}, the optimum *CF* and maximum E_{st} increases and finally approaches its upper limit. This could be explained in the analysis of *required heat transfer length*. A higher *CF* brings a larger thermal resistance, while a higher k_{eff} neutralizes the effect of a higher *CF* on the thermal resistance. As a result, *required heat transfer length*, l_p, decreases with the increase in k_{eff} and is gradually approaching the *ideal required heat transfer length*, l_w. Accordingly, the upper limits for maximum E_{st} and capacity effectiveness are determine by ratio of l_w to tube length, which are 4.85 and 67.9%, respectively. However, once l_p approaches 115% of l_w, the variation of maximum E_{st} over k_{eff} is slow; Thus, it is reasonable to regard the value of k_{eff} as the optimum. For the HTF with Re of 1000 in this section, the optimum k_{eff} is 8.5 W/(m·K) to obtain l_p of 4.40 m, optimum *CF* of 96.6%, capacity effectiveness of 63.3% and maximum E_{st} of 4.38.

To conclude, enhancing heat transfer in PCM could effectively shorten l_p and improve the optimum *CF* for PCM to obtain a higher maximum E_{st}. However, there are upper limits for E_{st} and capacity effectiveness, which are determined by the ratio of l_w to tube length. Thus, it is of great significance to analyze the effects of operating condition in HTF and tube length on the optimal designs.

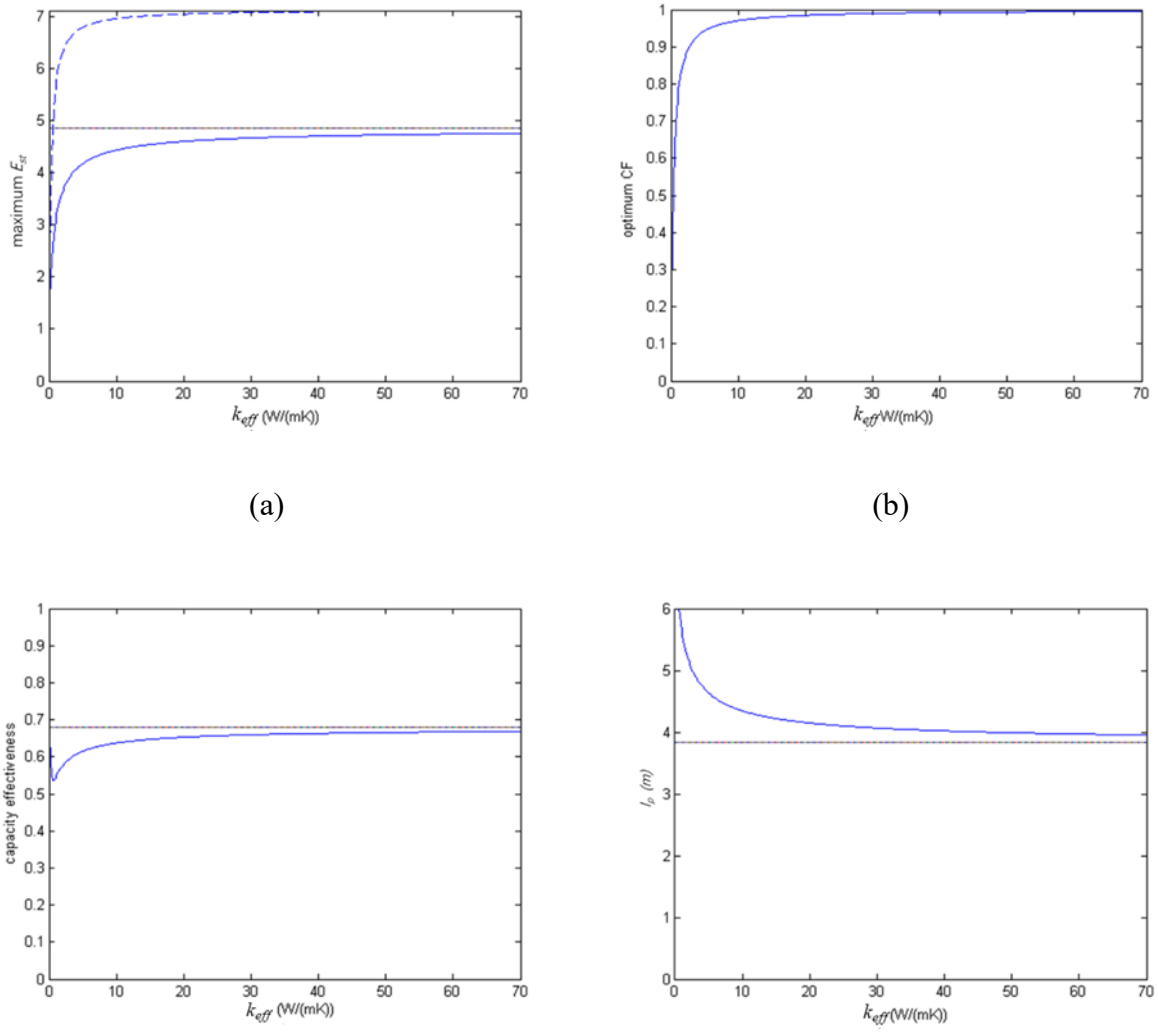

(a) (b)

(c) (d)

Figure 5-2 The comparison of optimal designs for PCM at different effective thermal conductivities, k_{eff}: a)the variation of maximum E_{st}, where the dashed curve represents the value of $E_{st,\infty}$, and dotted curve the upper limit for maximum E_{st}; b)the variation of optimum CF for PCM; c) the variation of capacity effectiveness, where the dotted curve represents the upper limit; d) the variation of l_p, where the dotted curve represents the value of l_w

5.4 Effect of inlet velocity

As indicated, the upper limits for E_{st} and capacity effectiveness in designs using PCM at high effective thermal conductivities are determined by the ratio of tube length to l_w. The increase in either inner tube diameter or inlet velocity could improve the mass flow rate and Re Number in Eq. (3-29) and thus results in a longer l_w. However, when Re Number exceeds the threshold for laminar flow, Nu Number could be also improved. The turbulence in HTF enhances the heat transfer and decreases the thermal resistance. As shown in Figure 5-3(d), l_w for turbulent HTF is about two-meter long, while that for laminar HTF varies linearly with the increase in mass flow rate and could be longer than six meters. Accordingly, the heat transfer enhancement in HTF is of great significance to improve the LHTES performance, and the parameters of inlet velocity and inner tube diameter should be optimized.

Figure 5-3, Figure 5-4 and Figure 5-5 present the effect of inlet velocity on the optimal designs. At low inlet velocity, HTF is in the laminar region and has an invariant low Nu, thus, l_w increases with inlet velocity; At high inlet velocity, HTF is in turbulent region and the ratio of Re to Nu is almost one, thus, l_w is short and almost invariant. However, the increase in Nu Number largely decrease the thermal resistance in HTF and causes a larger thermal resistance ratio of PCM to HTF. As a result, l_p is far longer than l_w and E_{st} is approaching one when PCM is at low k_{eff}. However, with the increase in k_{eff}, l_p could be decreased, and a higher CF and E_{st} could be obtained. As mentioned, the upper limits of capacity effectiveness for Re of 1000 is 63%, since the design uses laminar HTF; Here, using turbulent HTF and PCM at optimum k_{eff}, a capacity effectiveness of 80% could be obtained, although the optimum k_{eff}, as shown in Figure 5-4, could hardly be achieved. Even though the optimum k_{eff} for turbulent HTF is far from reality, using PCM at achievable k_{eff}, such as 7 W/(m·K), could also achieve high CF and high E_{st}. As shown in Figure

5-3, using HTF with RE of 5000 to 15,000 could all achieve an E_{st} over three, which is competitive to the performance of designs using HTF in laminar region. Hence, the heat transfer enhancement in PCM could enable the use of turbulent HTF and largely improve the discharging rate as well as effective storage capacity.

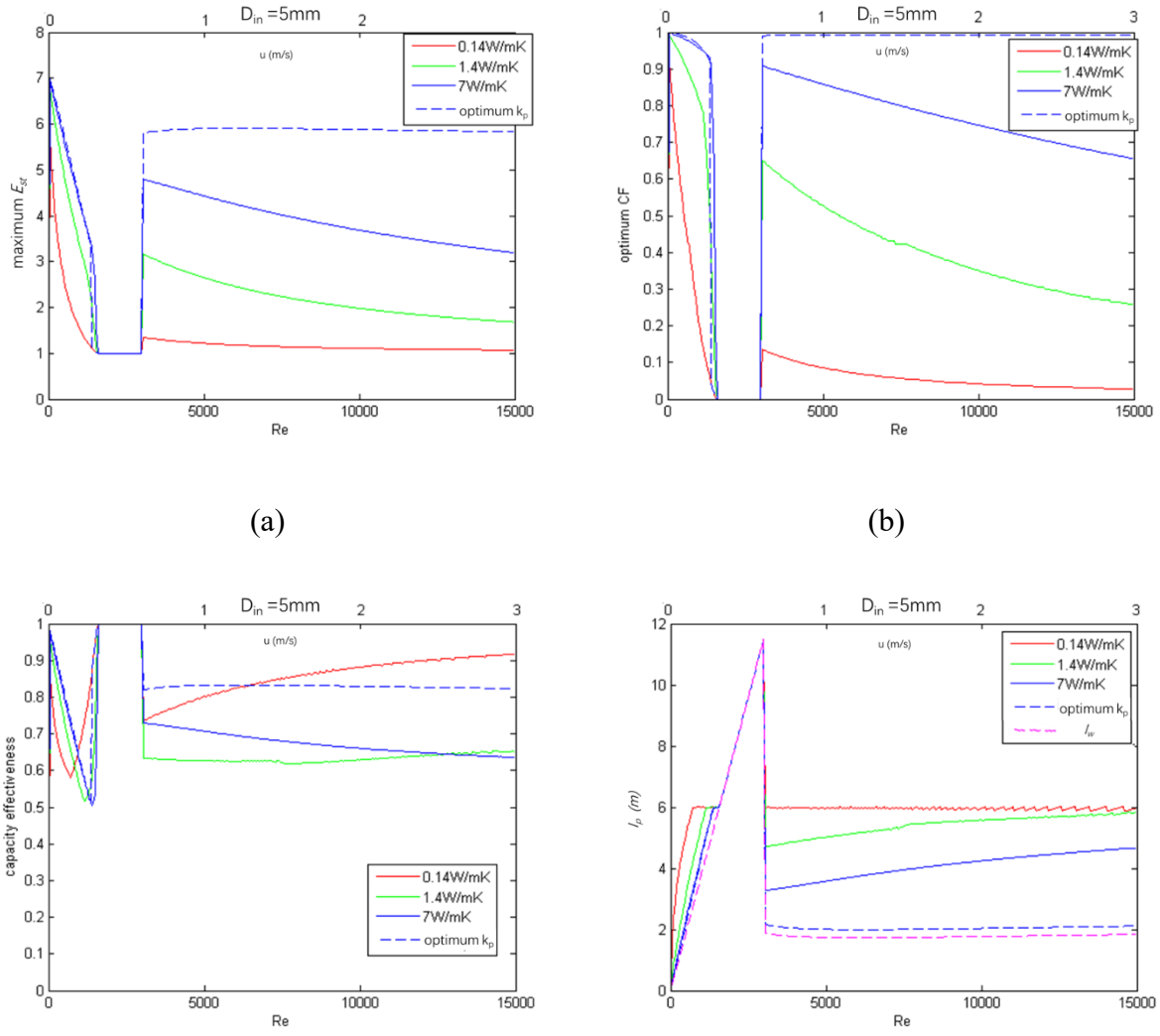

Figure 5-3 The comparison of optimal designs for HTF at different inlet velocities (Re): a) the variation of maximum E_{st}; b) the variation of optimum CF for PCM; c) the variation of capacity effectiveness; d) the variation of l_p

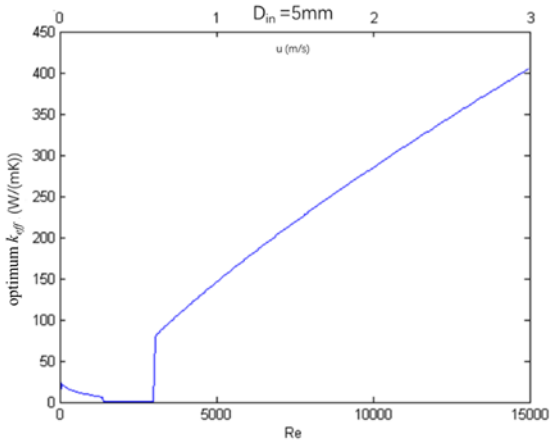

Figure 5-4 The variation of optimum k_{eff} for the optimal designs over inlet velocity (Re)

From the perspective of power consumption, the increase in Re from 0 to 15,000 would largely reduce the discharging COP from tens of thousands to tens, although a discharging COP of 100 is still very high. From the perspective of material, since the inner tube diameter is fixed, the total area of tube material is fixed. There are more tubes operating in parallel for low Re to meet the demand of discharging rate, and more tubes operating in serial for high Re to meet the demand of total discharging capacity. Thus, there is no additional material benefit in using a higher inlet velocity.

To conclude, it is possible to use HTF in turbulent region to obtain optimal design with high E_{st}, when there is adequate heat transfer enhancement in PCM. Note that there is a sudden drop and a sudden climb in the curves in this section. This accounts for the discontinuity between the Nu correlations for laminar flow and for turbulent flow. Further experimental work might fill in the gap and provide more detailed information in using low-Re HTF in LHTES systems.

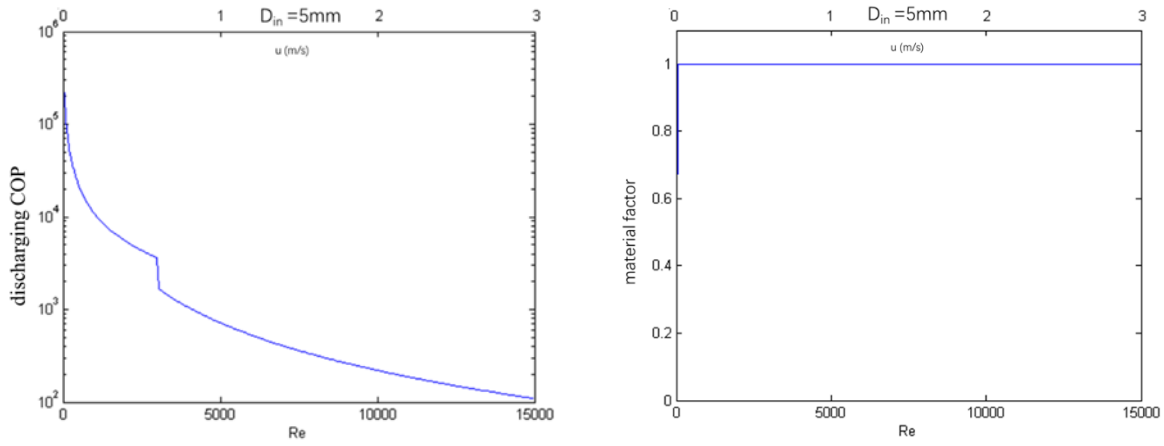

(a) (b)

Figure 5-5 The variation of a) discharging COP and b) material factor for the optimal designs over inlet velocity (Re)

5.5 Effect of inner tube diameter

As mentioned, the increase in inlet velocity could increase Nu and decrease the thermal resistance in HTF. When inlet velocity is fixed, the increase in inner tube diameter could have the similar effect. In this section, the tube is 100 m in length and the inlet velocity is fixed at 0.2m/s. As shown in Figure 5-6, the effect of heat transfer enhancement in HTF driven by a larger inner tube diameter is similar to that driven by a larger inlet velocity. The optimum *CF* and E_{st} for PCM decreases over Re in laminar region and turbulent region, respectively, while there is a sudden increase between the two regions. Accordingly, there might a peak of E_{st} for HTF in low-Re region.

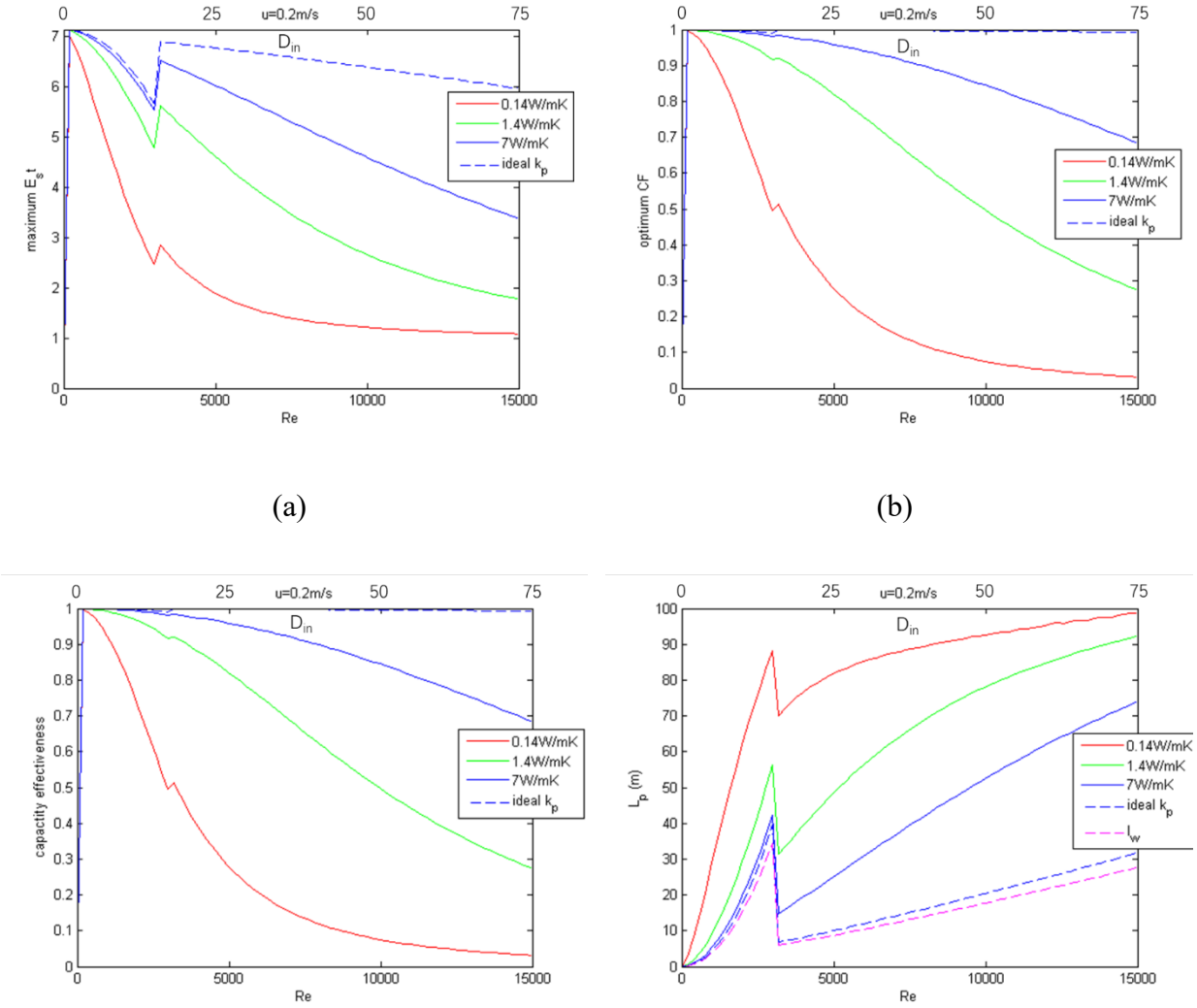

Figure 5-6 The comparison of optimal designs for HTF at different inner tube diameters (Re): a) the variation of maximum E_{st}; b) the variation of optimum CF for PCM; c) the variation of capacity effectiveness; d) the variation of l_p, where the dashed curve represents the value of l_w

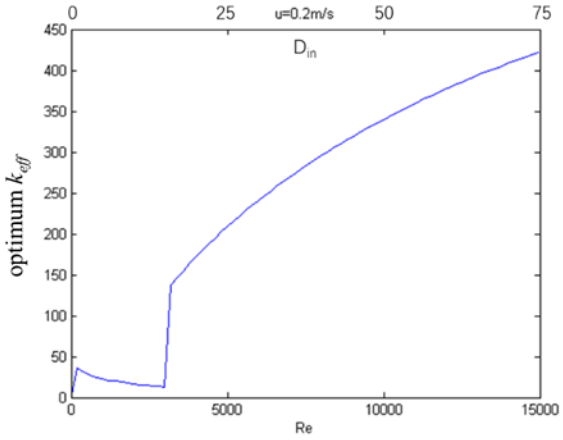

Figure 5-7 The variation of optimum k_{eff} for the optimal designs over inner tube diameter (Re)

Different conclusions could be drawn from aspects of power consumption and material cost. As shown in Figure 5-8, the increase of Re from 0 to 15,000 would largely increase the discharging COP due to the increase of inner tube diameter and the decrease in pressure drop. Moreover, the material factor decreases inversely over the increase in the inner tube diameter. The reason is easy to understand. When the inner tube diameter of a design is increased by N times, the area of an inner tube increases by N times and the total storage capacity of the design would increase by N^2 times. As a result, the inner tube with larger diameter has a smaller surface area and cost less material. If heat transfer in PCM is well enhanced, it is possible for LHTES to use inner tube with large diameters for both a high E_{st} and a high discharging COP.

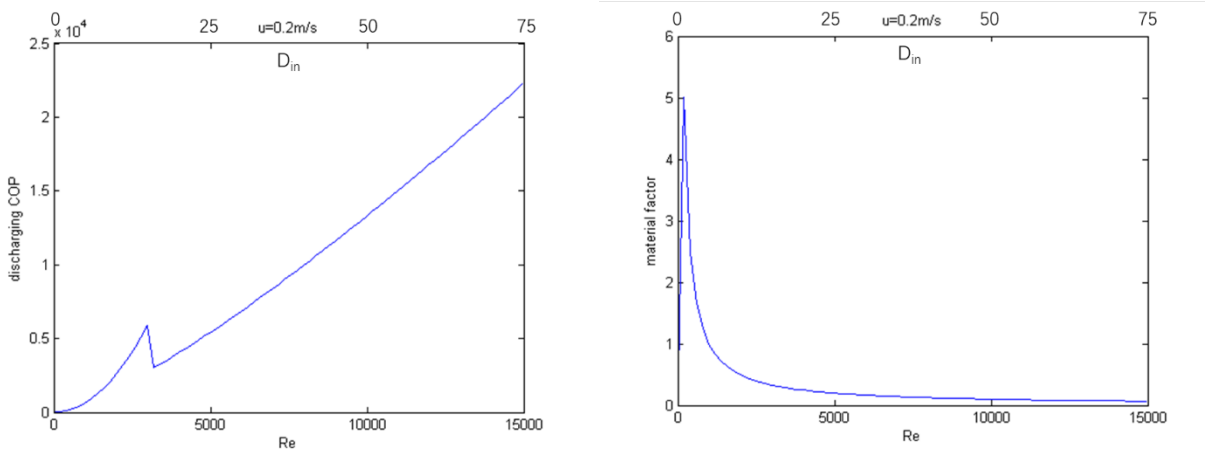

(a) (b)

Figure 5-8 The variation of a) discharging COP and b) material factor for the optimal designs over inner tube diameter (Re)

5.6 Effect of tube length

Figure 5-9 presents the effect of tube length on optimal designs. According to Eq. (3-27), l_p is independent of the value of tube length. However, for PCM at low $k_{eff,}$ a longer tube could accommodate a longer l_p, bringing in a higher optimum *CF* and a higher E_{st}; for PCM at high $k_{eff,}$ a longer tube could enlarge the ratio of tube length to l_p, thus achieve a higher capacity effectiveness and an E_{st} approaching $E_{st,\infty}$. As shown in Figure 5-8, the increase in tube length from 6 m to 150 m could improve the optimum *CF* for PCM at 0.14 W/(m·K) from 30% to over 90%, and the maximum E_{st} from below two to about six. However, at the same tube length, the design with a shorter l_p still has a higher E_{st}. Therefore, tube length should be optimized after the optimization of HTF and k_{eff}. The optimization of tube length aims at further improving the capacity effectiveness and E_{st} at the expense of pump power.

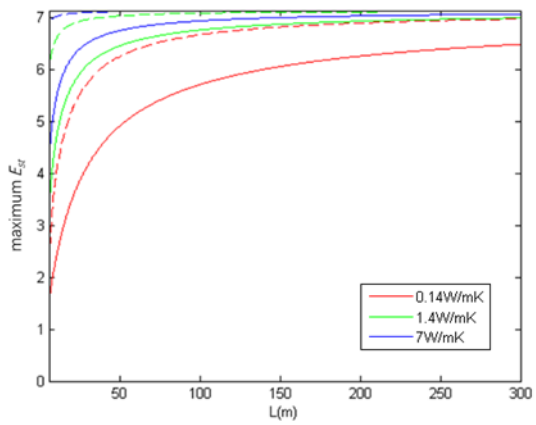

(a)

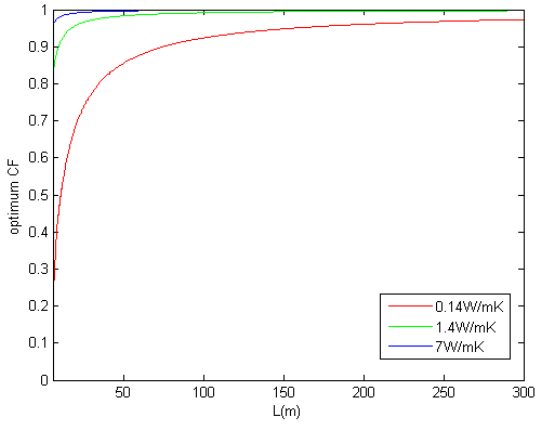

(b)

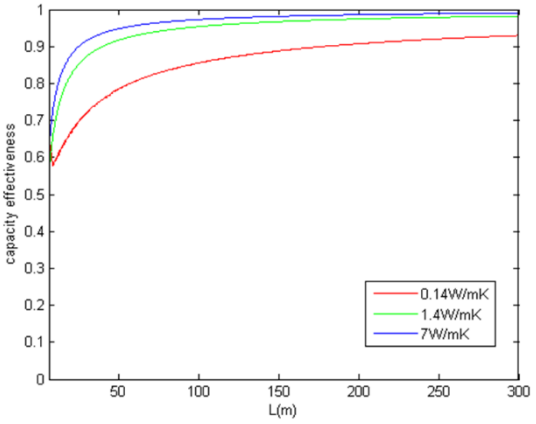

(c)

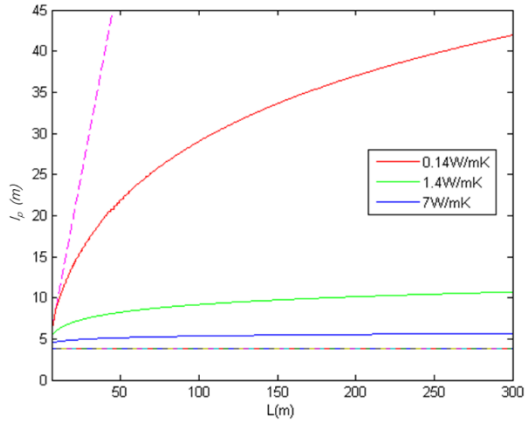

(d)

Figure 5-9 The comparison of optimal designs for tubes with different lengths: a) the variation of maximum E_{st}, where the dashed curve represents the value of $E_{st,\infty}$; b) the variation of optimum CF for PCM; c) the variation of capacity effectiveness; d) the variation of l_p, where the dotted curve represents the value of l_w, and the dashed curve the tube length

5.7 Summary

This Chapter revealed the effect of operating parameters on the optimal design for an LHTES system. The analytical technique of *required heat transfer length* was first validated and then used to predict the optimal design under different parameters. The following could be obtained.

- Enhancing heat transfer in PCM could effectively shorten l_p and improve the optimum *CF* for PCM to obtain a higher maximum E_{st}. However, when the effective thermal conductivity of PCM is above a certain threshold, *CF* and E_{st} approaches their upper limits, which are determined by the ratio of l_w to tube length. It is demonstrated that a decrease in l_w or increase in tube length could break the upper limits and further improve the system performance.

- By enhancing heat convection in HTF, the total thermal resistance could be further decreased. A high-degree heat transfer enhancement in PCM enables the use of turbulent HTF to obtain high *CF* and high E_{st}. The improvement of heat transfer enhancement in PCM could largely improve the discharging rate and effective storage capacity, and effectively reduce the material consumption of an LHTES system.

- After the heat transfer condition in HTF and PCM is optimized, tube length should be finally optimized. It is aimed to further improve the capacity effectiveness and approaches $E_{st,\infty}$ at the expense of pump power**.**

Chapter 6 Effect of charging parameters on discharging

6.1 Introduction

In previous Chapters, the index of effective energy storage ratio, E_{st}, and the analytical technique of *required heat transfer length* were used to find the optimal design for the basic unit of a tube-in-tank LHTES system. However, the optimization only considered the parameters in a discharging process. Since not all the thermal energy in PCM could be discharged from the system at the end of a discharging process, a charging process would be initiated in the system with the existence of an initial dead zone. This Chapter uses the numerical method in Chapter 3 to calculate the charging process of an LHTES system with an initial dead zone. By analysing the numerical results, the effect of charging parameters, including flow direction, flow velocity and flow temperature, on the power consumption in a charging process and E_{st} in a subsequent discharging process would be addressed. The analysis provides a complete understanding of the optimal designs for tube-in-tank LHTES systems.

6.2 The existence of initial dead zone

An LHTES system provides chilled water to air conditioning during a discharging process and consumes chilled water from water chillers during the charging process. During the discharging process, HTF is cooled down by the stored PCM, when flowing from tube inlet to tube outlet. The PCM near tube inlet always melts faster than that near the tube outlet, and the melting front is never parallel to the tube. For the optimal design with PCM at k_{eff} = 1.4 W/(m·K), an E_{st} of 3.46 could be obtained, but 43% of PCM was still at solid status when HTF was at the outlet temperature of 286K. Figure 6-1 presents the location of melting front when HTF was at outlet

temperature of 286K. Since the thermal energy in solid PCM could not be discharged, this bowl-shaped region with an inclined internal surface is called a dead zone for the discharging process. A subsequent charging process would be initiated with the existence of dead zone in the system.

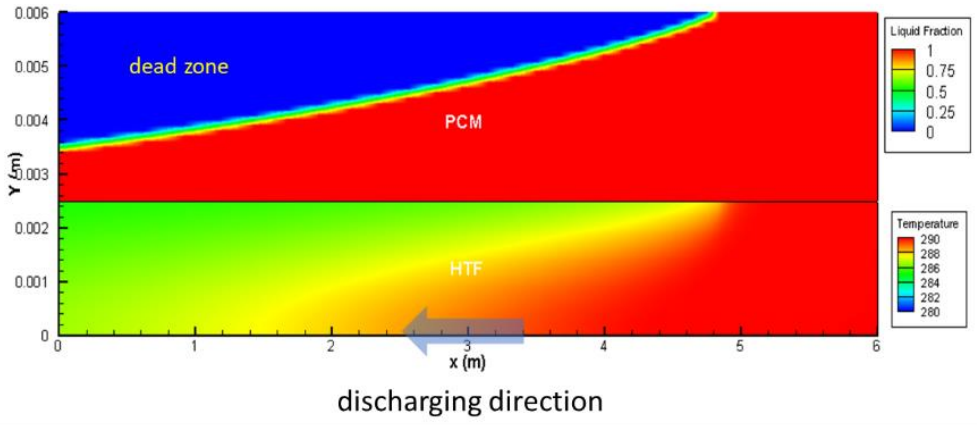

Figure 6-1 The distributions of temperature in the HTF and liquid fraction in the PCM at the instant when outlet temperature is about to exceed 286K after discharging in the optimal design for the default HTF and PCM at k_{eff} = 1.4 W/(m·K) (discharging HTF: 290K, 0.2m/s)

6.3 The parameter of charging direction

There are two potential flow directions for a charging process, i.e. parallel direction and counter direction. For parallel charging, the charging HTF flows from the discharging inlet to the discharging outlet; for counter charging, the charging HTF from the discharging outlet to the discharging inlet. The comparison between parallel charging and counter charging was conducted under the condition of the identical temperature difference between HTF and PCM and identical flow rate to that in a discharging process. To this end, the charging HTF of 280K flows into the system at a velocity of 0.2m/s. Figure 6-2 describes the variation of enthalpy, liquid fraction and outlet temperature of the system over the charging process.

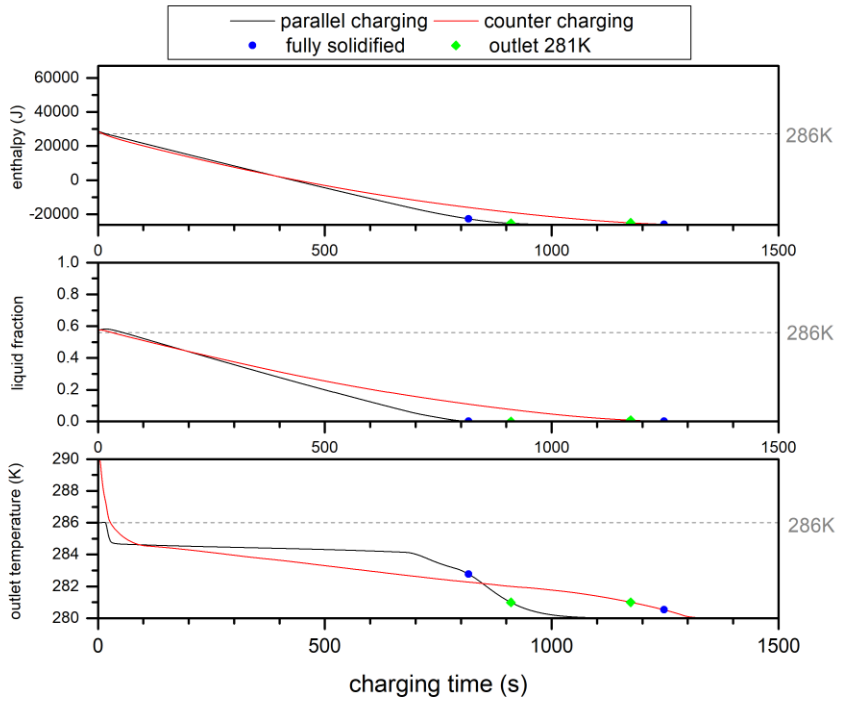

Figure 6-2 The variations of enthalpy, liquid fraction and outlet temperature over the charging process in the system with the initial condition as described in Figure 6-1. (charging HTF: 280K, 0.2m/s)

According to Figure 6-2, parallel charging is more effective to charge an LHTES system with an initial dead zone. For parallel charging, the solidification of PCM finishes at 817s; However, counter charging, PCM is not fully solidified until 1248s. Moreover, it takes around 1100s to fully charge the system to 280K in parallel charging, but over 1300s in counter charging. As shown, the rate of solidification in counter charging slows down over the charging process, but that in parallel charging almost remains constant. The reason for this phenomenon can be explained using Figure 6-3.

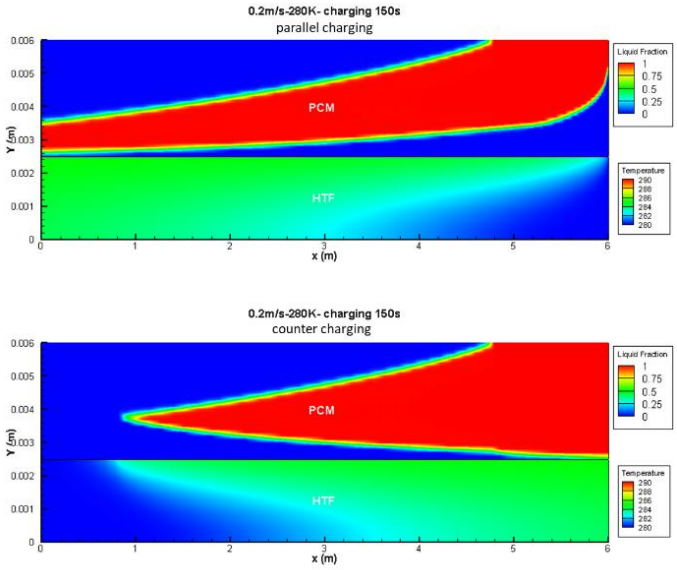

(a)

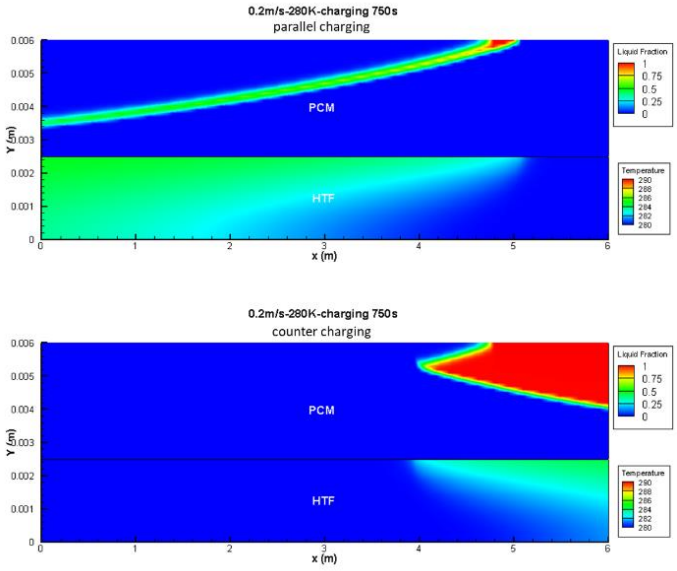

(b)

Figure 6-3 The distributions of temperature in the HTF and liquid fraction in the PCM at a) 150s and b) 750s, when parallel charging or counter charging is conducted in the system with the initial dead zone as described in Figure 6-1

As presented in Figure 6-3, the performance difference between parallel charging and counter charging lies in the existence of the initial dead zone. In a charging process, HTF acts as a heat sink for PCM and the solidification interface of PCM as the heat source for HTF. Once solidified zone fuses with the dead zone, the corresponding tube area, where fusion occurs, will lose its heat transfer effectiveness. In Figure 6-3, the fusion in counter charging starts as early as 150s, but that does not occur until the end of the parallel charging. Figure 6-4 depicts the variation of effective heat transfer length by monitoring the length of the tube with a surface temperature over 281K. As shown, the effective heat transfer length in counter charging decreases from the beginning to the end and that in parallel charging keeps at a high value before the completion of solidification. Thus, it is reasonable that parallel charging has a higher efficiency.

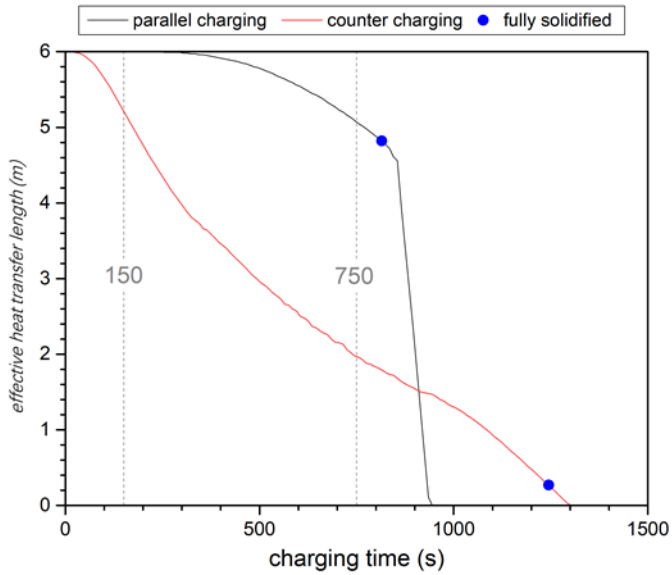

Figure 6-4 The variation of the effective heat transfer length over parallel charging and counter charging (charging HTF: 280K, 0.2m/s)

Figure 6-5 describes the variation of enthalpy over continuous discharging and charging process. In this comparison, the switches between discharging process and charging process are determined by the value of outlet temperature. For a discharging process, the outlet temperature of 286K indicates the end of discharging. In parallel, the outlet temperature of 281K could be the indicator for charging process, since enthalpy approaches the lower limit when outlet temperature reaches 281K in Figure 6-2. As shown in Figure 6-5, when the system is operating under the above rule, counter charging is still 29% slower than parallel charging in charging period, while the capacity effectiveness is not affected by the direction of charging flow.

.

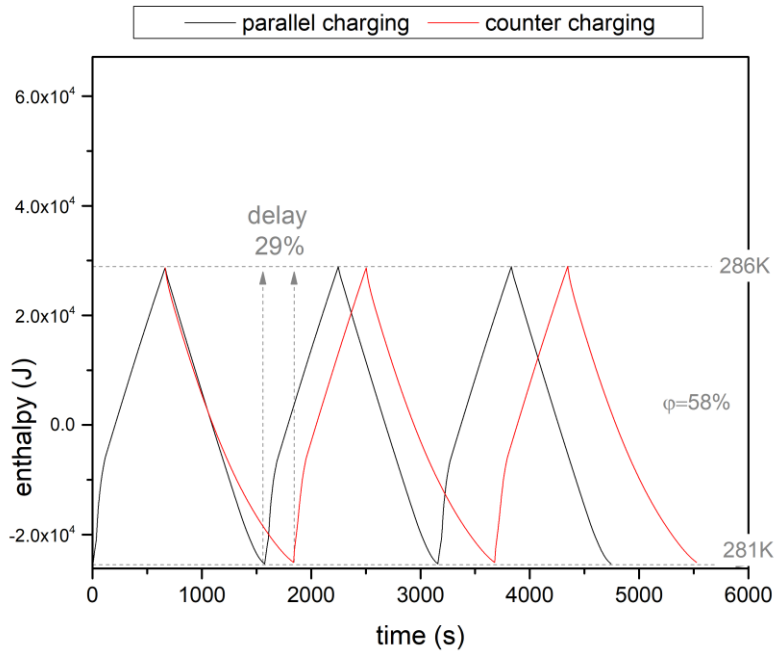

Figure 6-5 The variation of enthalpy over continuous discharging and charging process.

(discharging HTF: 290K, 0.2m/s; charging HTF: 280K, 0.2m/s)

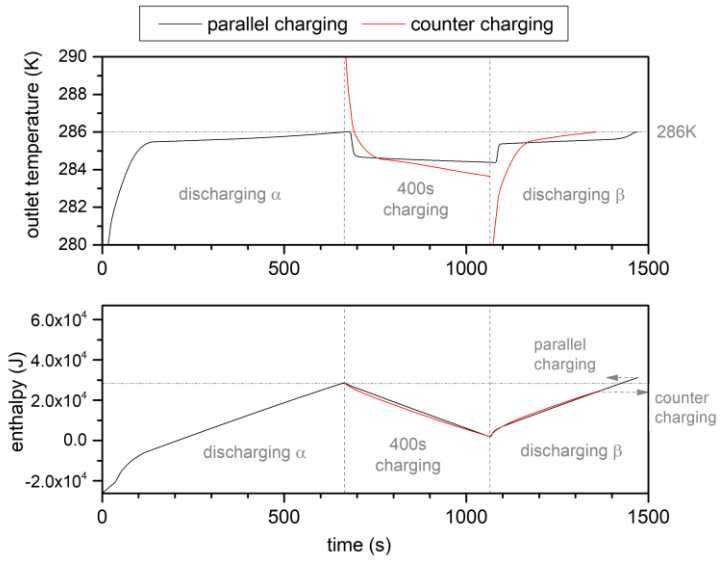

(a)

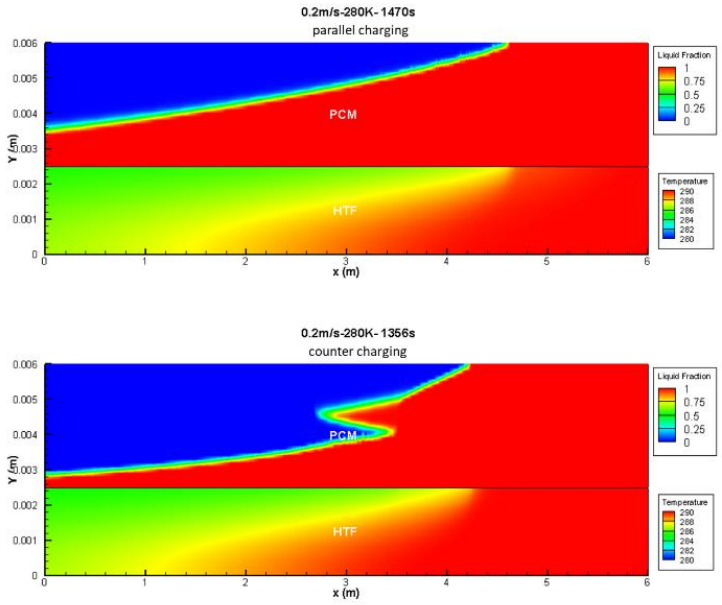

(b)

Figure 6-6 The comparison between discharging performance after an incomplete parallel charging and that after an incomplete counter charging: a) the variations of outlet temperature and enthalpy over time b) the distributions of temperature in the HTF and liquid fraction in the PCM after discharging (The texts above the contour describe the value of inlet velocity and inlet temperature of HTF in charging process and the local time in the continuous discharging and charging process)

However, an incomplete charging might damage the subsequent discharging performance. Figure 6-6 compares the discharging performance of the system after 400s of parallel charging and that of counter charging. After an incomplete counter charging, the dischargeable thermal energy in discharging process is even lower than the charged thermal energy in the previous charging process, leaving a larger dead zone in the system. On the contrary, all the energy charged during an incomplete parallel charging is dischargeable in the subsequent discharging process, and the region of dead zone is not affected. Thus, a complete charging is a demand for counter charging to avoid damaging system performance in discharging process, but parallel charging does not have such a requisite.

To conclude, parallel charging is a better choice for a system with an initial dead zone, since it is more efficient and has no negative effect on the subsequent discharging process.

6.4 The parameter of charging velocity

For an LHTES system with an initial dead zone, charging the system with HTF at a higher velocity can speed up the solidification of PCM at the expense of increased power consumption, which is in agreement with the conclusion under the condition without dead zone. Although parallel charging is still more effective than counter charging, the dead zone effect occurs when the system charges with an HTF at a different velocity from that in discharging process. As shown in Figure 6-7, the solidification curve of parallel charging and that of no-dead-zone charging overlap when the charging flow is at 0.2m/s, but the two curves deviate from each other when the charging flow is at 0.1m/s or 0.4m/s. Charging the system by an HTF at a different velocity destroys the parallel profiles of the solidified zone and that of the dead zone, which advances the fusion between the zones. However, this effect on charging rate could be neglected when compared with the effect of flow velocity.

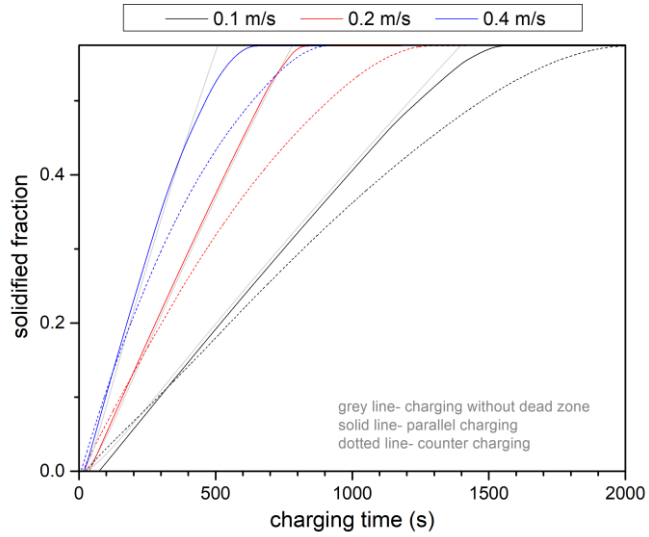

(a)

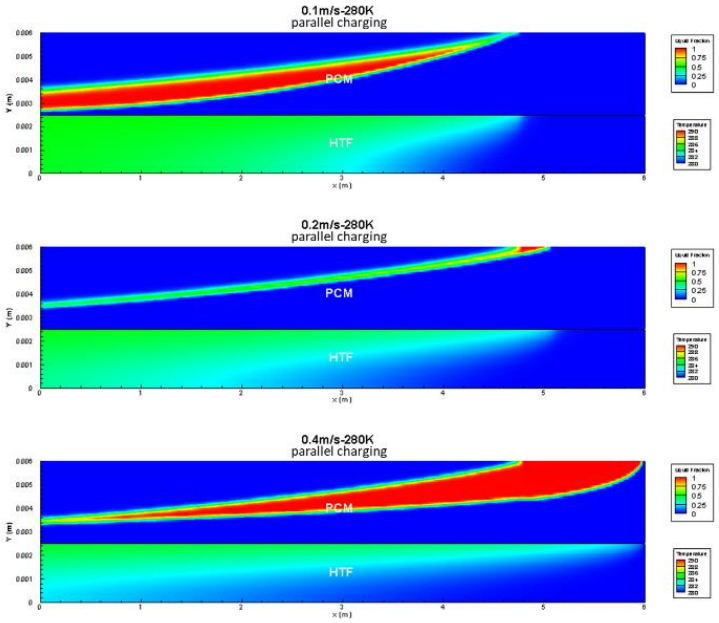

(b)

Figure 6-7 The comparison of designs using different charging velocities: a) the variation of solidified fraction of PCM over charging time; b) the distributions of temperature in the HTF and liquid fraction in the PCM when solidified zone begins to fuse with the dead zone in parallel charging (The texts above the contour describe the value of inlet velocity and inlet temperature of HTF in charging process)

The system performances of continuous discharging and charging are summarized in Table 6-1. The discharging process ceases at the outlet temperature of 286K, and the charging process stops at the outlet temperature of 281K. Overall speaking, the parameter of charging velocity has a subtle influence on the performance in a discharging process, but an evident impact on the time consumption and power consumption in a charging process. Charging the system with a flow of 0.1m/s only consumes 60% additional power of that in discharging process, but with a flow of 0.4 m/s consumes around 3.8 times additional power. A lower flow velocity in a charging process would largely improve the energy efficiency of an LHTES system, without much effect on the subsequent discharging process.

Table 6-1 The comparison of designs using different charging velocities

charging condition	280-0.1m/s		280-0.2m/s		280-0.4m/s	
	Parallel	counter	parallel	counter	parallel	counter
charging time, τ /s	1590	1907	912	1178	630	766
power factor, w	0.60	0.72	1.37	1.77	3.79	4.61
capacity effectiveness, φ	58.6%	58.3%	58.1%	57.9%	56.9%	56.2%
E_{st}	1.93	1.92	1.91	1.91	1.88	1.85

6.5 The parameter of charging temperature

Using charging flow at a lower temperature could speed up the solidification of PCM, since there is a larger temperature difference in heat transfer. As shown in Table 6-2, lowering down the temperature of charging flow from 282K to 275K could speed up the solidification from 1377 s to 570s, and decrease the power factor from 2.07 to 0.86. However, even though the power consumption is decreased, it is worth mentioning that the power consumption of chillers might also increase due to a lower evaporating temperature.

Moreover, counter charging is still less effective in solidifying PCM. Although the temperature difference between PCM and HTF in a charging process might be different from that in a discharging process, the dead zone effect does not occur in parallel charging. As shown in Figure 6-8(b), the profile of solidified zone is not influenced by charging temperature and is still parallel to that of the dead zone. As a result, the solidification curve of parallel charging overlap with that of no-dead-zone charging regardless of charging temperature in Figure 6-8(a).

The system performances of continuous discharging and charging are summarized in Table 6-2. The discharging process ceases at the outlet temperature of 286K, and the charging process stops when the temperature difference between charging inlet and outlet is within in 1K. According to the results, charging the system at a lower temperature can slightly improve the capacity effectiveness in the subsequent discharging process but largely decrease E_{st}. The reason lies in the increase in effective storage capacity of an SWS system. Overall speaking, the parameter of charging temperature is a key factor for the system E_{st} in a discharging process, but it also has an evident impact on the time consumption and power consumption in a charging process.

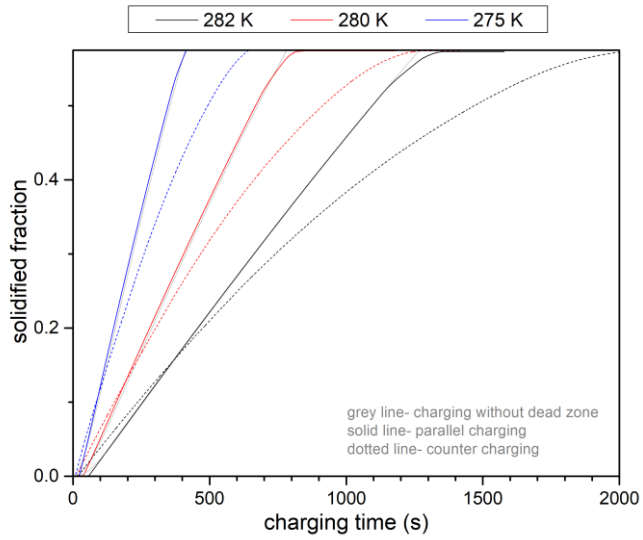

(a)

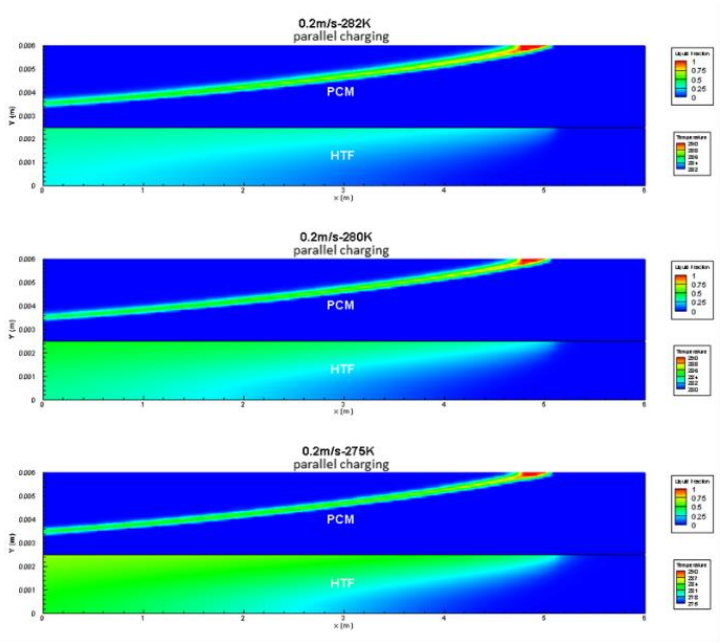

(b)

Figure 6-8 The comparison of designs using different charging temperatures: a) the variation of solidified fraction of PCM over charging time; b) the distributions of temperature in the HTF and liquid fraction in the PCM when solidified zone begins to fuse with the dead zone in parallel charging (The texts above the contour describe the value of inlet velocity and inlet temperature of HTF in charging process)

Table 6-2 The comparison of designs using different charging temperatures

charging condition	275K-0.2m/s		280K-0.2m/s		282K-0.2m/s	
	parallel	counter	parallel	counter	parallel	counter
charging time, τ /s	570	702	912	1178	1377	1645
power factor, w	0.86	1.06	1.37	1.77	2.07	2.47
capacity effectiveness, φ	61.7%	62.3%	58.1%	57.9%	56.5%	53.3%
E_{st}	1.46	1.47	1.91	1.91	2.26	2.13

6.6 Summary

This Chapter discussed the charging parameters of flow direction, flow velocity, and flow temperature, on the performances of subsequent discharging process. The followings are obtained.

- Counter charging consumes 20% additional power, thus is less effective than parallel charging due to the restriction of the initial dead zone, and an incomplete counter charging would damage the capacity effectiveness of the system in the subsequent discharging process;

-A charging HTF at a higher velocity can speed up the solidification of PCM and evidently increase the power consumption and slightly decrease the capacity effectiveness in the subsequent discharging process.

-A charging HTF at a lower temperature can speed up the solidification of PCM but causes a larger power consumption in water chillers. Although the capacity effectiveness in the subsequent discharging process can be improved slightly, the corresponding E_{st} is lowered down due to a larger range of working temperature.

In summary, it is appropriate to use HTF at a small velocity and a moderate temperature to charge an LHTES system with an initial dead zone. It is suggested to use parallel charging, since it consumes less pump power and has no negative effect on the system performance in a subsequent discharging process.

Chapter 7 Conclusions and future works

7.1 Conclusions

Stratified water storage (SWS) is of high energy efficiency, but of low energy density as it relies on the sensible heat of water. Latent heat thermal energy storage (LHTES) system using phase change material (PCM) is of higher energy density and might be an alternative to bulky SWS. In literature, the effect of many parameters on the LHTES performance has been studied. However, the characterization of the performance does not illustrate how much stored thermal energy could be utilized and whether the use of PCM in LHTES systems could provide a higher effective energy storage capacity than sensible thermal energy storage systems, such as SWS systems. Moreover, there lacks quantitative guidelines on optimizing LHTES systems. Thus, although the heat transfer enhancement technique in PCM has been largely developed, its benefit has not been well explored.

In this Thesis, a conjugate numerical fluid flow and heat transfer method was validated to solve the physical model of the basic unit of a tube-in-tank LHTES system. Then an index of effective energy storage ratio, E_{st}, was proposed to characterize the effective energy storage capacity of an LHTES system with reference to an equivalent SWS system. Other indices were also proposed to characterize the system performance from the perspective of power consumption, and material cost. Finally, an analytical technique of *required heat transfer length* was developed from the effectiveness-NTU theory to predict E_{st} and find the optimal designs for LHTES systems. Many conclusions could be drawn in this work.

Firstly, by characterizing the designs by the index of effective energy storage ratio, E_{st}, the effective storage capacity of the basic unit of a tube-in-tank LHTES system was compared with that of an SWS system. The effects of parameters on E_{st} and *required heat transfer length* were analyzed. The results show that a shorter *required heat transfer length* and a higher E_{st} could be obtained by enhancing heat transfer in PCM or lowering down the mass flow rate of the HTF by decreasing inlet velocity and inner tube diameter. Although the tube length has no effect on *required heat transfer length*, a longer tube could improve the effective *CF* or the ratio of tube length to *required heat transfer length*. Thus, E_{st} could be improved by lengthening tube. Most importantly, there is an optimal design with an optimum *CF* for PCM to achieve the maximum E_{st}.

Secondly, by using the analytical technique of *required heat transfer length*, an optimal design could be found and the effect of related parameters on the optimal designs for LHTES systems were demonstrated. For any HTF, enhancing heat transfer in PCM can effectively improve the optimum *CF* and E_{st}. However, when the effective thermal conductivity of PCM is above a certain threshold, *CF* and E_{st} would approach its maximum value. The maximum value is far lower than the $E_{st,\infty}$, which results from the low Nu of the HTF in the laminar flow region. By enhancing heat convection in HTF, the total thermal resistance could be further decreased. A high-degree heat transfer enhancement in PCM enables the use of turbulent HTF to obtain both a high E_{st} and a high COP at little cost of tube materials. However, if the use of heat transfer enhancement in PCM is limited, using long tubes could also improve the effective heat transfer length and achieve a higher optimum *CF* and E_{st}.

Thirdly, a complete optimization of LHTES should also consider the parameters in a charging process. Counter charging is less effective than parallel charging due to the mismatch of geometries between the solidified zone and an existing dead zone. An incomplete counter charging would

damage the capacity effectiveness of the system in the subsequent discharging process. For inlet velocity or inlet temperature of charging HTF, a higher velocity or a lower temperature could speed up the solidification of PCM while increasing the power consumption evidently. These two parameters have little effect on the capacity effectiveness in the subsequent discharging process. However, the corresponding E_{st} would be lowered down due to the larger range of working temperature when the system is charged by HTF at a lower temperature.

Through numerical and analytical studies, the Thesis provides both qualitative and quantitative instructions on designing optimal LHTES systems with higher effective energy storage capacity compared to SWS, and illustrate how LHTES systems could benefit from the heat transfer enhancement in PCM and convection enhancement in HTF.

7.2 Future works

This Thesis numerically studied the optimal designs for the basic unit of tube-in-tank LHTES system. Experimental works should be done according to the implications derived from the numerical and analytical work.

Firstly, in the numerical analysis, the effect of heat transfer enhancement in PCM was only described by the improvement in effective thermal conductivity of the PCM composite. However, the existence of the high-conductivity additives could also affect the volume fraction of PCM in the composite, and thus affect the latent heat of the composite. There might be some interesting findings due to the trade-off between a higher E_{st} and a lower latent heat driven by a higher degree of heat transfer enhancement in PCM. In addition, when the pore size and volume of the additives in PCM were large, the enhancement in heat conduction would be weak and the effect of natural convection should not be ignored. There can also be interesting findings due to the trade-off

between the suppression in natural convection and enhancement in heat conduction driven by a larger volume fraction of the additives in PCM.

Secondly, in analytical analysis, the heat transfer enhancement in HTF was caused by an increase in Nu over Re. Since the correlation of Nu in a low-Re region is weak, there is a sudden change of Nu around Re of 3000, resulting in the discontinuity of E_{st} over Re, as shown in Figure 5-7 and Figure 5-8. In experimental work, there might be a smooth increase in Nu over Re, and there might be a peak of E_{st} in the low-Re region. If so, the HTF in low-Re region might be the optimal for LHTES systems, since it has a small mass flow rate and a high Nu, which combines the merits of laminar flow and turbulent flow. Moreover, if thermal conductivity of HTF could be improved, or the vortex in the HTF could be enhanced without the increase of Re, the thermal resistance in HTF would be further decreased and E_{st} even higher.

Thirdly, the optimal designs discussed in the Thesis aimed at the basic unit of a tube-in-tank LHTES system. However, the arrangement of the tubes in the tank might also have effect on the E_{st} of the whole system. For example, if the tubes were arranged in parallel, the optimal spacing between the tubes should be smaller than the optimal outer tube diameter. This could be understood from the observation of locating round circles on a planar. However, if the volume of a dead zone in the basic unit could be decreased when tubes were arranged in the tank, E_{st} might be even increased. For an optimal design for the basic unit, as mentioned before, when E_{st} reaches its maximum, l_p would be around the length of the tube and the capacity effectiveness is only around 60%. Both future experimental and numerical studies are necessary to test the availability of increasing E_{st} by optimizing the arrangement of tubes in the tank.

To conclude, the numeral and analytical study presented in this Thesis has provided useful and interesting insights for the future experimental studies. By addressing the above issues, the

optimal designs and optimal operating strategies for a tube-in-tank LHTES system could be well understood.

References

Abhat, A., 1983. Low temperature latent heat thermal energy storage: Heat storage materials. *Solar Energy*, 30(4), pp.313–332.

Akhilesh, R., Narasimhan, A. & Balaji, C., 2005. Method to improve geometry for heat transfer enhancement in PCM composite heat sinks. *International Journal of Heat and Mass Transfer*, 48(13), pp.2759–2770.

Al-Saadi, S.N. & Zhai, Z., 2013. Modeling phase change materials embedded in building enclosure: A review. *Renewable and Sustainable Energy Reviews*, 21, pp.659–673.

Amin, N.A.M. et al., 2012. Optimising PCM thermal storage systems for maximum energy storage effectiveness. *Solar Energy*, 86(9), pp.2263–2272.

Azeem, S. & Zain-Ul-Abdein, M., 2012. Investigation of thermal conductivity enhancement in bakelite-graphite particulate filled polymeric composite. *International Journal of Engineering Science*, 52, pp.30–40.

Babapoor, A. & Karimi, G., 2015. Thermal properties measurement and heat storage analysis of paraffinnanoparticles composites phase change material: Comparison and optimization. *Applied Thermal Engineering*, 90, pp.945–951.

Belmonte, J.F. et al., 2016. A simplified method for modeling the thermal performance of storage tanks containing PCMs. *Applied Thermal Engineering*, 95, pp.394–410.

Belusko, M., Halawa, E. & Bruno, F., 2012. Characterising PCM thermal storage systems using the effectiveness-NTU approach. *International Journal of Heat and Mass Transfer*, 55(13–14), pp.3359–3365.

Bo, H., Gustafsson, E.M. & Setterwall, F., 1999. Tetradecane and hexadecane binary mixtures as phase change materials (PCMs) for cool storage in district cooling systems. *Energy*, 24(12), pp.1015–1028.

Cabeza, L.F. et al., 2011. Materials used as PCM in thermal energy storage in buildings: A review. *Renewable and Sustainable Energy Reviews*, 15(3), pp.1675–1695.

Cao, Y. & Faghri, A., 1990. A Numerical Analysis of Phase-Change Problems Including Natural Convection. In *Journal of Heat Transfer*. pp. 812–816.

Castell, A. et al., 2011. Maximisation of heat transfer in a coil in tank PCM cold storage system. *Applied Energy*, 88(11), pp.4120–4127.

Chen, X. et al., 2014. Experimental investigation on PCM cold storage integrated with ejector cooling system. *Applied Thermal Engineering*, 63, pp.419–427.

Dutil, Y. et al., 2011. A review on phase-change materials: Mathematical modeling and simulations. *Renewable and Sustainable Energy Reviews*, 15(1), pp.112–130.

Faghri, A., 2008. Transport Phenomena in Multiphase Systems.

Fan, L.W. et al., 2013. Effects of various carbon nanofillers on the thermal conductivity and energy storage properties of paraffin-based nanocomposite phase change materials. *Applied Energy*, 110, pp.163–172.

Fopah Lele, A. et al., 2015. Thermal decomposition kinetic of salt hydrates for heat storage systems. *Applied Energy*, 154, pp.447–458.

Francis, A., Philip, E. & Mervyn, S., 2009. A comparison of heat transfer enhancement in a medium temperature thermal energy storage heat exchanger using fins. *Solar Energy*, 83(9), pp.1509–1520.

Fu, Y.X. et al., 2014. Thermal conductivity enhancement of epoxy adhesive using graphene sheets as additives. *International Journal of Thermal Sciences*, 86, pp.276–283.

Al Ghossein, R.M., Hossain, M.S. & Khodadadi, J.M., 2017. Experimental determination of temperature-dependent thermal conductivity of solid eicosane-based silver nanostructure-enhanced phase change materials for thermal energy storage. *International Journal of Heat and Mass Transfer*, 107, pp.697–711.

Gil, A. et al., 2014. Experimental analysis of hydroquinone used as phase change material (PCM) to be applied in solar cooling refrigeration. *International Journal of Refrigeration*, 39, pp.95–103.

Gong, Z. & Majumdar, A., 1997. Finite-element analysis of cyclic heat transfer in a shell-and-tube latent heat energy storage exchanger. *Applied Thermal Engineering*, 17(6), pp.583–591.

Haillot, D. et al., 2008. Storage composites for the optimisation of solar water heating systems. *Chemical Engineering Research and Design*, 86(6), pp.612–617.

Hashemi, H.T. & Sliepcevich, C.M., 1967. A numerical method for solving two-dimensional problems of heat conduction with change of phase. *Chem. Eng. Prog. Symp. Series*, 63, pp.34–41.

Ismail, K.A.R., Alves, C.L.F. & Modesto, M.S., 2001. Numerical and experimental study on the solidification of PCM around a vertical axially finned isothermal cylinder. *Applied Thermal Engineering*, 21(1), pp.53–77.

Jana, S., Salehi-Khojin, A. & Zhong, W.H., 2007. Enhancement of fluid thermal conductivity by the addition of single and hybrid nano-additives. *Thermochimica Acta*, 462(1–2), pp.45–55.

Jones, B.J. et al., 2006. Experimental and numerical study of melting in a cylinder. *International Journal of Heat and Mass Transfer*, 49(15–16), pp.2724–2738.

Kalaiselvam, S. & Parameshwaran, R., 2014. Chapter 11 - Review on the Modeling and Simulation of Thermal Energy Storage Systems. *Thermal Energy Storage Technologies for Sustainability*, pp.247–278.

Kalnas, S.E. & Jelle, B.P., 2015. Phase change materials and products for building applications: A state-of-the-art review and future research opportunities. *Energy and Buildings*, 94(7491), pp.150–176.

Khan, Z., Khan, Z. & Ghafoor, A., 2016. A review of performance enhancement of PCM based latent heat storage system within the context of materials, thermal stability and compatibility. *Energy Conversion and Management*, 115, pp.132–158.

Khodadadi, J.M. & Hosseinizadeh, S.F., 2007. Nanoparticle-enhanced phase change materials (NEPCM) with great potential for improved thermal energy storage. *International Communications in Heat and Mass Transfer*, 34(5), pp.534–543.

Lacroix, M., 1993. Study of the heat transfer behavior of a latent heat thermal energy storage unit with a finned tube. *International journal of heat and mass transfer*, 36(8), pp.2083–2092.

Lacroix, M. & Voller, V.R., 1990. Finite Difference Solutions of Solidification Phase Change Problems: Transformed Versus Fixed Grids. *Numerical Heat Transfer, Part B: Fundamentals*, 17(1), pp.25–41.

Lamberg, P., Lehtiniemi, R. & Henell, A.M., 2004. Numerical and experimental investigation of melting and freezing processes in phase change material storage. *International Journal of Thermal Sciences*, 43(3), pp.277–287.

Languri, E.M., Aigbotsua, C.O. & Alvarado, J.L., 2013. Latent thermal energy storage system using phase change material in corrugated enclosures. *Applied Thermal Engineering*, 50(1), pp.1008–1014.

Li, G., Hwang, Y. & Radermacher, R., 2012. Review of cold storage materials for air conditioning application. *International Journal of Refrigeration*, 35(8), pp.2053–2077.

Li, Z. & Wu, Z.G., 2015. Analysis of HTFs, PCMs and fins effects on the thermal performance of shell-tube thermal energy storage units. *Solar Energy*, 122, pp.382–395.

Lin, Y. et al., 2018. Review on thermal conductivity enhancement , thermal properties and applications of phase change materials in thermal energy storage. *Renewable and Sustainable Energy Reviews*, 82(September 2017), pp.2730–2742.

Ling, Z. et al., 2015. Thermal conductivity of an organic phase change material/expanded graphite composite across the phase change temperature range and a novel thermal conductivity model. *Energy Conversion and Management*, 102, pp.202–208.

Liu, L. et al., 2016. Thermal conductivity enhancement of phase change materials for thermal energy storage: A review. *Renewable and Sustainable Energy Reviews*, 62, pp.305–317.

Liu, M., Saman, W. & Bruno, F., 2012. Development of a novel refrigeration system for refrigerated trucks incorporating phase change material. *Applied Energy*, 92, pp.336–342.

Liu, Y.F. & Wang, R.Z., 2002. Method to design optimal scheme for cold storage air conditioning system. *Energy Conversion and Management*, 43(17), pp.2357–2367.

Liu, Z., Sun, X. & Ma, C., 2005. Experimental investigations on the characteristics of melting processes of stearic acid in an annulus and its thermal conductivity enhancement by fins. *Energy Conversion and Management*, 46(6), pp.959–969.

Longeon, M. et al., 2013. Experimental and numerical study of annular PCM storage in the presence of natural convection. *Applied Energy*, 112, pp.175–184.

López-Navarro, A. et al., 2014. Performance characterization of a PCM storage tank. *Applied Energy*, 119, pp.151–162.

Lorente, S., Bejan, A. & Niu, J.L., 2014. Phase change heat storage in an enclosure with vertical pipe in the center. *International Journal of Heat and Mass Transfer*, 72(2014), pp.329–335.

Lv, Y., Zhou, W. & Jin, W., 2016. Experimental and numerical study on thermal energy storage of polyethylene glycol/expanded graphite composite phase change material. *Energy and Buildings*, 111, pp.242–252.

Mackenzie, J.A. & Robertson, M.L., 2002. A Moving Mesh Method for the Solution of the One-Dimensional Phase-Field Equations. *Journal of Computational Physics*, 181(2), pp.526–544.

Mat, S. et al., 2013. Enhance heat transfer for PCM melting in triplex tube with internal-external fins. *Energy Conversion and Management*, 74, pp.223–236.

Mehrali, M. et al., 2013. Preparation and characterization of palmitic acid/graphene nanoplatelets composite with remarkable thermal conductivity as a novel shape-stabilized phase change material. *Applied Thermal Engineering*, 61(2), pp.633–652.

Mills, A. et al., 2006. Thermal conductivity enhancement of phase change materials using a graphite matrix. *Applied Thermal Engineering*, 26(14–15), pp.1652–1661.

Mills, A.F., 1998. *Basic heat and mass transfer* 2nd revise., Pearson Education.

Nomura, T. et al., 2015. High thermal conductivity phase change composite with percolating carbon fiber network. *Applied Energy*, 154, pp.678–685.

Oya, T. et al., 2013a. Thermal conductivity enhancement of erythritol as PCM by using graphite and nickel particles. *Applied Thermal Engineering*, 61(2), pp.825–828.

Oya, T. et al., 2013b. Thermal conductivity enhancement of erythritol as PCM by using graphite and nickel particles. *Applied Thermal Engineering*, 61(2), pp.825–828.

Park, S.S. & Kim, N.J., 2014. Influence of the oxidation treatment and the average particle diameter of graphene for thermal conductivity enhancement. *Journal of Industrial and Engineering Chemistry*, 20(4), pp.1911–1915.

Pham, Q.T., 2006. Modelling heat and mass transfer in frozen foods: a review. *International Journal of Refrigeration*, 29(6), pp.876–888.

Py, X., Olives, R. & Mauran, S., 2001. Paraffin/porous-graphite-matrix composite as a high and constant power thermal storage material. *International Journal of Heat and Mass Transfer*, 44(14), pp.2727–2737.

Rahimi, M. et al., 2014. Analysis of geometrical and operational parameters of PCM in a fin and tube heat exchanger. *International Communications in Heat and Mass Transfer*, 53, pp.109–115.

Rathod, M.K. & Banerjee, J., 2015. Thermal performance enhancement of shell and tube Latent Heat Storage Unit using longitudinal fins. *Applied Thermal Engineering*, 75, pp.1084–1092.

Şahan, N., Fois, M. & Paksoy, H., 2015. Improving thermal conductivity phase change materials - A study of paraffin nanomagnetite composites. *Solar Energy Materials and Solar Cells*, 137, pp.61–67.

Sari, A. & Kaygusuz, K., 2001. Thermal energy storage system using stearic acid as a phase change material. *Solar Energy*, 71(6), pp.365–376.

Shatikian, V., Ziskind, G. & Letan, R., 2005. Numerical investigation of a PCM-based heat sink with internal fins. *International Journal of Heat and Mass Transfer*, 48(1), pp.3689–3706.

Swaminathan, C.R. & Voller, V.R., 1997. Towards a general numerical scheme for solidification systems. *International Journal of Heat and Mass Transfer*, 40(12), pp.2859–2868.

Tan, F.L., 2008. Constrained and unconstrained melting inside a sphere. *International Communications in Heat and Mass Transfer*, 35(4), pp.466–475.

Tay, N.H.S., Belusko, M. & Bruno, F., 2012a. An effectiveness-NTU technique for characterising tube-in-tank phase change thermal energy storage systems. *Applied Energy*, 91(1), pp.309–319.

Tay, N.H.S., Belusko, M. & Bruno, F., 2012b. Designing a PCM storage system using the effectiveness-number of transfer units method in low energy cooling of buildings. *Energy and Buildings*, 50, pp.234–242.

Tay, N.H.S., Belusko, M. & Bruno, F., 2012c. Experimental investigation of tubes in a phase change thermal energy storage system. *Applied Energy*, 90(1), pp.288–297.

Tay, N.H.S., Bruno, F. & Belusko, M., 2013. Comparison of pinned and finned tubes in a phase change thermal energy storage system using CFD. *Applied Energy*, 104, pp.79–86.

Trp, A., 2005. An experimental and numerical investigation of heat transfer during technical grade paraffin melting and solidification in a shell-and-tube latent thermal energy storage unit. *Solar Energy*, 79(6), pp.648–660.

Trp, A., Lenic, K. & Frankovic, B., 2006. Analysis of the influence of operating conditions and geometric parameters on heat transfer in water-paraffin shell-and-tube latent thermal energy storage unit. *Applied Thermal Engineering*, 26(16), pp.1830–1839.

Viswanath, R. & Jaluria, Y., 1993. a Comparison of Different Solution Methodologies for Melting and Solidification Problems in Enclosures. *Numerical Heat Transfer, Part B: Fundamentals*, 24(1), pp.77–105.

Vyshak, N.R. & Jilani, G., 2007. Numerical analysis of latent heat thermal energy storage system. *Energy Conversion and Management*, 48(7), pp.2161–2168.

Wang, S., Faghri, A. & Bergman, T.L., 2010. A comprehensive numerical model for melting with natural convection. *International Journal of Heat and Mass Transfer*, 53(9–10), pp.1986–2000.

Wang, W.W., Wang, L.B. & He, Y.L., 2016. Parameter effect of a phase change thermal energy storage unit with one shell and one finned tube on its energy efficiency ratio and heat storage rate. *Applied Thermal Engineering*, 93, pp.50–60.

Wang, W.W., Wang, L.B. & He, Y.L., 2015. The energy efficiency ratio of heat storage in one shell-and-one tube phase change thermal energy storage unit. *Applied Energy*, 138, pp.169–182.

Xiao, X. & Zhang, P., 2015. Numerical and experimental study of heat transfer characteristics of a shell-tube latent heat storage system: Part I - Charging process. *Energy*, 79(C), pp.337–350.

Xiao, X., Zhang, P. & Li, M., 2014. Effective thermal conductivity of open-cell metal foams impregnated with pure paraffin for latent heat storage. *International Journal of Thermal Sciences*, 81(1), pp.94–105.

Xiao, X., Zhang, P. & Li, M., 2013. Preparation and thermal characterization of paraffin/metal foam composite phase change material. *Applied Energy*, 112, pp.1357–1366.

Xu, T. et al., 2016. Preparation and thermal energy storage properties of d-Mannitol/expanded graphite composite phase change material. *Solar Energy Materials and Solar Cells*, 155, pp.141–146.

Yau, Y.H. & Rismanchi, B., 2012. A review on cool thermal storage technologies and operating strategies. *Renewable and Sustainable Energy Reviews*, 16(1), pp.787–797.

Zalba, B. et al., 2003. *Review on thermal energy storage with phase change: materials, heat transfer analysis and applications*,

Zhai, X.Q. et al., 2013. A review on phase change cold storage in air-conditioning system: Materials and applications. *Renewable and Sustainable Energy Reviews*, 22, pp.108–120.

Zhang, Q. et al., 2017. Preparation and thermal properties of short carbon fibers/erythritol phase change materials. *Energy Conversion and Management*, 136, pp.220–228.

Zhang, Z. & Fang, X., 2006. Study on paraffin/expanded graphite composite phase change thermal energy storage material. *Energy Conversion and Management*, 47(3), pp.303–310.

Zhao, D. & Tan, G., 2015. Numerical analysis of a shell-and-tube latent heat storage unit with fins for air-conditioning application. *Applied Energy*, 138, pp.381–392.